Optimised Use of Independent Component Analysis for EEG Signal Processing

By

Zohreh Zakeri

A Thesis Submitted to
The University of Birmingham
for the Degree of
Doctor of Philosophy

School of Engineering
College of Engineering
and Physical Sciences
The University of Birmingham
January 2016

Abstract

Electroencephalography (EEG) is the prevalent technique for monitoring brain function. It employs a set of electrodes on the scalp to measure the electrical activity of the brain. EEG is mainly used by researchers to study the brain's responses to a specific stimulus - the event-related potentials (ERPs). Different types of unwanted signals, which are known as artefacts, usually mix with the EEG at any point during the recording process. As the amplitudes of the EEG and ERPs are very small (in the order of microvolts), they can be buried in the artefacts which have very high amplitudes in the order of millivolts. Therefore, contamination of EEG activity by the artefacts can degrade the quality of the EEG recording and may cause error in EEG/ERP signal interpretation.

Several EEG artefact removal methods already exist in the literature and these previous studies have concentrated on manual or automatic detection of either one or, of a few types of EEG artefacts. Among the proposed methods, Independent Component Analysis (ICA) based techniques are commonly applied to successfully detect the artefacts.

Different types of ICA algorithms have been developed, which aim to estimate the individual sources of a linearly mixed signal. However, the estimation criterion differs across various ICA algorithms, which may deliver different results. Additionally, the estimated sources are not labelled by the ICA algorithms. Therefore, a criterion to select the proper ICA algorithm, with the aim of source separation and a method to label different types of artefacts, to clean the EEG signal for extracting the ERP information is required.

This thesis therefore contributes to the systematic comparison of commonly applied ICA algorithms, to be employed for automatically detecting and removing various types of artefacts mixed with EEG and furthermore to improve the extraction of ERP information. In this context, the thesis tackles three major problems, namely: (i) the problem of selecting the optimum data preparation steps, applied prior to ICA and the ICA algorithm

variant for better source separation; (ii) the state of the art-of-the-art method for the detection of only a few types of commonly occurring artefacts, during EEG recording; (iii) weak performance of the conventional ERP classification methods.

To deal with these problems, a literature review was carried out associated to each step. A wide range of signal processing was performed in MATLAB, which is computationally fast and easy to implement with the EEGLAB plug-in, to analyse the EEG data. The proposed methods were evaluated using EEG data collected from ten healthy subjects.

The first body of work outlined in this thesis proposes a pipeline to select an ICA algorithm variant that is most suitable for separating the artefactual sources from the EEG mixture. The criteria to compare different ICA algorithms are selected based on the independence and physiological plausibility of the components. Also, 24 pre-processing conditions are proposed by combining 5 commonly used data pre-processing steps. The results highlight the importance of selecting the data pre-processing condition, before ICA decomposition, rather than a type of ICA algorithm itself.

The proposed signal processing chain is the first of its kind and offers the possibility of selecting a data preparation condition based on the output of ICA algorithms' decomposition that may be employed in different EEG studies. In this thesis, a pre-processing condition and an ICA algorithm variant are selected based on their suitability for separation of the desired artefacts from non-artefact sources.

The optimum data preparation condition and ICA algorithm variant are consequently adapted for employing in an automated ICA-based EEG artefact removal method. A set of temporal, spatial and frequential features are proposed to automatically detect the commonly occurring EEG artefacts. The proposed artefact removal method compares favourably with the state-of-the-art ADJUST method [1] and detected five types of EEG artefacts successfully, with the balanced accuracy above 95%.

The proposed method is further improved by detecting one of the prominent EEG artefacts, blink, by means of combining the epoch-based and regression-based Sparse Component Analysis (SCA) methods. Simulated data is used to evaluate and compare

the proposed method with a recent study [2]. The result demonstrates an almost 2% improvement in terms of residual variance.

Finally, the ERP classification rate is improved by proposing an ICA-based method which does not require any artefact removal. The proposed method outperforms the *recursive backward channel elimination* method which is used to select a number of channels, including higher ERP information, from the artefact-free data; and compares favourably with the state-of-the-art xDAWN [3] for ERP classification. Using the proposed method, a rejection of the artefacts that may contain EEG information is no longer required; hence more ERP information is extracted.

To Imam Muhammad ibn Ali al-Baqir (PBUH)

Acknowledgements

Firstly, I would like to express my sincere thanks to my supervisors, Dr. Neil Cooke and Dr. Peter Jancovic who helped me throughout my PhD. It was an honour for me to work with them and confront through the difficulties with their help.

I would also like to thank my initial supervisors, Dr. Theodoros Arvanitis, Dr. Andrew Bagshaw and Dr. Sara Assecondi for their help and support during the formation and initial steps of my PhD and for helping me to build-up my knowledge. This project was done on a dataset recorded by Dr. Dirk Ostwald and without his generosity and sharing his dataset with me, this project would have been much harder to accomplish. Likewise, I would like to thank Dr. Reza Sameni for sharing the implementation of his method with me for comparison purposes.

I would also like to thank Dr. Biman Chakraborty (department of Mathematics-University of Birmingham) for his help and support in statistical analysis of the results of this research.

The members of staff in my school were always helping and make me feel welcomed and enjoy my studies. The list is endless but in particular, I would like to thank Prof. Chris Baber, Prof. Peter Gardner, Dr Tony Childs, Dr. Phil Atkins, Mary Winkles, Ben Clarke, Andy Dunn and other members of staff in my school.

My mother and my father, have always been by my side, not only through my PhD but also entire my life, holding my hand and believing in me. Without their love, help and support I would never have been able to accomplish so much this far. They are my everything.

My siblings, Nasrin, Mohsen, Masoud and my niece Melika have always been caring and provide me with emotional support; they encouraged me to carry on with my studies and I will never forget their support.

I would like to acknowledge the help, encouragement and support by my friends Mohammadreza Hajisamadi, Amani Algharibi and Laleh Akbarzadeh and whoever has helped me during my studies over the past years.

Last, but not least, I would like to thank Mrs. Janet Hingley for copy editing this thesis for conventions of language, spelling and grammar.

Contents

1 Introduction **1**

1.1 Aims and Scope of the Thesis 3

1.2 Major Contributions 5

1.3 Thesis Structure 7

1.4 List of Publications 9

1.5 Summary 10

2 Background **11**

2.1 EEG Historical Background 11

2.2 Anatomy and Physiology of the Brain 13

2.2.1 Neuronal Activity 14

2.2.2 Action Potentials 15

2.3 EEG Generation 17

2.4 EEG Recording 18

2.5 EEG Artefact Removal 23

2.6 Blind Source Separation 24

2.6.1 Blind Source Separation Principles 25

2.6.2 Independent Component Analysis 27

2.6.3 Application of ICA to EEG 33

2.7 EEG Applications 34
2.8 Summary 37

3 Systematic Comparison of ICA Algorithms 38

3.1 Introduction 38
3.2 Materials and Method 40
3.2.1 Data Acquisition and Pre-processing 40
3.3 ICA Performance Evaluation 48
3.3.1 Independence of Sources 49
3.3.2 Biological Plausibility 53
3.3.3 Statistical Analysis 54
3.4 Result Analysis 55
3.4.1 Pre-processing Conditions, Independence and Dipolarity of Sources 55
3.4.2 Processing Time 59
3.5 Summary 62

4 Automatic ICA-Based EEG Artefact Removal 64

4.1 Introduction 64
4.2 Methodology 67
4.2.1 Feature Extraction 67
4.2.2 Feature Normalisation 75
4.2.3 Artefact Classification 75
4.3 Evaluation Criteria 77
4.3.1 Visual Inspection 78
4.3.2 Balanced Accuracy 78
4.3.3 Receiver Operator Curve 79
4.3.4 Signal-to-Noise Ratio 79
4.3.5 Relative Variance 80
4.3.6 Event-related Potential Classification 81

4.3.7 Cross Validation . . . 82
4.4 Results Analysis . . . 83
4.4.1 Artefact Classification at Segment-Level . . . 83
4.4.2 Artefact Classification at IC-Level . . . 85
4.4.3 Comparison with ADJUST . . . 87
4.5 Summary . . . 91

5 Enhanced Blink Artefact Removal via Sparse Component Analysis 93
5.1 Introduction . . . 93
5.2 Methodology . . . 95
5.2.1 Blink Segment Detection . . . 96
5.2.2 Method-1: Time Masking . . . 97
5.2.3 Method-2: Regression-Based SCA . . . 98
5.3 Evaluation . . . 101
5.3.1 Simulated Data . . . 101
5.3.2 Real Data . . . 105
5.3.3 Evaluation Measures . . . 106
5.4 Results Analysis . . . 106
5.4.1 Simulated Data . . . 107
5.4.2 Real Data . . . 109
5.5 Summary . . . 113

6 ICA-Based Event-Related Potential Classification 114
6.1 Introduction . . . 114
6.2 Methodology . . . 116
6.2.1 Recursive Backward Channel Elimination . . . 117
6.2.2 ICA-based ERP Classification . . . 118
6.2.3 Stage 1: Automatic Task-related IC Detection . . . 118
6.2.4 Stage 2: ERP Classification . . . 121

6.2.5 xDAWN Algorithm . . . 121
6.3 Evaluation . . . 122
6.3.1 Visual Inspection . . . 122
6.4 Results Analysis . . . 123
6.4.1 Recursive Backward Channel Elimination . . . 123
6.4.2 Task IC Classification . . . 125
6.4.3 ERP Classification from Task ICs . . . 127
6.4.4 Comparison with xDAWN . . . 128
6.5 Summary . . . 130

7 Conclusion **131**
7.1 Summary of Findings . . . 133
7.2 Future Research Directions . . . 134

A Pairwise comparison of the ICA algorithms **137**

B Automatic Artefact Detection **139**

C Distribution of Artefactual ICs **141**

D Task-Related IC Detection **144**

List of References **146**

List of Figures

1.1 Block diagram of the thesis structure. 7

2.1 Anatomical division of the brain in to four brain lobes of frontal, parietal, occipital and temporal 13
2.2 Schematic structure of a neuron 14
2.3 Changes of the membrane potential in a neuron 16
2.4 The 10-20 international electrode placement 19
2.5 A differential amplifier of the EEG recording connected to each channel. . 21
2.6 Illustration of the brain rhythms: delta (δ), theta (θ), alpha (α), beta (β) and gamma (γ) 35
2.7 A sample of EEG time series recorded during ERP experiment 36

3.1 Experimental design of the visual stimulation. 40
3.2 A sample of continuous multichannel EEG data 43
3.3 A sample of multichannel EEG data epoched based on stimulus onset . . . 43
3.4 A sample of not filtered EEG data versus band-pass filtered EEG data . . 45
3.5 A sample of potential distribution of an EEG bad channel and a fitted normal distribution. 46
3.6 Marked bad channels in the EEG data whose kurtosis value exceeds the threshold 47

3.7 Example of component scalp maps resembling the equivalent current dipole 54
3.8 The pre-processing hierarchy of the raw EEG data and the performance of ICA algorithms based on MIR, PMI and dipolarity 56
3.9 Processing time of AMICA algorithms through different pre-processing conditions 60
3.10 Block diagram of the obtained optimum pre-processing steps, where the raw EEG signal is band-pass filtered and concatenated with ECG and EOG channels 62

4.1 A sample of typical blink artefact IC in time, frequecy and spatial domains 68
4.2 A sample of a blink IC histogram with a negative skewness 69
4.3 The subdivisions of the scalp map according to the brain lobes used as spatial features 70
4.4 A sample of saccade artefact IC in time, frequency and spatial domains . . 71
4.5 A sample of muscle artefact IC in time, frequency and spatial domains . . 72
4.6 A sample of focal artefact IC in time, frequency and spatial domains 73
4.7 A sample of ECG artefact IC in time domain 74
4.8 A sample of the averaged QRS complex used as a temporal feature of the ECG artefact 74
4.9 The averaged BA of the proposed method in detecting artefactual segments classified as blink, ECG, muscle, focal and saccade 84
4.10 ROC curves of the proposed method for blink, ECG, muscle, focal and saccade IC classification, when different thresholds are used 86
4.11 Distribution of the blink IC scores for 10 subjects 87
4.12 Comparison of the proposed method and ADJUST in detecting the artefactual components 88
4.13 The averaged BA of the ERP classification for the raw, cleaned data when removing artefacts labelled in the ground truth, by the proposed method and ADJUST method 90

4.14 Block diagram of the proposed automatic artefactual segment and IC detection method 92

5.1 Diagram of the proposed methods to enhance the blink artefact removal . . 96
5.2 A sample of blink segments detected within the blink IC 97
5.3 A sample of simulated 9-channel EEG data generated by MVAR model . . 102
5.4 Simulated blink IC modelled by two Gaussian waveforms 103
5.5 The effect of the blink artefact on the EEG channels, with SNR equal to $0dB$ and -30dB 105
5.6 The normalised residual variance obtained for time masking, regression-based SCA, DEFL and the Proposed_method_IC blink artefact removal methods, for different SNR values 107
5.7 Comparison of the proposed blink artefct correction methods and the raw EEG 109
5.8 A fragment of multichannel EEG data contaminated by blink artefact . . . 110
5.9 A fragment of multichannel EEG data cleaned by the regression-based SCA method 111

6.1 Block diagram of the proposed ICA-based ERP classification method . . . 118
6.2 A sample of a task-related IC in time, frequency and spatial domains . . . 119
6.3 The ERP classification rates obtained by the recursive backward elimination method 123
6.4 Comparison of ERP classification rates calculated using channel subsets selected by different channel selection methods 125
6.5 Number of task-related ICs, for each participant, detected automatically by the proposed method 126
6.6 ERP classification rate for different number of channels selected by the xDAWN algorithm 129

6.7 Comparison of the ERP classification rate using the 3 channels selected by xDAWN algorithm and task-related ICs 129

B.1 A sample of artefact ICs, automatically labelled by the proposed method in Chapter 4 140

C.1 The distribution of IC scores for ECG, muscle, focal and sccade artefacts . 143

D.1 The time series of the multichannel EEG data decomposed by AMICA algorithm, including the correctly and incorrectly detected task-related ICs 145

List of Tables

4.1 The automatic ICA-based EEG artefact removal methods in the literature 65

4.2 The threshold ranges for artefactual IC detection obtained from the ROC curve 85

4.3 Comparing ADJUST with the proposed artefact removal method in terms of RV 88

5.1 Comparison of DEFL and the proposed blink artefact removal methods . . 112

6.1 Performance of task-related IC classification for all participants, measured by sensitivity, specificity and balanced accuracy 126

6.2 Accuracy of ERP classification for the cleaned data obtained by the proposed automated task-IC detection compared with the cleaned data by the task-ICs in the ground truths 127

A.1 Pairwise comparison of the ICA algorithms in terms of MIR. 138

A.2 Pairwise comparison of the ICA algorithms in terms of PMI. 138

A.3 Pairwise comparison of the ICA algorithms in terms of the mean percentage of dipolar sources. 138

List of Acronyms

AC	Alternating Current.
AMICA	Adaptive Mixture of Independent Component Analysers.
ANOVA	Analysis of Variance.
AUC	Area Under the Curve.
BA	Balanced accuracy.
BCG	Ballistocardiogram.
BSS	Blind Source Separation.
CLT	Central Limit Theorem.
CNS	Central Nervous System.
ECG	Electrocardiography.
EEG	Electroencephalography.
EM	Expection Maximisation.
EOG	Electrooculography.
EPSP	Excitatory Post Synaptic Potential.
ERPs	Event Related Potentials.

FA	False Acceptance.
FIR	Finite Impulse Response.
FL	Frontal Lobe.
GT	Ground Truth.
HCI	Human Computer Interaction.
ICA	Independent Component Analysis.
ICs	Independent Components.
IIR	Infinite Impulse Response.
IPSP	Inhibitory Post Synaptic Potential.
MI	Mutual Information.
MIR	Mutual Information Reduction.
MVAR	Multivariate Autoregressive.
NB	Naive Bayesian.
NS	Nervous System.
PCA	Principle Component Analysis.
PMI	Pairwise Mutual Information.
PNS	Peripheral nervous System.
PSD	Power Spectral Density.
ROC	Receiver Operator Curve.
RV	Relative Variance.
SCA	Sparse Component Analusis.
SNR	Signal-to-Noise-Ratio.
SSNR	Signal to Signal plus Noise Ratio.

std. error	Standard error.
TA	True Acceptance.
TNR	True Negative Rate.
TPR	True Positive Rate.

"Knowledge and science are the coffers and caches to the treasures of Perfection; and the only access to them is to ask and question."

Imam Ali al-Rida (PBUH)

1

INTRODUCTION

The recording of the brain's electrical potentials or Electroencephalography (EEG), as it is known in a scientific context, is widely used by clinicians, neurologists and researchers in monitoring and evaluating the brain's function; and for diagnosis and treatment of mental issues and brain disorders [4,5]. The term *Electroencephalography* refers to the recording of the brain's activity through a set of electrodes which are placed on the scalp [6]. The neurons' firing creates a flow of current in the brain which causes a voltage fluctuation that can be measured - the EEG potential. If the corresponding activities in the brain are happening in response to a stimulus (sensory, motor or cognitive), the measured EEG potential is called the event-related potential (ERP). A subject's brain in different states of consciousness (sleeping, waking, etc.) can generate EEG signals that seemingly vary in

characteristics such as amplitude and frequency [7].

A common ERP paradigm is the flashing checkerboard used in clinical applications to measure the visual cortex response [8]. Extracting the ERP responses buried in the EEG data is a crucial task in the analysis of brain information. In addition to the clinical application, there is an increased interest in employing EEG-ERP paradigms to understand brain function and develop brain control interfaces in the field of Human-Computer Interaction (HCI) and assistive technologies [9,10]. Impeding in this interest is the fact that EEG recordings are attenuated and contaminated by unwanted artefactual electrical signals originating from physiological and non-physiological sources [11]. To avoid misinterpretation of EEG data or the brain's responses to different stimuli, it is desirable to improve the signal-to-noise ratio (SNR) of EEG data by removing the EEG artefacts. Usually, the non-physiological artefacts are removed using linear filtering, or data preparation steps performed according to the specific experimental data. However, it is not possible to effectively remove physiological artefacts by simple filtering as the frequency bands of the recorded EEG signal and the artefacts overlap.

Different approaches have been proposed to reject or reduce physiological artefacts in EEG signals. The earliest approaches rejected artefacts by simply discarding temporal segments of multichannel EEG contaminated by artefacts [12,13] resulting in a great amount of information loss. More recently, artefact reduction methods have been adopted to reduce EEG information loss. Independent Component Analysis (ICA) is one popular and successful EEG artefact reduction method which belongs to the Blind Source Separation (BSS) technique [14]. ICA assumes that EEG is a multivariate signal of independent cerebral and non-cerebral sources whose distributions do not follow the Gaussian distribution. An ICA decomposition via an estimated un-mixing matrix creates Independent Components (ICs), each representing a source signal. By removing the ICs identified as artefactual sources and recombining the remaining ICs by inverting the un-mixing matrix, the cleaned EEG signal is reconstructed, potentially improving ERP classification accuracy.

There are various ICA algorithms which estimate the ICs in different ways. One active topic of the research is to systematically compare the performance of different ICA algorithms in source separation and select the best performing algorithm. However, assessing the effect of different data preparation steps (e.g. segmenting the continuous data prior to ICA) on the performance of the ICA decompositions has not received a great deal of attention. Although all the ICA algorithms potentially separate brain sources from artefactual sources, they do not provide information about labelling the ICs. Thus, labelling the artefactual sources is essential prior to artefact removal. Another active topic of research is to automatically label the artefactual sources to be removed from the data; in order to increase the SNR of EEG data or ERP detection reliability [12, 15]. This thesis, therefore, is mainly interested in extracting more ERP information reliably, by investigating the optimum signal pre-processing chain and ICA algorithm variant to be employed for the automatic detection of EEG artefacts.

1.1 Aims and Scope of the Thesis

The ultimate goal of this research is to effectively use ICA for EEG signal processing. In order to reach this goal, the following steps have to be taken:

- Evaluating the effect of data pre-processing steps on the performance of ICA algorithms.
- Assessing the source separation of different ICA algorithms which employ different metrics to estimate independent components.
- Effective use of source separation of ICA to increase the SNR of the signal.

Based on the aims of the thesis, first the performance of different ICA algorithms based on the independence and physiological plausibility of the estimated sources are systematically compared. Furthermore, the influence of different data pre-processing steps, prior to ICA decomposition, on the performance of ICA algorithms are evaluated and assessed.

Therefore, the optimum type of ICA algorithm with respect to the type of the given pre-processed data and the decomposition quality can be selected for source separation.

Secondly, an ICA-based method is proposed to automatically detect the common EEG artefacts, namely: blink, saccade, muscle, heartbeat and focal, reliably. The accuracy of ERP classification calculated from the cleaned data by removing the artefacts using the proposed method is then evaluated. Methods for removing one of the prominent artefacts in EEG data, blink, are improved by proposing two approaches which preserve more ERP information that are buried in the EEG signal and reduce the amount of data loss with the aim of improving ERP classification rate. The thesis also further improved the accuracy of ERP classification by proposing the automatic ICA-based method which does not require any artefact removal.

This study has raised the following research questions:

- Is there any difference between the performance of various ICA algorithms?
- What is the influence of different data pre-processing steps on the performance of ICA algorithms?
- What is the optimum type of ICA algorithm for source separation with respect to the type of the given pre-processed data?
- How can ICA be used to remove all the common EEG artefacts reliably and how is it compared to the existing state-of-the-art ADJUST method?
- Given the blink as the most prominent artefact in EEG data, how can it be effectively removed from the EEG while ERP information within EEG is preserved?
- How can ICA be effectively employed to enhance ERP classification?

1.2 Major Contributions

The research introduced in this thesis provides original contributions to EEG signal processing to enhance ERP classification rate and to improve the SNR of EEG data via the optimised use of ICA. The major contributions can be summarised as follows:

- Providing a pipeline to effectively select the pre-processing steps and ICA algorithm variant for optimum source separability;
  - systematic evaluation of the ICA algorithms for source separation based on the independence and physiological plausibility of the recovered sources;
  - assessment of the effect of all common pre-processing steps (24 different conditions) on the performance of the most commonly used ICA algorithms (via 960 different ICA decompositions).
- Proposal of a fully automated artefact IC removal method to detect and remove the common artefacts that occur in normal EEG recordings, including: blink, saccade, electrocardiogram (ECG), muscle and focal artefacts;
  - proposing a set of spatial, temporal and frequential features to discriminate different artefact ICs, based on the characteristics of different artefacts;
  - proposing a two-layered artefact classification algorithm, for labelling artefact ICs and artefact segments within different ICs;
  - building a ground truth by labelling more than 640 ICA decompositions by two individual experts.
- Improvement of ICA-based blink artefact removal, by proposing a Sparse Component Analysis (SCA) based method to detect and regress out the impact of the blink artefacts within the blink ICs and keeping the EEG information within those blink ICs intact.

- Improvement of the ERP response classification via using ERP response sources as a new representation of EEG data and extracting ERP features from the automatically detected ERP sources;
  - proposing a set of spatial, temporal and frequential features to discriminate sources including ERP responses (task-related ICs) from all other activity sources;
  - proposing a fully automated ERP response IC labelling method.

The statistical analysis of the results plays an important role in research studies and helps researchers to make inferences about the data and evaluate the certainty or uncertainty of the methods. The absence of statistical analysis does not guarantee the validity and reliability of the research findings; as the interpretation of the findings and the obtained relationships of the results may not be correct or meaningful and could be simply chance occurrences. Thus, the full reliability of the findings depend upon a robust statistical assessment of the methods. Therefore, in order to ensure the reliability of the proposed methods and obtained results, the Analysis of Variance statistical test, which is one the most commonly used tests in statistics, is applied to all of the findings of this research.

This thesis is organised in seven chapters. Following this chapter, the necessary background is provided in Chapter 2 and the main contributions of the research are presented in Chapter 3 to Chapter 6, followed by the conclusion in Chapter 7. Each chapter is started by an introduction section which includes the related existing works and literature review followed by a discussion of their shortcomings. Subsequently, the proposed methods are introduced and the obtained results are discussed. The chapters end with an overview section which concludes and summarises the associated chapter. Figure 1.1 illustrates a block diagram of the thesis structure. A summary of the information provided in each chapter is given below:

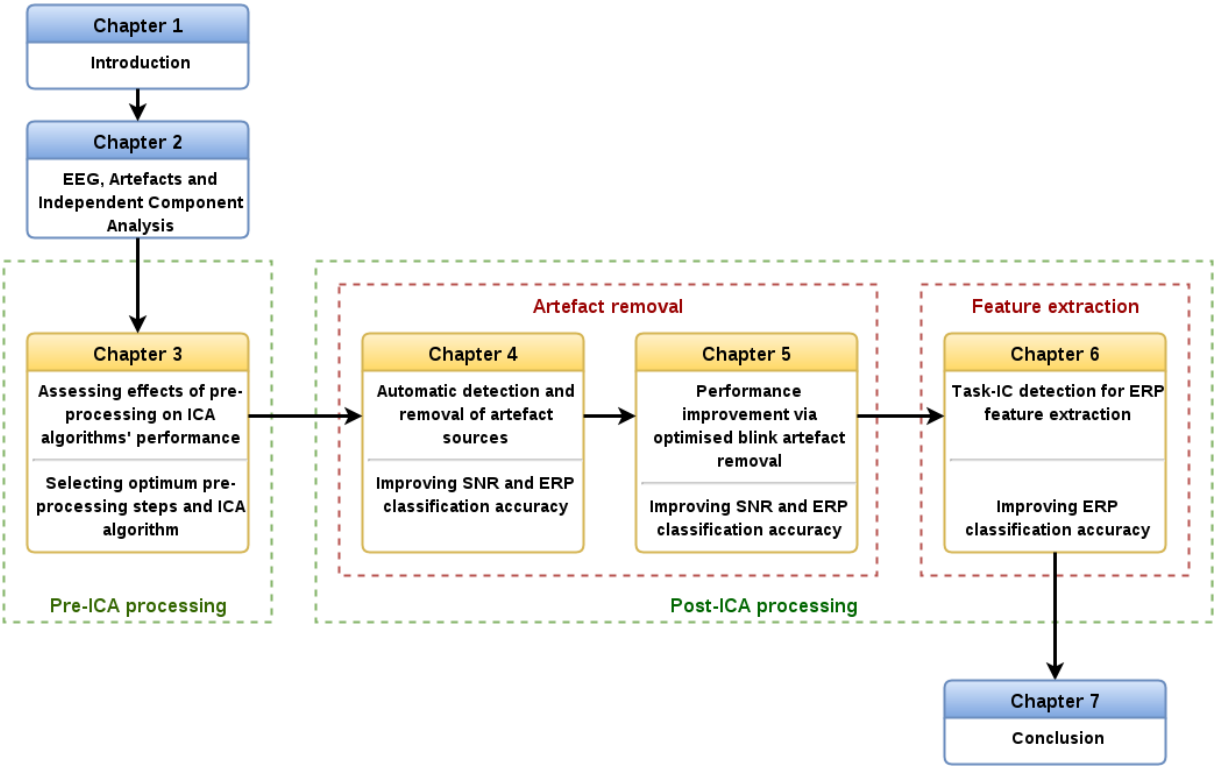

Figure 1.1: Block diagram of the thesis structure.

1.3 Thesis Structure

Chapter 2 - Background

In this chapter, the background required to understand the EEG concept is provided. It begins with a brief historical background of EEG; the anatomy and physiology of the brain; the process of EEG generation and the basic concepts of EEG recording. Then, the common and conventional EEG pre-processing steps are given followed by an introduction of the different types of EEG artefacts. Furthermore, the conventional EEG artefact removal methods are generally discussed and the most recent and commonly used method, ICA, which is employed in this thesis is explained in more details. Next, ICA principles, the commonly used ICA algorithms and the application of ICA to EEG are outlined. Finally, this chapter ends with a discussion on the application of EEG.

Chapter 3 - Systematic Comparison of ICA Algorithms

This chapter provides the pipeline for selecting the optimum ICA algorithm with the aim of removing artefacts from the EEG data. The effect of different data preparation and pre-processing on the performance of ICA algorithms is assessed. Based on the assessment, the optimum pre-ICA processing chain and ICA algorithm variant is introduced and employed for the rest of this research to detect and remove artefacts from EEG data.

Chapter 4 - Automatic ICA-Based EEG Artefact Removal

In this chapter, an automatic EEG artefact removal method, based on ICA, is proposed to remove several types of EEG artefacts as a post-ICA processing step. The EEG datasets are decomposed into independent components by ICA. For each type of artefact, a joint set of temporal, spatial and frequential features representing artefact characteristics is extracted. Then, the desired artefacts are detected and removed, based on a two-layered artefact classification algorithm.

An ERP classification method is employed to evaluate the cleaned reconstructed data, after detecting and removing artefacts by the proposed method and the existing state-of-the-art ADJUST method [1] relative to the ground truth and raw data.

Chapter 5 - Enhanced Blink Artefact Removal via Sparse Component Analysis

In this chapter, the blink artefact is considered as an important and most contributed artefact to EEG data, and two methods are developed to further improve the proposed blink artefact removal method in Chapter 4. Both methods are based on detecting the segments of blink IC in which the blink occurred, to either reject or eliminate the effect of blinking. The first method removes the effect of blink by setting the ample point of the blink segments to zero. In the second method, the effect of blink is eliminated by regressing out the blink peak in the blink segments. Real and simulated data are used to

evaluate the performance of the proposed methods; and also to compare these methods to the recently developed method, DEFL [2].

Chapter 6 - ICA-Based Event-Related Potential Classification

In this chapter, the ERP classification rate is improved by means of two methods. First, the recursive backward channel elimination method is applied to the cleaned EEG in order to select the optimum set of channels that provide the highest ERP classification rate. Furthermore, the result is compared to the ERP classification rate obtained in Chapter 4, where the ERP channels were selected by a human-based method.

Second, an automated ICA-based Event-Related Potential classification method is proposed in which the ERP is not classified from EEG channels. This way, instead of the conventional use of ICA to detect and remove artefactual sources to obtain cleaned data, the ERP is merely calculated from the task-related sources. The task-related ICs are automatically detected by extracting a set of features based on the visual stimulation paradigm in this experiment. The result of ERP classification from task-related ICs is compared to the state-of-the-art xDAWN algorithm [3], which has been reported to enhance ERP classification.

Chapter 7 - Conclusion

In the final chapter of this dissertation, a summary of the results and achievements in the thesis are provided, along with the conclusion and future trends of the work.

1.4 List of Publications

The list of publications of the author is as follows:

- Zakeri Z, Assecondi S, Bagshaw AP, Arvanitis TN. Influence of signal preprocessing on ICA-based EEG decomposition. In XIII Mediterranean Conference on Medical

and Biological Engineering and Computing 2014 (pp. 734-737). Springer International Publishing.

- Zakeri Z, Samadi MR, Cooke N, Jancovic P. Automatic ERP classification in EEG recordings from task-related independent components. In 2016 IEEE-EMBS International Conference on Biomedical and Health Informatics (BHI) 2016 Feb 24 (pp. 288-291). IEEE.

- Haji Samadi MR, Zakeri Z, Cooke N. VOG-enhanced ICA for removing blink and eye-movement artefacts from EEG. In 2016 IEEE-EMBS International Conference on Biomedical and Health Informatics (BHI) 2016 Feb 24 (pp. 603-606). IEEE.

- Zakeri Z, Cooke N, Jancovic P. An Effective ICA-Based Processing Chain For Automatic Artefact Removal In EEG. In: International Journal of Psychophysiology [under revision].

1.5 Summary

This chapter provides a brief introduction to this research, its aims and scopes and its contributions, including a brief summary of each chapter of the thesis, followed by the list of publications of the author.

"Teach others your knowledge and learn knowledge of others so you will bring your knowledge to perfection and learn something which you do not know."

Imam Hassan ibn Ali (PBUH)

2

BACKGROUND

2.1 EEG Historical Background

The discovery of the potential of EEG goes back to 1877 as a result of research conducted by the physician Richard Caton (1842-1926) on the exposed brains of rabbits and monkeys [16]. However, it was not until 1912 that the first measurements and demonstration of electrical activity were performed by Vladimir Pravdich-Neminsky in the brain of dogs [17]. Eight years later, in 1920, the German neuropsychiatrist Hans Berger (1873-1941) revealed the first recordings of the electrical activities of a human's brain and reported the results on photographic paper. He used the German word $'electroenkephalogram'$ to name these recordings; a term which later was altered to *electroencephalogram* or

EEG. He also realised that recorded brain signals vary with the individual's state of consciousness from relaxation to alertness [18].

In 1935, Gibbs et al. described the characteristic form of spike waves, which started the field of clinical electroencephalography [19]. Subsequently, in 1936, Gibbs and Jasper reported the interictal spikes as the focal signature of epilepsy [20, 21]. After World War II, the researchers tended to develop different methods of detection, purification and classification of brain signals that enabled them to diagnose abnormal signals. In the 1950s, English physician William Grey Walter developed EEG topography that allowed for the mapping of electrical activity across the surface of the brain; this topography was used in psychiatry until the 1980s. From 1990 to 2000, different techniques such as Blind Source Separations (BSS) [22–27] and Independent Component Analysis ICA [28–30] were developed to process EEG signals .

Presently, ERP is widely used in cognitive neuroscience research. Since over the ensuing decades, EEG has proved to be useful in both scientific and clinical applications [7]. Furthermore, the processing and analysing of the EEG signals for a better understanding and interpretation of these signals has also gained importance. As the recorded EEG data on the scalp is usually contaminated by various artefacts, which are typically comparable with or of higher amplitudes than the desired brain signal [11], EEG interpretation may be impaired by the presence of these artefacts [31], resulting in misdiagnosis in patients in clinical applications. Therefore, in order to maintain clean and clinically meaningful cerebral activity, improving the EEG signal-to-noise ratio (SNR) via artefact removal is in demand.

In this chapter, a short introduction of the physical anatomy of the human brain and the underlying mechanism of EEG signal generation are given. Additionally, the basics of EEG measurement and pre-processing and application of EEG signals are discussed. The chapter concludes with introducing the common EEG artefacts and methods employed to remove their effects from EEG recordings.

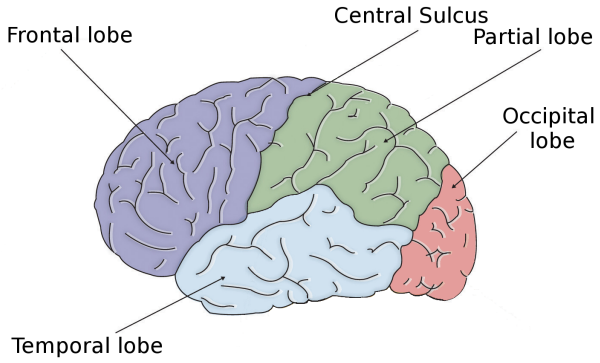

Figure 2.1: Anatomical division of the brain in to four brain lobes of frontal, parietal, occipital and temporal. The central sulcus, which separates the frontal and parietal lobes, and the spinal cord, are also shown. The figure is adopted from [32]

2.2 Anatomy and Physiology of the Brain

To gain a better understanding of how an EEG signal is generated, it is important to realise the neuronal functions of the brain as well as the underlying mechanism of the EEG.

The Nervous System (NS) is composed of nerve cells (neurons) and glial cells (neuroglia) that control and respond to the interaction between the human body and its external environment [11]. The NS has two major divisions: the Central Nerve System (CNS) and the Peripheral Nerve System (PNS). The CNS comprises the brain and spinal cord and controls most functions of the body by receiving information from the PNS and processing and sending it back. The human brain is the most important organ in the CNS, which anatomically is divided into different regions, known as the frontal, parietal, occipital and temporal lobes and the central sulcus (Figure 2.1) [11]. Each lobe performs a specific function. The *frontal* lobe is associated with skills of planning and decision making, control of movement and mood. The *parietal* lobe is involved in processing the somatic information derived from external stimuli, namely perception of stimuli. The *occipital* lobe is responsible for the perception and elaboration of visual stimuli (visual processing). The *temporal* lobe deals with hearing and, through its deep structures (amygdaloid nuclei and hippocampus), with learning, memory and emotion (i.e. the perception

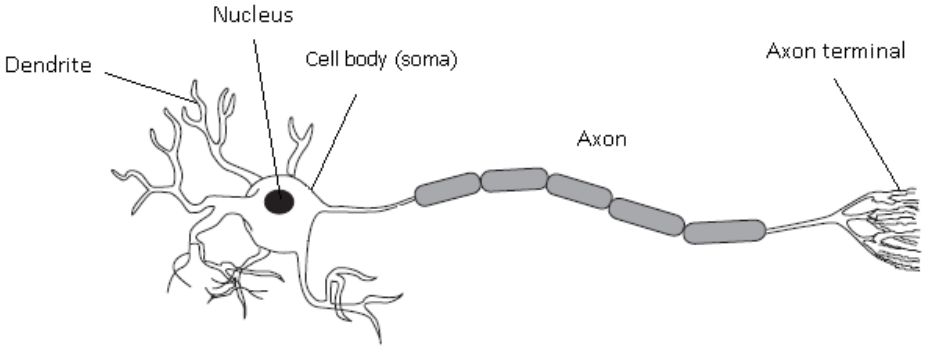

Figure 2.2: Schematic structure of a neuron. The figure is adopted from [11]

and recognition of auditory stimuli, memory, and speech). The *centralsulcus* separates the parietal lobe from the frontal lobe.

The brain consists of billions of neurons connected to each other. The neurons' structure and behaviour are described below.

2.2.1 Neuronal Activity

Neurons are the core components of the nervous system in charge of receiving and transmitting electrochemical nerve impulses. In response to physical and chemical stimuli, neurons perform their specialised tasks of conducting electrochemical signals and releasing chemicals that govern different body processes. Neurons' activities and nutrition are supported by glial cells. Neurons exist in a variety of shapes and sizes with specialised characteristics that enable them to transmit nerve impulses. They can be categorised by function as [33]: sensory neurons, motor neurons, communication neurons and computation neurons. However, they share the same structure comprising *dendrites*, the *cell body* (*Soma*) and *axon*, as shown in Figure 2.2. A neuron usually has just one single axon but can have several dendrites. Dendrites are the branching fibres extended from the soma responsible for carrying the received signals from other nerve cells towards their corresponding soma. The soma is the central part of the neuron that contains the nucleus of the cell (Figure 2.2) and is responsible for metabolic reactions of the neuron. It processes the incoming signals from the dendrites and decides whether a signal has to be transmitted

to the axon. In this case, a neuron is said to fire the signals in the form of electrochemical impulses called action potential or spikes that propagates along the axon [7, 11]. The axon is a slender projection of a neuron that conducts the signals away from the soma to other neurons, muscles and glands via the axon's terminal. The transmission of impulses from one neuron to another happens through an interface called a synapse. A synapse is a physiological connection between the axon's terminal of a presynaptic neuron and dendrites of the postsynaptic neuron, forming a cleft. Small rounded swellings at the axon terminal release chemicals called neurotransmitters which ease the transmission of impulses through the synapse. As a result, nerve impulses are sent from the axon of one neuron to dendrites of another through synaptic junctions and the received signals by the dendrites are transmitted to the soma and carried away via the axon.

2.2.2 Action Potentials

Different concentrations of the ions and cations between two opposite sides of a neuron, known as intra-cellular and extra-cellular environments, result in a potential difference of about $-70\ mV$ to $-80\ mV$ across the membrane of the neuron at the rest state, known as the resting potential [11]. The concentration of sodium (Na^+) and chloride (Cl^-) ions are higher in the extra-cellular compared to the intra-cellular and the concentrations of potassium (K^+) ions are more in the intra-cellular; as a result of which the intra-cellular and extra-cellular gain negative and positive voltages, respectively. In the case of activation of a neuron by an action potential, the neurotransmitter will be released at the synaptic side of the presynaptic neuron [11]. On the other side of the synapsis, the postsynaptic neuron has many receptors on its membrane which are sensitive to the neurotransmitter. The released neurotransmitter in contact with the receptors changes the permeability of the membrane for charged ions and allows the potential of the postsynaptic neuron at rest to change.

Neurotransmitters can affect the postsynaptic membrane in two ways: excitatory or inhibitory. In the excitatory effect, the ion channels on the membrane are open and allow

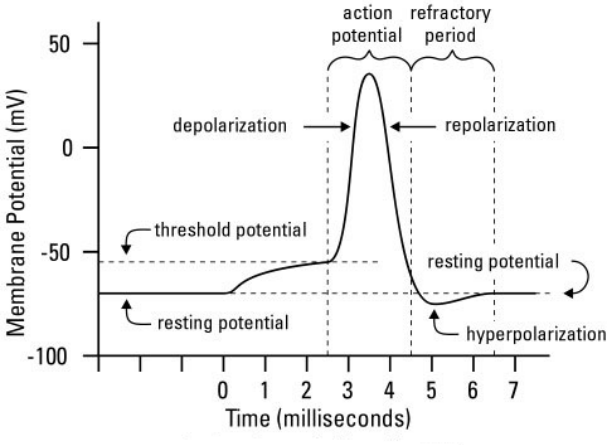

Figure 2.3: Changes of the membrane potential in a neuron, from [34].

the positively charged Na^+ ions to flow across the neuron. As a result, the potential of the intra-cellular becomes more positive than the extra-cellular. This is called depolarisation of the intra-cellular site or Excitatory-Post-Synaptic-Potential (EPSP) [11]. In consequence, the potential difference between extra- and intra-cellular is increased and reaches to about $-40\ mV$ (Figure 2.3). If the depolarisation is large enough to hit a given threshold (about 15 mV higher than the resting potential), the action potential is generated within the soma that stimulates all points along the axon to constitute the nerve impulse. In other words, the action potential moves rapidly along the axon and transmits the nerve impulse from one neuron to the next through the synapse. Therefore, for a very short time, the cross membrane potential difference is reversed (the intra-cellular is positive while the extra-cellular is negative). If neurotransmitters have an inhibitory effect, the ion channels are open and allow the positively charged K^+ ions to flow out to the extra-cellular site and carry a positive charge out of the postsynaptic neuron. This results in the repolarisation of the membrane; so that again the intra-cellular and extra-cellular potentials become negative and positive, respectively and the membrane resumes its previous polarisation (Figure 2.3). This effect is known as Inhibitory-Post-Synaptic-Potential (IPSP) and results in hyperpolarisation of the intra-cellular site such that the intra-cellular potential becomes more negative than the extra-cellular, until eventually the cross-membrane potential overshoots to nearly $-90\ mV$ [11]. After the sodium-potassium

exchange and the membrane overshooting, the membrane returns to its normal resting potential. For the next few milliseconds after an action potential, the membrane cannot be stimulated and undergo another action potential. This brief period of time is called the $refractory$ period of the membrane [11]. There are many synapses from different presynaptic neurons in contact with one postsynaptic neuron. So, all the EPSP and IPSP signals are summed up in the soma and the action potential is generated when a net depolarisation of the intra-cellular site at the soma reaches a certain threshold. The neuron fires, the action potential is generated and propagates along the axon, it arrives at the end of a presynaptic neuron and causes the release of the neurotransmitter into the synaptic cleft to reach the dendrites of the postsynaptic neuron.

2.3 EEG Generation

As mentioned previously, Electroencephalography (EEG) is the measurement of the electrical activity of the brain using electrodes placed on the scalp. The electrical activity of neurons comes from action potentials and Post-Synaptic-Potentials (PSPs). Action potentials are a rapid series of discrete voltage spikes that travel down from the beginning of the axon at the soma to the axon terminals where neurotransmitters are released. PSPs, on the other hand, are voltages that are restricted to the soma and dendrites and do not flow through the axon. They occur when neurotransmitters are in contact with receptors on the membrane of the postsynaptic neuron and the cross-membrane potential changes by the exchange of intra- and extra-cellular ions. However, although the amplitude of PSPs is smaller than action potentials, it is more likely that EEG recording reflects PSPs rather than action potentials due to their longer duration which makes it possible to detect and measure the integrated PSPs of neighbouring neurons on the scalp, unlike the action potentials.

Pyramidal neurons are special types of neurons that are suggested to be the main generators of EEG. These types of neurons have a triangular (pyramidal) shaped soma,

a single axon and long parallel dendrites (called apical dendrites) which are oriented orthogonally to the cortex [35]. The neighbouring pyramidal neurons in the cerebral cortex have parallel dendrite trees and orthogonal direction to the surface. Pyramidal neurons are polarised at the resting state, in the same way that was mentioned in section 2.2.1. By receiving an action potential at the axon terminals, the excitatory neurotransmitter is released in the cleft. The neurotransmitter in contact with apical dendrites causes a current flow into the neuron, due to the flow of positive ions in the cell membrane which depolarised the membrane potential at the soma. Consequently, by the outward flow of the positive ions, another current flows out of the membrane to keep the equilibrium, which makes the neuron a tiny dipole [7]. This current produces an electric field that extends to the scalp. The electric potentials generated by a single neuron is too small to be picked up by the electrodes on the scalp or they can be cancelled out by electrical activity of neighbouring neurons with opposite polarity. If thousands or millions of neurons in one or more cortical patches with similar synaptic stimuli (excitatory or inhibitory) align in the same direction and fire together, they can generate a measurable potential, of the order of μV, at the scalp [7]. A group of simultaneously active pyramidal neurons in a small patch of the cortex that produces potentials can be modelled as an equivalent dipole on macroscopic level [36].

2.4 EEG Recording

To record an EEG signal, a set of electrodes are placed over the scalp with the aid of a conductive gel in order to boost the scalp conductivity and to enhance the contact between the electrodes and the skin [37]; how many electrodes to use and where exactly to place them depends on the application. However, it is essential for any protocol to be viably reproducible in different laboratories to allow the comparison of results and also over time in the case of long-term monitoring studies. To make this possible, the $10-20$ system has been introduced by Jasper et al. [38]. The $10-20$ refers to the distance between

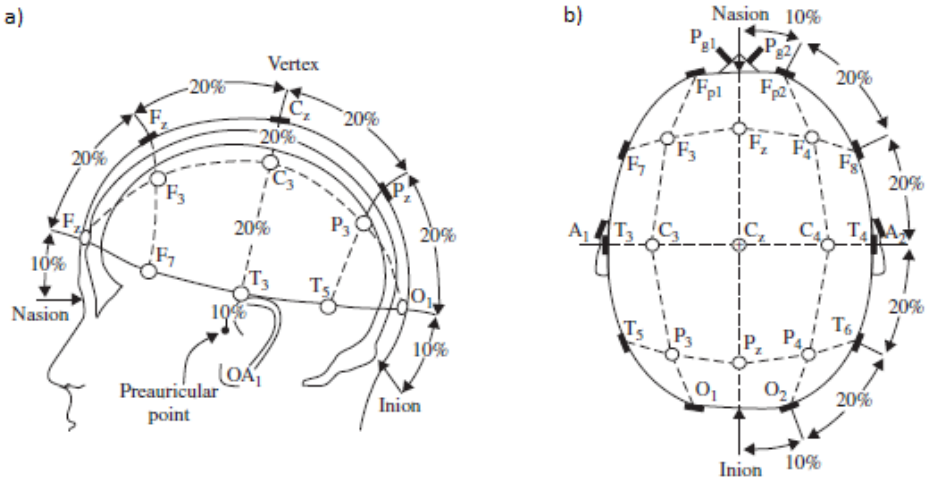

Figure 2.4: The 10-20 international electrode placement; a) and b) represent the three dimensional view of of the electrode placement on the scalp.

the electrodes as 10% or 20% of the distance between given anatomical landmarks. The electrodes are labelled by the initial of their corresponding lobe and their position is then labelled by an increasing odd (left) or even (right) number (Figure 2.4). The American EEG society has introduced an extended setup [11]. Some applications may use extra electrodes or only a subset of them.

As the potential is a differential quantity where its value in each point has to be measured with reference to another point, the same principle is used in EEG recordings; that is the potential difference needs to be measured between each electrode and a reference point. Therefore, EEG or potential difference measurements are not valid unless a reference point (electrode) is defined. A reference point can be assigned per electrode or it can be commonly assigned for all electrodes [37, 39]. The former is called *bipolarmontage* which represents measuring the potential difference between an adjacent pair of electrodes at each channel (a pair of electrodes usually make up a channel).

In the latter, each channel represents the potential difference between a certain electrode on the scalp and the assigned reference electrode (*referential montag*). The reference electrode is usually placed at a different position to the recording electrodes, like ear lobes. Also the reference can be the average of all the recording electrodes' signals (*average ref-*

erence montage). Furthermore, each channel can represent the difference between an electrode and a weighted average of the surrounding electrodes (*Laplacian montage*) [39].

The EEG is measured by placing electrodes on the scalp (non-invasive EEG) or on the cortex (invasive EEG) [7]. In the case of invasive EEG, because the microelectrodes are placed directly on the cortex and so are closer to the brain compared to the scalp electrodes, the amplitude of the signal is higher than scalp EEG and as a result, the signal is less contaminated by artefacts [40]. In non-invasive EEG, the electrical field produced by synchronous active pyramidal neurons are varied by their passage to the scalp and mixed linearly on the scalp [5]. The cerebral fluid, skull and the skin constitute a conductive medium. As mentioned previously, EEG sources inside the brain which generate potentials, can be considered as an equivalent dipole. When a dipole is placed inside the homogeneous conductive medium with infinite extent, the current flow in the medium and the generated potential measured at each point is proportional to the inverse of the squared distance between the dipole and the point of measurement. If the medium is inhomogeneous, in addition to the inverse square of the distance, a factor related to the conductivity of different materials will also be considered. The head conductive volume has different biological tissues with different conductivity [11]. The produced current by a dipole is conducted through the head volume among different brain tissues towards measurement sensors. Due to the variations in conductivity of brain tissues, the potential field will be distorted and attenuated. When the potential field reaches the scalp surface, the dispersion of the field occurs and they spread all over the head volume surface because of the lower conductivity of the scalp in comparison to other brain tissues. Therefore, the recorded far-field potentials that are conveyed by volume conduction to the scalp electrodes are relatively smooth and is mixed linearly at the recording site. This is called non-invasive EEG, which measures the mixed and smoother far-field potentials by using electrodes placed on the scalp [7,41]. Each channel (a recoding electrode and the reference) is connected to a differential amplifier (Figure 2.5); since the EEG signals have very weak amplitude, in the order of microvolts (μVs) and need to be amplified. Therefore, the

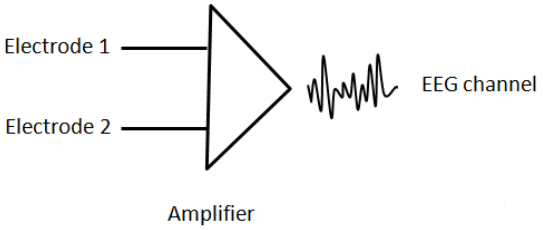

Figure 2.5: A differential amplifier of the EEG recording connected to each channel.

measured continuous analogue signal of each channel is then amplified and high-pass filtered (to reduce noise) through an analogue filter. The continuous analogue signal is then digitised and converted into a series of discrete samples by means of an analogue-to-digital converter to be stored in a computer for further analysis. The digitisation consists of sampling and quantization of the signal. The channels of the analogue signal are sampled at a fixed time interval (sampling interval) such that the sampling frequency must be at least twice the maximum frequency present in the signal to fulfil the Nyquist sampling theorem [42]. The sampling frequency determines the temporal resolution of the EEG and the voltage resolution is determined by the quantization step.

Once the data have been recorded, they are generally pre-processed in order to reduce the effect of artefacts and increase the signal to noise ratio without losing information [43]. Several steps are usually applied to the raw EEG, for further processing of the data, but the application of a particular method depends on the kind of data that is being processed, how noisy it is and what techniques will be used in the subsequent processing stages. Nonetheless, digital filtering and re-sampling of the recorded signal are two common initial stages in EEG data pre-processing.

The EEG signal is usually recorded at a high sampling rate (e.g. up to $20kHz$ for different research applications) which increases the required memory for storage in and decreases the speed of evaluation and computation. Therefore, the measured EEG is down-sampled to smaller frequencies to reduce the computational and storage costs. It is important to mention that it is essential to down-sample the data after filtering with

regards to the Nyquist sampling theorem.

Digital filtering is another stage in EEG data pre-processing to extract signals within a predefined frequency band of interest. Applying a filter to the data presupposes that the information carried by signals will be mostly preserved, to the benefit of attenuating other frequency components which are not desired. Normally EEG data is band-pass filtered to reduce the slow drifts and high frequency artefacts. It is also common to use a $50Hz$ or $60Hz$ notch filter to eliminate power line interference. Filtering is widely carried out by using Finite Impulse Response (FIR) or Infinite Impulse Response (IIR) linear filters [44]. IIR filters are usually more computationally efficient than FIR filters, but with the inconvenience of introducing non-linear frequency-dependent phase delays and hence some non-equal delays in the temporal domain at all frequencies; which is unacceptable for EEG signal analysis where timing and phase measurements are crucial. FIR filters delay signals in the time domain equally at all frequencies, which can be conveniently compensated for by applying the filter twice: once forward and once backward on the EEG time series [45]; which results in a zero-phase shift.

Electrical signals in the EEG that are originated from a non-cerebral origin are called artefacts. After the above pre-processing steps, removing the well-defined artefacts, such as eye movements and muscle activity, is often desired in EEG signal processing [19, 128]. At many points during the recording of the EEG data, the signal is likely to be contaminated by artefacts typically with the same amplitude as the desired brain signal or higher [11]. Artefacts are undesirable signals that may affect the signal of interest which can lead to misinterpretation of EEG analysis. It is, therefore, important to be able to identify common artefacts before interpreting the recorded signals. Artefacts can be divided into two categories [39, 46]: physiological and non-physiological. Physiological artefacts are generated by sources inside the subject itself, like those generated by eye movement (i.e. blink and saccade artefacts) and muscle movement. Non-physiological artefacts originate from sources outside the human body, which is the case in instrumentation artefacts. While transferring from the scalp electrodes to the recording device,

the EEG signal can be corrupted by the strong fields of alternating current (AC) power supplies. A significant rise in the impedance of an active electrode between the ground of the amplifier and the electrode causes the ground to act as an active electrode; which consequently produces the 50 Hz (in Europe) or 60 Hz (in the USA) mains artefact [11]. Moreover, electrode and equipment-related artefacts such as impedance change due to electrode displacement and may also compromise the quality of the data. In Chapter 4, the common artefacts in EEG data are discussed in detail; the intention is to detect and remove these from the data.

In addition to the above common pre-processing steps, there are a few more pre-processing stages such as segmenting the data into epochs and removing the baseline, which are discussed in Chapter 3.

2.5 EEG Artefact Removal

Artefacts can be handled by either avoidance, rejection or removal. To avoid artefacts, in many studies the subjects are instructed to suppress limb movement, eye movement and blinking. However, artefact occurrence is inevitable because movements and blinks can be involuntary, especially in children and elderly people [47, 48]. Several techniques have been proposed to remove artefacts from EEG recording to improve the signal-to-noise ratio(SNR). One of the basic approaches is the epoch-based method in which the whole temporal segments of EEG contaminated by artefacts are rejected. However this way, a large amount of useful cerebral information in the EEG is also discarded, especially when the artefacts occur frequently [12, 13].

To prevent losing whole EEG segments when removing artefacts, methods which remove them while preserving the underlying neural activity, are employed. Regression-based methods emerged in the time [49, 50] and frequency domains [51, 52] and are the most common type of artefact removal methods in EEG studies. They require additional reference noise channels (e.g. Electrooculography-EOG) so that the activity measured at

a reference channel is subtracted from the EEG channels. However, regression methods cannot be used to remove all artefact types. The fact is that a reliable reference channel for a specific type cannot always be realised due to the artefact source being spatially dispersed, e.g. power line noise and muscle movement. Another weakness of regression methods is that bidirectional contamination of brain signal and artefact sources, the same as removing whole temporal segments, will risk the removal of relevant neural information [53, 54].

An alternative successful artefact removal method is based on blind source separation (BSS) techniques that can recover the source signals from a mixture of multichannel EEG recordings. The process of estimating the source signals is without prior knowledge of the sources and their mixing process. As a result, the estimated sources may correspond to artefact or cerebral activities. Once the source signals associated to the artefact are detected and removed, the cleaned EEG data can be obtained.

Recently, methods based on the concept of BSS, have been widely employed in order to separate neural activity from different artefacts in spontaneous EEG data [37, 55–57].

The rest of this thesis concentrates on the BSS method and its principles. Among different BSS algorithms, the most widely used and effective algorithm, Independent Component Analysis (ICA) is described, with the aim of comparison (covered in Chapter 3) followed by the application of ICA to EEG.

2.6 Blind Source Separation

BSS was first initiated in 1982 from a discussion between neuroscientists Bernard Ans, Jeanny Herault and Christian Jutten with Jean-Pierre Roll about modelling the biological problem of motion decoding in muscle contraction [58] to separate sources corresponding to the angular position and velocity of a moving joint. In 1986 Jutten and Herault presented an algorithm to separate two mixed independent source signals based on neural networks [22, 59] (using the search method). In 1994, Comon formulated BSS and

introduced a BSS algorithm, Independent Component Analysis (ICA), based on minimisation of mutual information between the sources [60]. A year after, in 1995, Bell and Sejnowski proposed the Infomax ICA based on a maximum entropy approach [23]. This algorithm was further refined by Amari and his colleagues using the natural gradient [61,62]. The originally proposed algorithm by Bell and Sejnowski (1995) was only able to separate super-Gaussian sources. To overcome this limitation, Lee et al. [63] developed the Extended-Infomax algorithm which was able to simultaneously separate both sub- and super-Gaussian sources.

A few years later, Hyvärinen and Oja presented the fixed-point or FastICA algorithm [64], which has contributed to the application of ICA to large-scale problems due to its computational efficiency. Another recent algorithm has been proposed by Palmer et al. and is called the Adaptive Mixture of Independent Component Analysers (AMICA) [65], which is based on the modelling of each source component as a sum of extended Gaussians.

Up to now, a large number of ICA algorithms have been proposed which cover research areas such as EEG, speech and digital image processing [14]. However, in this thesis only the EEG signal and the application of ICA to EEG signal processing are considered.

2.6.1 Blind Source Separation Principles

Blind Source Separation (BSS) is a statistical approach to recover and estimate the source signals (components) from a set of observations. It assumes that the mixture signal is generated by uncorrelated sources. The BSS method has been developed for a so-called 'cocktail party problem' in which individual speech is found from mixtures recorded simultaneously by several microphones located at different positions in a room. The term blind refers to the fact that in the BBS approach very little is known about the nature of the source signals and the mixing process. In the concept of an EEG signal, a single scalp electrode records a mixture of signals from different sources in the brain when the individual sources of the mixed signal are desired [66]. The individual source signals can be obtained by the BSS approach in such a way that BSS tries to estimate the optimal

set of uncorrelated brain sources that best represent the measured signal, while little is known about their mixing process. BSS appears to be suitable for artefact rejection in which a subset of sources that generates artefacts is likely to be removed and the EEG is reconstructed by the remaining sources. A BSS model can be formulated as follows:

$$X(t) = A \times S(t) \tag{2.1}$$

Where $X(t)$ represents the observed mixed data matrix ($m \times n$); the EEG data matrix time course, with m and n equal to the number of sensors and sample points, respectively; A is the unknown mixing matrix of the dimension $m \times m$; $S(t)$ represents a $m \times n$ matrix of the time series of sources. Since the A and $S(t)$ are unknown, an assumption on the number of sources has been made, in addition to the un-correlation of the sources. The number of sources are considered to be known in such a way that it should not be more than the number of sensors. It can be equal or less than the number of scalp sensors. If it is assumed to be more than the number of sensors, the signal sources are under-determined and cannot be estimated by BSS due to the imperfect knowledge about sources and the mixing process [67, 68].

In order to estimate sources, the un-mixing matrix, $W = A^{-1}$ has to be estimated to recover the time series of sources in such a way that:

$$\hat{S}(t) = W \times X(t) \tag{2.2}$$

The un-mixing matrix W is also known as a topography matrix in which the columns represent the contribution of each source to the EEG data. When the estimated sources are recovered, the unwanted (i.e. noise) sources can be removed and the clean EEG data, $\hat{X(t)}$, can then be reconstructed by backprojecting the remaining set of sources. This can be done by using the new mixing matrix $\hat{A}$ which is obtained by setting the columns of

the corresponding unwanted sources in matrix A to zero:

$$\hat{X}(t) = \hat{A} \times S(t) \tag{2.3}$$

Several BSS algorithms have been developed which employ different assumptions to estimate the un-mixing matrix W and sources $S(t)$. In this research, one of the most widely used BBS-based algorithms, ICA, is selected and its principles are described next.

2.6.2 Independent Component Analysis

ICA is a BSS technique that employs higher order statistics to estimate the constitutive source signals of linearly mixed signals. The estimated sources by ICA are assumed to be statistically independent; which do not provide any information about each other [14]. Statistically, independent sources are uncorrelated; however, the reverse statement is not necessarily correct. For example, if X is a continuous random variable uniformly distributed on $[-1, 1]$ (i.e. $X \sim U(-1, 1)$) and $Y = X^2$, then X and Y are uncorrelated; however, they are not independent, as a particular value of Y can be produced by only one or two values of X. In EEG context, ICA assumes that the reading at each electrode is a linear mixture of independent physiological activities (independent sources); and it attempts to estimate the original sources corresponding to different physiological processes.

Prior to applying ICA to decompose EEG data, the ICA principles and assumptions [69], regarding the nature and characteristics of the EEG signal, are discussed in the following section:

Linear representation - ICA assumes that the observed data is generated from a linear combination of a number of independent sources. In the context of the EEG signal, the potential fields are linearly mixed on the scalp by the head conductive volume (section 2.4).

Instantaneous mixing model - The time delays that may occur in the mixing of the sources of the mixed signal are neglected by ICA. This is often called an instantaneous

mixing model. In EEG recording, there is a delay between the transmissions of the generated signal from the sources to the measurement sites on the scalp (i.e. electrode locations). The EEG electrodes are relatively close to each other and the propagation speed are relatively high compared to the signal frequency and sampling frequency. Therefore, it can be assumed that the source signals are measured at the same time as they have been emitted from the sources, which is called instantaneous EEG recording [11].

Spatial stationarity - The estimated sources by ICA are assumed to have spatially stationary location. This assumption is plausible for constitutive sources of EEG data, as the EEG sources are assumed to be generated from independent activities of neurons in a small number of spatially stationary brain networks (spatially-fixed cortical patches) which fire together and generate EEG potential [7].

Independence - The original sources should be statistically independent to be able to be estimated by ICA, which means that the sources do not contain any information about each other. Based on the Central Limit Theorem (CLT) [70], the distribution of the linear summation of a large enough number of independent random variables approaches a Gaussian distribution. The ICA method can be seen as the reverse process of the CLT with the assumption of independence and non-Gaussianity of the sources [60]. Aligned with this theorem, since the number of neurons is very large, the mean of all the EEG activity sources also tends to have Gaussian distribution. Neurons work like independent oscillators and can generate oscillatory potentials. These potentials are added together and can be detected and measured by electrodes on the scalp. The EEG signal is a mixture of both brain and non-brain sources. The EEG non-brain sources have non-Gaussian distribution; most of the non-brain sources have super-Gaussian distribution (i.e. blink and ECG sources) [71] and the main sub-Gaussian source in EEG is the 50 Hz power line signal [72]. The sources associated to the response of the stimuli and the epileptic spikes can be extracted by ICA due to their spiky activation pattern and non-Gaussian distribution. Thus, this assumption is plausible for EEG data to separate artefactual sources from the mixed EEG signal. Therefore, if S(t) from equation 2.1 is assumed to

be a set of independent sources, the observed mixed signal X(t) will be more Gaussian than each source from S(t), by the CLT. A single independent source is a linear mixture of X(t) given by the weights in the un-mixing matrix W. The process of finding the un-mixing matrix W is an optimisation process that maximizes the non-Gaussianity (with minimal Gaussian properties) of independent sources S, such that sources are maximally independent [73].

There are several ICA algorithms developed to estimate the optimised un-mixing matrix W, which employ different metrics to quantify the non-Gaussianity of the ICs.

The estimated source signals could be associated with either cerebral or artefactual activities. Despite source separation, ICA does not label the estimated sources. Usually, the estimated sources by ICA are labelled manually by visual inspection. Once the sources are labelled, the artefact-free EEG can be reconstructed by removing the artefactual sources from the data.

ICA Algorithms

In the previous section, it was highlighted that different ICA algorithms employ different criteria to maximise the non-Gaussianity of ICs. Nevertheless, two initial steps of centring and whitening (or sphering) are usually taken to simplify the ICA algorithms before estimating the un-mixing matrix W.

Centring: the mean of the observed signal X is subtracted from the signal itself. So the observed signal has zero mean by the centring process.

Whitening: whitening is a simple and standard procedure to reduce the complexity of the ICA problem by a linear change of the coordinate of the mixed data. Then applying ICA only means "rotating" this representation back to the original axis space. Thus one can say that whitening solves half of the problem of ICA. From a mathematical point of view, whitening is a linear transformation in which the components of the measured data X become uncorrelated and their variances are equal to one (unity). It can be obtained by linear transformation of data X by linearly multiplying it with a matrix V, so that the

new vector z is obtained which is the whitened data:

$$z = VX \tag{2.4}$$

Such a transformation may be estimated by Principle Component Analysis (PCA); the covariance matrix of the observed data is formed by taking the covariance between every point of the measured data X. The Eigen decomposition is performed. Therefore, the whitening matrix can be obtained in such a way that it transforms the covariance matrix into an identity matrix and the whitened data is achieved.

After the above two steps, the uncorrelated data with zero mean and unit variance undergoes further transformation by different ICA to estimate the sources as independently as possible.

All ICA algorithms are based on the same fundamental approach to find an un-mixing matrix W in such a way that the non-Gaussianity of sources $S(t)$ is maximised resulting in maximising the independence of $S(t)$. The process of finding W is an optimisation process to maximise the non-Gaussianity of the estimated sources. However, different criteria have been employed by different types of ICA algorithms to estimate sources as independently as possible [11]. The most commonly used ICA algorithms namely: AMICA, Infomax, Extended-Infomax and FastICA are considered in this research and are explained below.

The *FastICA* algorithm was introduced by A. Hyvarinen in 1999 [64]; it provides a fast iterative algorithm. It is based on the CLT and attempts to separate underlying sources from the given measurement set based on maximising their non-Gaussianity as a measure of statistical independence. FastICA uses this fact by building up a weight matrix column-by-column, where each column maximizes the non-Gaussianity of the corresponding component.

Non-Gaussianity can be measured by *kurtosis* or *negentropy* [74]. Kurtosis measures

the peakedness of a distribution. It can be calculated by:

$$kurt(y) = E\{y^4\} - 3E\{y^2\}^2 \tag{2.5}$$

where, $E\{\dots\}$ is the expectation operator. When y is normalised, its variance is equal to one, $E\{y^2\} = 1$; so, the kurtosis ($kurt(y)$) is simplified to $E\{y^4\} - 3$. (For a variable y with unit variance, $kurt(y) = E\{y^4\} - 3$, which is simply a normalised version of the fourth moment $E\{y^4\}$.)

If the kurtosis is zero the distribution is Gaussian. The distribution of all non-Gaussian variables have non-zero kurtosis; if it is positive, the distribution is super-Gaussian which is spikier than a Gaussian distribution and if it is negative, the distribution is sub-Gaussian which is flatter than Gaussian. Therefore, in ICA the absolute value or square of kurtosis can be used as a measure of non-Gaussianity. However, kurtosis is sensitive to the outliers in the dataset and is more influenced by values in the tails of the distribution, than in the centre of the distribution, which may be erroneous or irrelevant observations. Therefore it is not a robust measure of non-Gaussianity [75].

Negentropy (differential entropy) measures the distance from the Gaussian distribution. An important property of a Gaussian distribution is that it has maximum entropy among all distributions with the same variance. Therefore, non-Gaussian distributions have less entropy than Gaussian distribution and the more distance from Gaussianity yields more non-Gaussianity. Negentropy is defined as the difference between the entropy of a Gaussian random variable y_{gaussi} and the entropy of y:

$$J(y) = H(y_{gaussi}) - H(y) \tag{2.6}$$

where J is the differential entropy (negentropy) and H is the entropy of a distribution,

which is given by

$$H(y) = -\int f(y)\log(f(y))dy \tag{2.7}$$

where $f(y)$ is the density function of y. Negentropy is almost always greater than zero and is zero only if the signal is Gaussian. Because Gaussian random variables have the largest entropy, H among all random variables with the same variance [76], maximizing $J(y)$ leads to the separation of independent source signals.

The problem in using negentropy is that it is computationally difficult to calculate and requires estimation of the probability density function of the sources ($f(y)$). Several entropy approximations are introduced in the literature, which are beyond the scope of this research. In [77–79], there is an exhaustive list of entropy approximations in detail.

Infomax was developed by Bell and Sejnowski [23] to estimate the independent sources with super-Gaussian distributions [63], using the information-maximization principle. This ICA algorithm identifies the un-mixing matrix W in such a way that the joint entropy of the estimated sources is maximised; so that the mutual information among the sources is minimised, resulting in maximally independent and non-Gaussian sources. Mutual information measures the dependence of variables. It tells how much information a variable gives about the other. Mutual information is explored in more depth in Chapter 3 section 3.3.1.

Mutual information can also be thought of as a reduction in uncertainty about a variable. A high level of mutual information specifies a large reduction in uncertainty; while a low level of mutual information specifies a small reduction. Zero mutual information means the variables are independent. Mutual information is defined in terms of entropy which is a measure of uncertainty. The minimisation of entropy equals minimising the mutual information. Since non-Gaussians have less entropy than Gaussians, minimising the entropy, which results in minimising the mutual information, is equivalent to minimizing Gaussianity.

Extended-Infomax is an extension of the Infomax ICA algorithm that brings the ability of estimating sources with sub-Gaussian distributions to Infomax. It preserves the Infomax architecture, while considering both sub- and super-Gaussian distributions to estimate sources. Therefore, it may be slower than the original Infomax algorithm, which does not consider sources with sub-Gaussian distribution [80].

The *AMICA* algorithm was proposed by Palmer et al. [81]; that uses a generalised Gaussian scale mixture model [80, 82, 83] to flexibly model the density of each source signal as a sum of sub- or super-Gaussians. In order to estimate the independent sources, the non-Gaussianity of the sources is maximised by maximising the likelihood of the data; which is equivalent to mutual information minimisation used in the Infomax ICA algorithm [84]. This algorithm segments the data in an unsupervised manner by using an expectation maximisation (EM) algorithm [85, 86]. An EM algorithm is a statistical estimation to model the density of data based on maximisation of likelihood [84]. It has an adaptive approach in which the models in the mixture compete with each other to fit the data. This allows modelling of non-stationarity in the source structure by allowing different models to account for different time periods [65]. Similar to Extended-Infomax, AMICA is also able to estimate sources with both sub- and super-Gaussian distributions [87].

2.6.3 Application of ICA to EEG

ICA can be applied to EEG data to reveal the information associated to the brain activities which are hidden in the observed mixture of the EEG signal. In this manner, EEG can be decomposed into artefact and non-artefact sources. The artefact sources can then be detected either manually [88–91] or automatically [1,92] and removed from the data. Thus, the cleaned and artefact-free EEG can be reconstructed by backprojecting the remaining non-artefact sources [12, 93–97].

Another application of ICA to EEG concerns feature extraction [75], where the independent components estimated by ICA are used as a new representation of the data, from

which the meaningful features can be extracted from their time series and power spectra. ICA has been successfully employed to extract features for detection of Alzheimer's disease [98], epilepsy seizures [99] and epileptic spikes [100].

2.7 EEG Applications

EEG provides high temporal resolution in the range of milliseconds and low spatial resolution of a few centimetres, depending on the number of electrodes [11, 46]. As the EEG can provide a non-invasive measure of the brain activity with high temporal resolution, it has been widely used in different areas such as clinical and scientific research.

EEG waves have been extensively studied and analysed in recent years as a way of understanding brain activities and also as an objective approach to recording brain stimulation. EEG signals are composed of different oscillations, named rhythms [37]. The identification of specific rhythms or features in the EEG is a way to quantitatively diagnose brain disorders. In healthy subjects, brain activity in specific frequency bands is related to the state of consciousness or sleep. These frequency bands are called delta (δ), theta (θ), alpha (α), beta (β) and gamma (γ) -bands respectively. The δ-band (0.5-4 Hz) is associated with deep sleep; the θ-band (4-7.5 Hz) appears during the transition from consciousness to drowsiness and it is related to the level of arousal; the α-band (7.5-13 Hz), mainly visible in the occipital region, indicates a relaxed state of awareness without attention; the β-band (13-26 Hz) is a waking rhythm associated with attention and concentration; the γ-band (above 26 Hz) contributes to some brain diseases as well as to event-related synchronization. These rhythms are illustrated in Figure 2.6. Variations in the main EEG rhythms or abnormal patterns may be related to diseases, such as epilepsy or mental disorders.

Analysis of the evoked brain response to a specific stimulus is a common application of EEG which is known as Event-Related Potential (ERP) analysis. ERPs represent the electrical activity of the brain specifically associated to a given external stimulus. They are

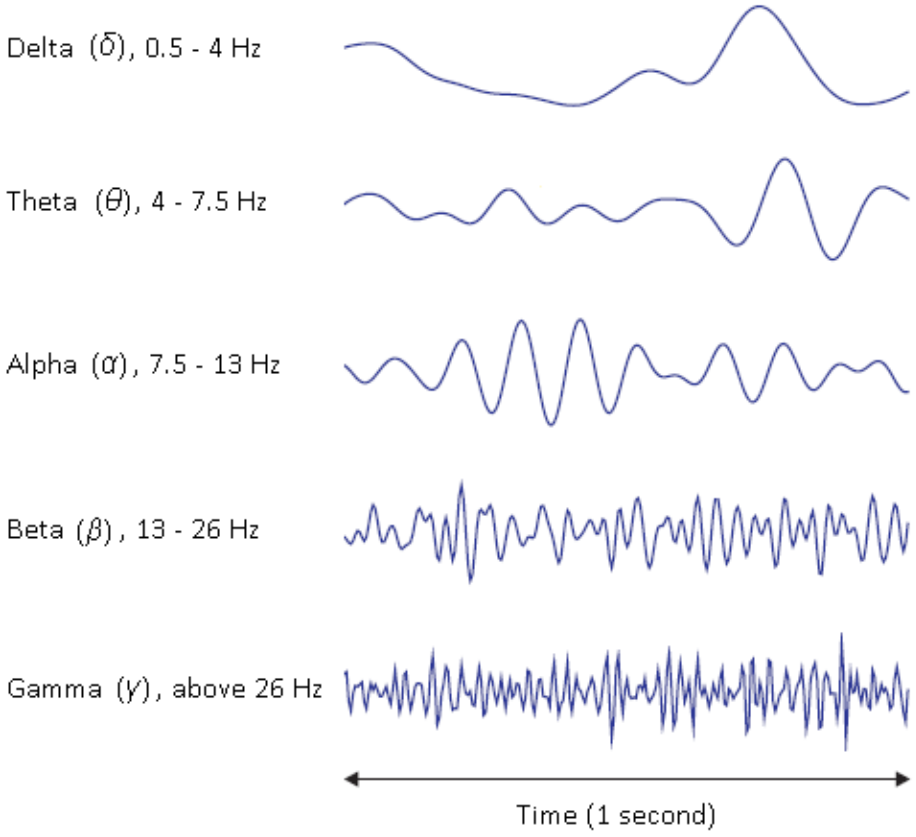

Figure 2.6: Illustration of the brain rhythms: delta (δ), theta (θ), alpha (α), beta (β) and gamma (γ), from [101].

commonly used in psychological or neurological sciences to probe cognitive functions [102]. A typical ERP experiment is shown in Figure 2.7.

In an ERP experiment, a subject is presented with stimuli that are related to the cognitive function of interest and the subject's EEG is recorded (Figure 2.7 (a)). A single response is called a trial (Figure 2.7 (b)). The amplitude of ERPs (10 μ V) is much smaller than EEG recordings (100 μ V). This activity is extracted from the EEG by synchronous averaging of single trials, triggered by the stimulus time. In this manner, background stochastic activity is averaged out while the event-related component is highlighted. The number of trials to be averaged depends on the original signal-to-noise ratio of the data and the ERP component of interest. However, it can be proved that the factor of improvement of the signal-to-noise ratio is equal to the square root of the number of trials over which averaging has happened. The single trials are obtained by segmenting the EEG around

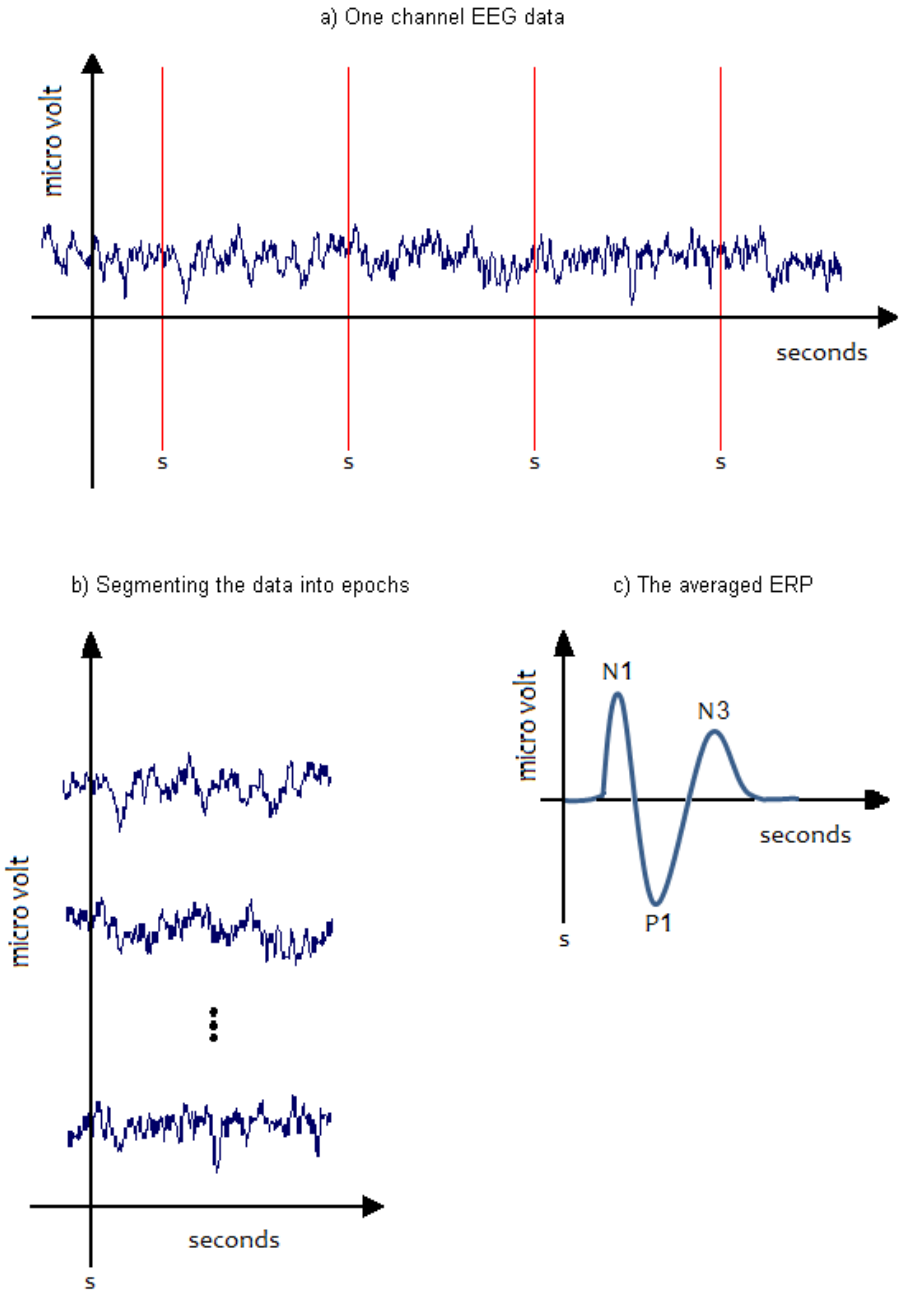

Figure 2.7: A typical ERP experiment; a) One channel EEG data recorded during the presentation of the stimulus (s); b) Segmenting the EEG data into epochs based on stimulus onset; c) Averaging the data epochs to obtain the averaged ERP.

the stimulus time, in a time window that depends on the process under investigation. The resulting average usually contains peaks and troughs, commonly called components, with respect to a baseline, i.e. brain electrical activity at rest (Figure 2.7 (c)). The trials are usually plotted with a negative voltage upward, by convention. The peaks are named

by a letter, N (negative) or P (positive), according to their polarity and a number that indicates a precise latency, in milliseconds, or the component's ordinal position. Due to the correspondence between a peak and a specific stage of the cognitive processes arisen by the stimulus, amplitude and latency of these peaks (i.e. the time interval between the stimulus onset and the peak) may provide convenient measures for tracking practical neuronal mechanisms. The absence of some peaks or significant changes in amplitude and latency with respect to a normal population may depict particular brain pathology or dysfunction. The ERPs, averaged separately for each condition present in the experiment, are then compared and tested for significant differences.

2.8 Summary

In this chapter the basic concepts of EEG generation and brain electrical activity were discussed, followed by the application of EEG data. Different artefact types can affect the quality of EEG data and make it difficult to be interpreted and analysed. Various methods, either artefact rejection or artefact removal methods, exist to remove artefacts from EEG data. The most recent successful EEG artefact removal method is the BSS-based method, ICA, which unlike artefact rejection methods can remove the artefacts while preserving the underlying neural activity. In this thesis, ICA algorithms are considered to be employed for EEG artefact removal; they are described in the following chapter.

"Seek Knowledge and adorn it with forbearance and dignity."

Imam Ja'far al-Sadiq (PBUH)

3

SYSTEMATIC COMPARISON OF ICA ALGORITHMS

3.1 Introduction

ICA has been widely used for the analysis of EEG data and separating the brain and non-brain sources (commonly known as artefacts) from the EEG mixture [14,23,103,104]. ICA estimates the independent components (ICs) by maximising their non-Gaussianity [73,105, 106]. Various ICA algorithms employ different metrics to quantify the non-Gaussianity of the ICs resulting in components that may differ across algorithms [11,104]. Consequently, the systematic evaluation of the ICA algorithm variants to find the best performing al-

gorithm for source separation, is an active topic of research. Some ICA algorithms have been compared based on the independence of estimated ICs in ocular artefact removal from EEG [107]. The performance of ICA algorithms in separating and removing different types of artefact such as EOG and ECG from EEG data has also been evaluated [96, 108, 109]. Delorme et al. [110] assessed the ability of ICA algorithms in separating the stereotyped artefact sources from brain sources using higher order statistics.

Ilavennila et al. [111] compared the quality of source separation based on the non-Gaussianity of estimated sources and the percentage of variance accounted for in the data among four ICA algorithms, along with their computational demands.

The effect of removing the linear trend of data epochs on the reliability of the estimated sources by ICA is also assessed by Groppe et al. [112]. Furthermore, the independence and physiological plausibility of the estimated sources by several types of ICA algorithms have recently been evaluated by Delorme et al. [104]. Korats et al. [113] compared the performance of ICA algorithms in terms of using different initialisation steps (whitening and sphering) of the ICs estimation and different lengths of data undergoing ICA decomposition. The performance of two ICA algorithms in effective EOG artefact separation and removal has also been compared by Kusumandari et al. [96].

However, the effect of various pre-processing steps on the output of different ICA algorithms has not yet received a great deal of attention [114]. As the initial step after recording the raw EEG data is to pre-process and prepare it for further analysis, it is crucial to select the data pre-processing chain and apply it to the raw data prior to ICA decomposition (pre-ICA processing).

In this chapter, the decomposition results of the most commonly applied ICA algorithms, namely AMICA, Extended-Infomax, Infomax and FastICA are compared. These ICA algorithms are most aligned with the purpose of this research which is separating artefactual components, such as eye artefacts, from EEG activities. Also, the effect of several pre-processing steps prior to ICA on the ICA source separation quality is assessed. In total, 24 EEG data pre-processing conditions have been examined and the independence

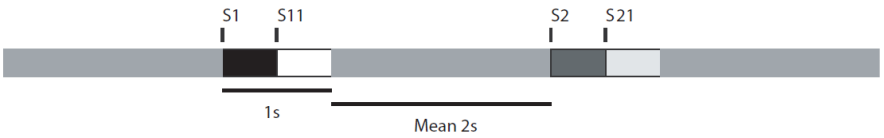

Figure 3.1: Experimental design of the visual stimulation.

and physiological plausibility of the recovered components have been assessed. The processing times of the best performing algorithm across different pre-processing conditions were also evaluated. Finally, the optimum pre-ICA processing chain and ICA algorithm variant for better source separation is reported.

3.2 Materials and Method

3.2.1 Data Acquisition and Pre-processing

EEG data recordings were obtained from ten healthy subjects who attended to a visual stimuli paradigm. As illustrated in Figure 3.1, each trial was started with a presentation of either high contrast (distinct) or low contrast (blurred) checkerboard ($t = 0$). After 500 ms ($t = 500ms$), the checkerboard was phase-reversed and was presented for another 500 ms. Usually, the repeated stimulus presentation on the fixed time intervals may lead to a decrease in the amplitude of subjects' brain responses recorded in the EEG - an effect known as habituation [115]. In order to avoid habituation, the inter-trial interval was randomised between $1.5 - 2.5$ s (mean 2 s). During each recording session, 100 high contrast ($S1$) and 100 low contrast ($S2$) stimuli were presented randomly over an approximate duration of 10 minutes. Each of 10 subjects attended at one session, resulted in collecting a total of 2000 trials (10 subjects $\times$ 200 trials). Subjects were asked to avoid moving their eyes and body as much as possible.

The data was collected using 64 channels (connected to a BrainAmp MR-Plus Amplifier, BrainProducts, Gilching, Germany) with current limiting safety resistors of $5k\Omega$ at the amplifier input and in each electrode. The EEG cap including 62 scalp electrodes

following the standard $10-20$ system [38] was used along with one EOG and one ECG electrodes, which were attached below the left eye and 2 cm below the left collarbone, respectively. The datasets were recorded at sampling rate of 5 kHz and the impedance at all recording electrodes was less than $20k\Omega$ [116].

It could be beneficial if there was the possibility of collecting different EEG datasets with more complex paradigms for the aim of this research. However, due to the lack of resources, we had to employ the described EEG dataset which is collected at the school of Psychology and shared with the Electronics department at the university of Birmingham.

As an initial pre-processing step, raw EEG data was first band-pass filtered at $0.016-100Hz$ [117]. The value of the low cut-off frequency of the filter is the same as the low cut-off frequency of the high-pass filter ($0.016Hz$) in the AC amplifier of the EEG equipment which filters out the DC components and non-neural potential (i.e. skin potentials) [118]. Thus, as the data was kept intact at this stage, the same low cut-off as the AC amplifier was chosen. Generally, EEG signals are not extended beyond $100Hz$ in normal EEG-analysis [119]. Therefore, the high cut-off frequency of $100Hz$ was selected for the band-pass filter. In the next step, the EEG data was down-sampled to $250Hz$ to reduce computational and storage cost. The sampling frequency of $250Hz$ was selected in order to fulfil the Nyquist theorem and to ensure the sampling rate is at least twice the highest frequency component [46, 120].

The beginning and end parts of the data that do not include any stimuli are removed. If electrodes are periodically noisy, it is not necessary to exclude them. This type of noise can originate from the gross movements of the subjects' body during EEG recording, which can bury the low amplitude signals of interest. Thus, the fragments of data which contain substantial noise with high frequency and high amplitude waves are intended to be deleted [1, 104]. This is done by segmenting the data into 500 ms windows and removing the fragments in which at least one of the channels exceeds the identified threshold ± 200 μV.

Before entering ICA decomposition, the pre-processed data undergo further processing

steps, which are a combination of the following [114]:

- ExG: the non-EEG channels (ECG and EOG) are included (*withExG*) or excluded (*w/o ExG*) from further analysis;
- FILTER: the EEG data are further band-pass filtered at $0.16 - 40$Hz (*Filtered (40HzBandwidth)*) or no additional filter is applied (*Not Filtered (100Hz Bandwidth)*);
- SEGMENTATION: the EEG data is segmented (*Epoched*) into epochs ($100ms$ before and $900ms$ after stimulus onset) or continuous data is used (*Continuous*) for ICA decomposition;
- EPOCH MEAN REMOVAL: in the case of epoched data, the mean values across the epoch are removed (*Mean Removal*) or not removed (*No Mean Removal*) before ICA decomposition. Based on the study performed by Groppe et al. [112], removing the epoch mean leads to more reliable sources, thus, it is recommended rather than removing the pre-stimulus baseline.
- BAD-CHANNEL REMOVAL: the bad-channels are removed from the data (*Bad-Channels Removal*) or not removed (*No Bad-Channels Removal*).

More discussion on each of these pre-processing steps is provided in the following sections.

Continuous and epoched EEG data

EEG data is collected continuously and can be analysed and processed as either continuous (Figure 3.2) or epoched data (Figure 3.3). Segmenting the signal into time-locked epochs to the stimulus onset is desired in studying the brain response to the presentation of a specific stimulus type [7]. Also, it has been reported that segmentation can divide the non-stationary EEG signal into pseudo-stationary segments [37, 121, 122].

A signal is non-stationary if the statistical characteristics of it change over time (in other words, if the signal is time-variant). Due to the fact that the state of the brain

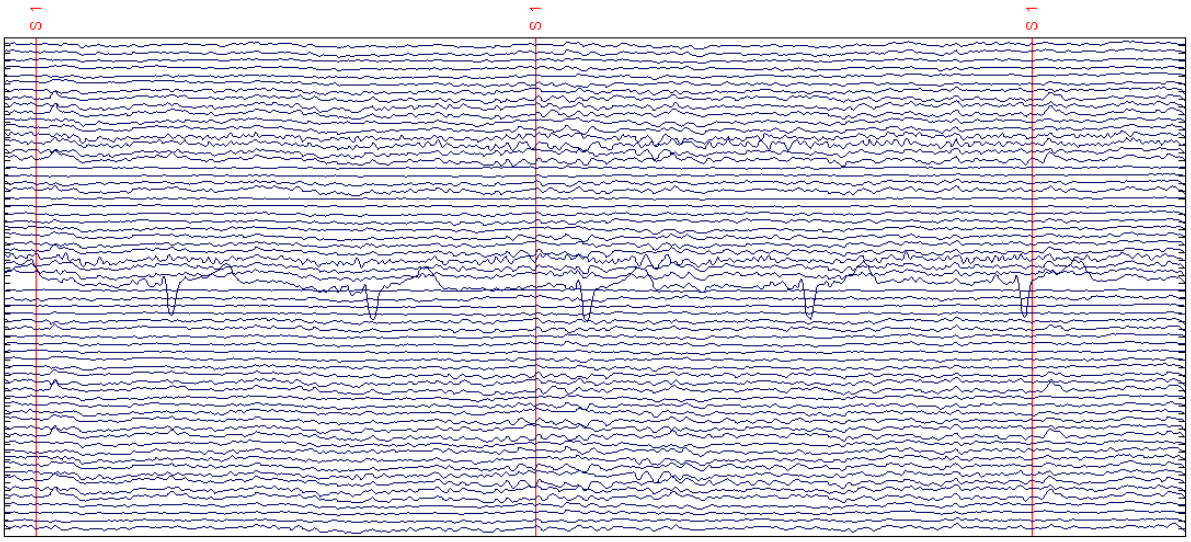

Figure 3.2: A sample of continuous EEG data; red lines depict the stimulus; $S1$ onset in the data.

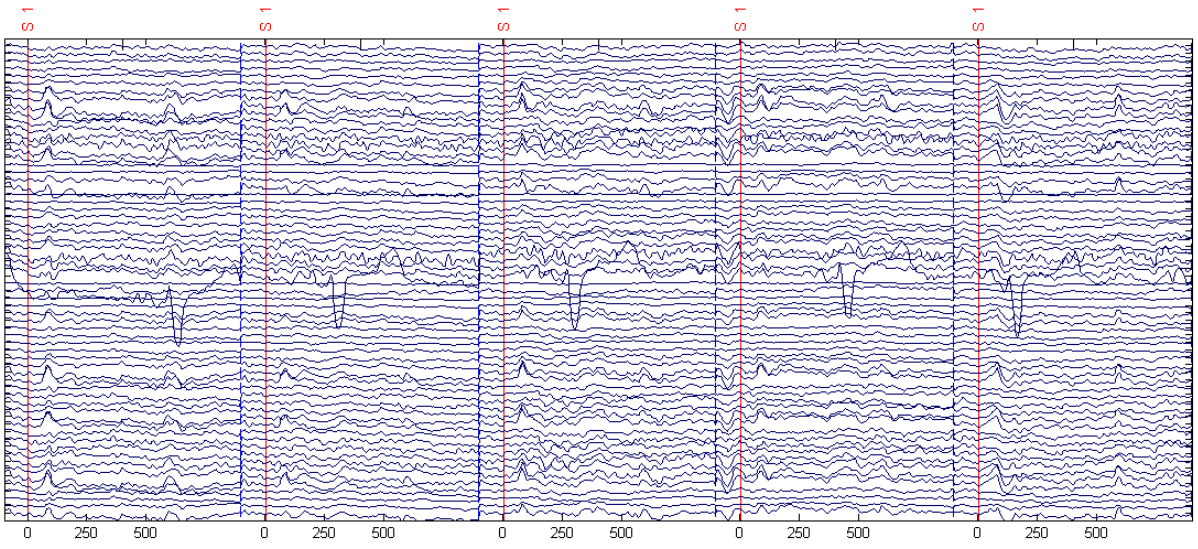

Figure 3.3: A sample of epoched EEG data based on stimulus onset $S1$.

varies over time, such as changes in the physiological state (e.g. different stages of sleep) or pathological changes (e.g. epileptic seizures), the multichannel EEG signals can also be considered as non-stationary. Since the scalp electrodes measure the mixed signal coming from different neurons, each transmits a signal with different intensity. Also, a single non-stationary source can make the whole mixed signal appear non-stationary even if the rest of the sources are stationary [123]. However, the EEG signal can be assumed to be stationary only within short intervals of time. This assumption holds during a normal

brain condition in which the subject is in a particular state [124].

Therefore, EEG signal segmentation into epochs is suggested as a pre-processing step that can improve the non-stationarity of the EEG signal and reduce the noise [125–128], while resulting in some data sample points loss. The process of selecting specific time intervals of EEG data time-locked to the stimulus and discarding all other samples is called epoching (segmenting). Normally, the time interval of the epochs starts from tens of milliseconds before and hundreds of milliseconds after stimulus onset, respectively. The pre-stimulus and post-stimulus intervals are selected in such a way that the baseline (i.e. resting) EEG and the brain response to the stimulus are captured, respectively.

In contrast, the continuous EEG data could be of interest, rather than the epoched data, in order to prevent information loss, especially in clinical environments and for monitoring epileptic seizures [129–134].

In this research, the effect of both continuous and epoched EEG data on the ICA decomposition are analysed. The epoched data is obtained by segmenting the continuous EEG data from $100ms$ before to $900ms$ after stimulus onset.

Baseline Correction

In the case of the epoched data, there could be baseline level differences between the data epochs. The presence of the baseline (DC) level differences in the data could lead to misinterpretation in EEG data analysis. Baseline correction is another option in the pre-processing steps which removes the DC component due to overall voltage offset from the waveform in each epoch. Therefore, it would be beneficial to have a time interval where there is no obvious stimulus-related brain activity (pre-stimulus interval); and any shifts from the baseline can be assumed as artefact contamination in the data. There are two major baseline correction methods for each epoch in every EEG channel:

- subtracting the mean signal over pre-stimulus interval, from the signal at all time points [135, 136].

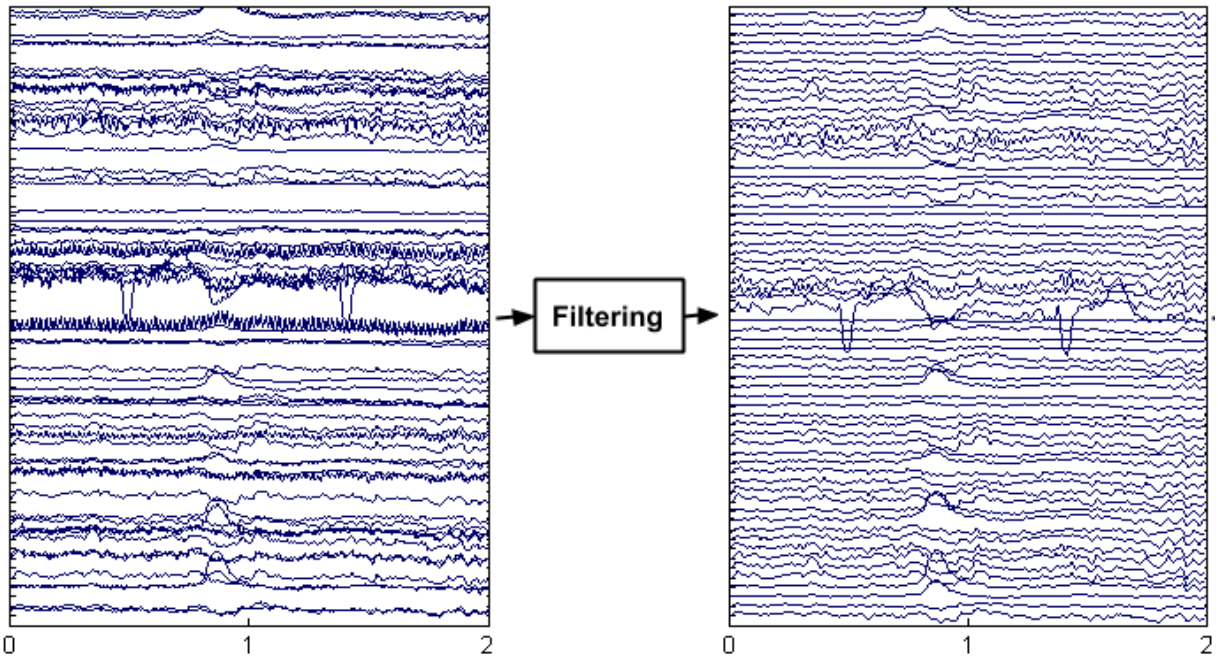

Figure 3.4: Not filtered EEG data (left) versus band-pass filtered EEG data with high cut-off frequency of $40Hz$ (right).

- subtracting the mean signal over the whole epoch interval, from the signal at all time points.

The latter method is used in this study for baseline correction, since Groppe et al. [112] demonstrated that removing the whole epoch mean rather than the pre-stimulus mean, before ICA decomposition, leads to less data discontinuity. Thus it considerably improves the reliability of ICA decomposition by blocking the generation of high amplitude and high frequency noise. The effect of both baseline corrected epoched data and no-baseline corrected epoched data on the ICA decomposition is evaluated.

Filtering

Normally EEG data is band-pass filtered to reduce the slow drifts and high frequency artefacts (Figure 3.4). Commonly, the EEG activities below $40Hz$ are used in clinical applications and EEG/ERP studies [1, 92, 137, 138]. Additionally, in order to analyse the brain function during mental and motor activities, a high cut-off frequency up to $100Hz$ is used for EEG band-pass filtering [139–142]. In this experiment, two band-pass filters

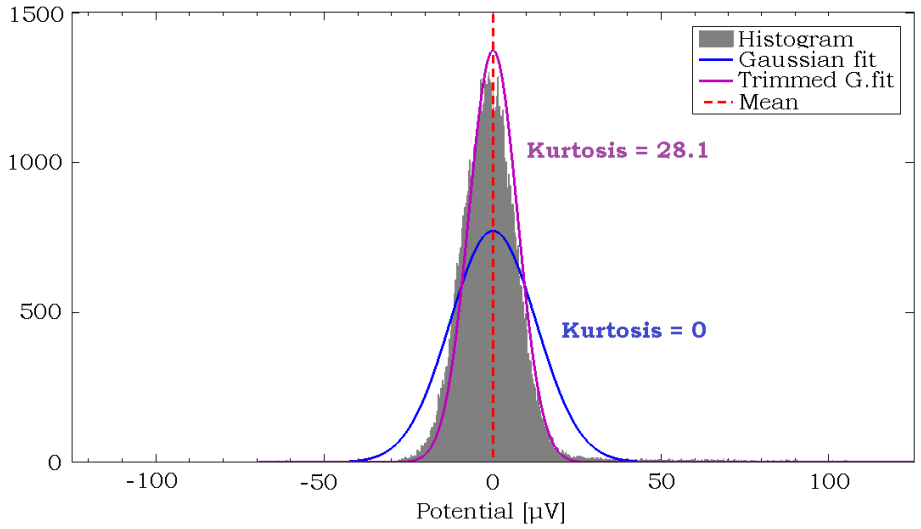

Figure 3.5: A sample of potential distribution of an EEG bad channel and a fitted normal distribution. The kurtosis value of the bad channel is also provided with respect to the kurtosis of normal distribution which is zero.

of 100 order Hamming-window based linear-phase FIR filters with a passband frequency of $0.16Hz$ to $40Hz$ and $100Hz$ are used for filtering out the undesired frequencies.

Bad channel removal

Multi-channel EEG data often have some channels known as *bad-channels* (i.e. channels with low SNR). Bad-channels can result from a poor connection between electrodes and the scalp and usually are characterised with: higher variability than other channels in time and a stronger deviation from a Gaussian distribution (Figure 3.5). They can be identified by the outlying values of their statistics (e.g. kurtosis) relative to the normal distribution. Since the EEG mixtures typically have near zero kurtosis values [143], the electrodes at which the resulting potential values exceed a pre-defined value (e.g. kurtosis value more than 5 [144–147]) are considered as bad channels (Figure 3.6) and are removed from the data. Although the kurtosis is known to be sensitive to outliers, bad-channel removal is done on EEG channels (not ECG and EOG channels) after slight cleaning of the data by removing the gross movements. Therefore, the effect of outliers on the kurtosis can be reduced.

Several researchers recommend removing bad-channels prior to ICA [143, 148–151],

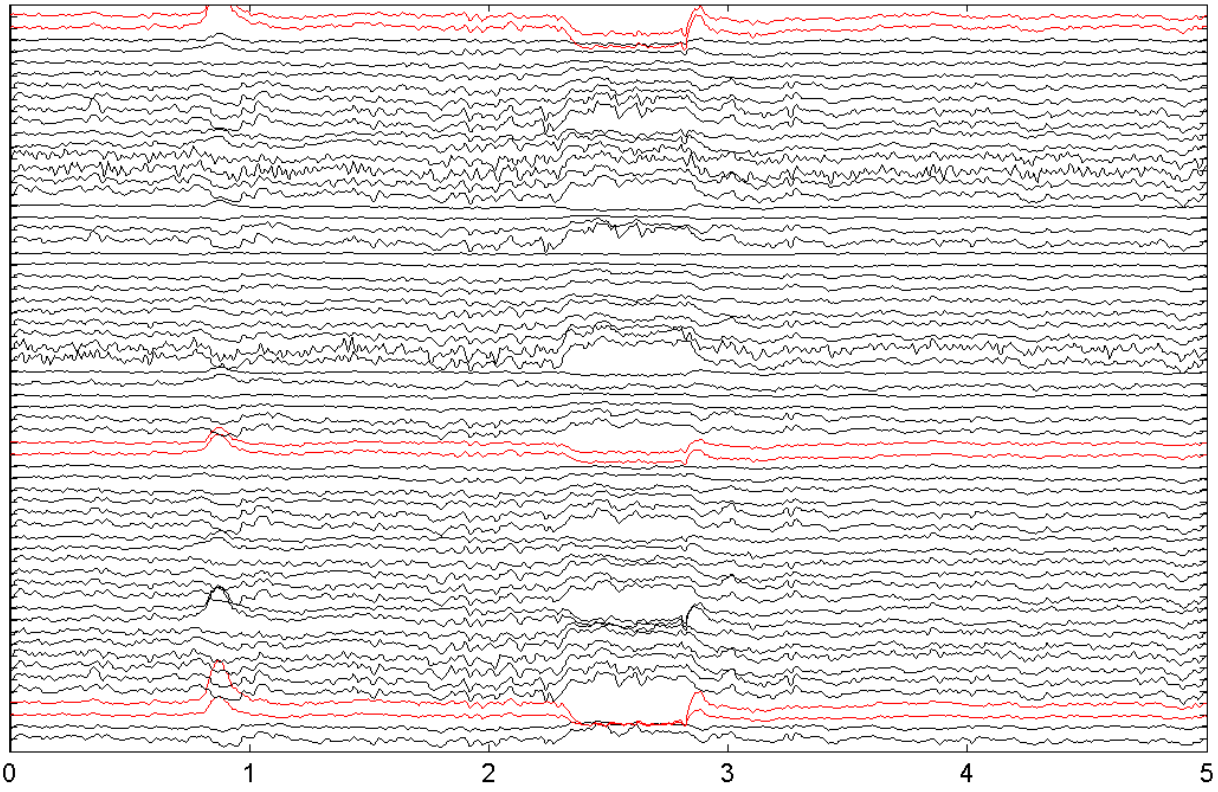

Figure 3.6: Marked bad channels in the EEG data whose kurtosis value exceeds the threshold.

because ICA decomposition might be biased by bad-channels leading to a reduction in degrees of freedom assigned to decomposition of other source signals such as cerebral activities. However, ICA can be applied to EEG data without bad-channel removal to separate brain and non-brain sources [12, 104, 152, 153]. In this study, both cases in which bad channels are excluded and included for ICA decomposition are considered.

Excluding EOG and ECG

Some studies suggest that heart rate variability and eye movements have a relationship with cognition [154–157]. Therefore, in some EEG recording setups, extra EOG and ECG channels are available parallel to the EEG in order to measure the electrical potentials produced by eye movements and heartbeats, respectively. However, EOG and ECG channels are not always included in ICA decomposition along with EEG scalp channels. Some researchers state that including the EOG and ECG channels for ICA decomposition is

not necessary for isolating the eye and heartbeat activities due to their independence from the brain activities [158–161]. In contrast, EOG and ECG channels are suggested to be included in the ICA decomposition to improve the identification and separation of eye-related and ECG artefacts due to the extra information provided by these additional channels [162–167]. Thus, both the inclusion and exclusion of EOG and ECG channels in ICA decomposition will be assessed.

The combination of the above 5 pre-processing steps resulted in a total of 24 different pre-processing categories (conditions). The hierarchy in Figure 3.8 (a) illustrates the obtained pre-processing conditions. Each condition was individually applied to the data of a single subject described in section 3.2.1 and resulted in 240 different pre-processed datasets (i.e. 10 subjects $\times$ 24 conditions). Consequently, the four ICA algorithms were applied to all 240 pre-processed datasets. In the first 12 pre-processing conditions, where the bad channels are not removed, each dataset was decomposed into either 62 or 64 independent components by ICA depending on the existence or non-existence of the EOG and ECG channels in the data. However, using the pre-processing conditions of $C13$ to $C24$, the datasets were decomposed into fewer independent components compared to the first 12 pre-processing conditions as the number of channels are reduced by removing the bad channels from the data. In total, 37284 independent components were obtained by applying the four pre-selected ICA algorithms to all 240 pre-processed datasets.

3.3 ICA Performance Evaluation

ICA algorithm variants are assessed based on two criteria - the independence, and physiological plausibility of the estimated ICs. To assess independence, Mutual Information Reduction (MIR) and Pairwise Mutual Information (PMI) are considered [104]. MIR measures the total amount of Mutual Information (MI) reduced in the data when EEG channels are decomposed into ICs. PMI considers the pairwise dependencies between ICs' time series and measures the amount of information that each IC gives about the other

ICs. The larger MIR and lower PMI values specify the desirable higher independence of the estimated sources.

To assess physiological plausibility, sources are assumed to have dipolar behaviour in the far-field at the scalp electrodes' distance. Dipolarity is measured by fitting a dipole for each IC using the method proposed by Delorme et al. [104]. The higher the numbers of ICs that can be fitted by a dipole, the more biologically plausible the ICs are.

One can use simulated data to evaluate the performance of ICA algorithms and to find out how well the known original sources (based on the ground truth) are estimated by the different algorithms. However, the ultimate goal of this study is to assess the performance of ICA algorithms in separating independent sources which correspond to sources mostly from biological origins, when ICA is applied to real data (in which there is no ground truth). Therefore, the described evaluation measures are selected in such a way that the performance of ICA algorithms can be measured based on independence and at the same time, physiological plausibility of the ICA decompositions, when ICA is applied to real data.

3.3.1 Independence of Sources

As described in section 2.6.2, one of the ICA assumptions on the times series of components extracted from the mixed EEG signal is statistical independence of those components. Two mutual information-based measures of MIR and PMI proposed by Delorme et al. [104], are considered to assess the independence of the estimated EEG sources for each type of ICA algorithm.

Mutual Information Reduction

Mutual Information (MI) is a measure of independence of random variables and determines how much information one random variable provides about another. It is a non-negative quantity and is equal to zero if variables are independent [14]. It can be considered as the reduction in uncertainty of one random variable based on knowledge of another. Higher MI

reduction indicates a large reduction in uncertainty, whereas lower MI reduction implies a small reduction in uncertainty. The mutual information between two random variables X and Y is defined as the difference between the sum of individual (marginal) entropies of X and Y, taking away the joint entropy of X and Y [106]:

$$I(X;Y) = h(X) + h(Y) - h(X,Y) \tag{3.1}$$

Correspondingly, the mutual information between components of random vector $Y = [y_1; y_2; ...; y_n]$ is defined as:

$$I(y_1; y_2; ...; y_n) = h(y_1) + h(y_2) + ... - h(Y) \tag{3.2}$$

As discussed in section 2.6.2, MI has been used as a criterion for ICA transformations that involves estimating the un-mixing matrix, W, such that the mutual information of the transformed components, Y, is minimised.

$$Y(t) = W \times X(t) \tag{3.3}$$

where $X(t)$ is the data matrix; W is an un-mixing matrix; and $Y(t)$ is the ICA component activation time series.

The entropy of the continuous vector variable Y is given by [104]:

$$h(Y) = log|detW| + h(X) \tag{3.4}$$

So the mutual information of the transformed data $I(Y(t))$ is defined by:

$$\begin{aligned} I(Y) &= h(y_1) + h(y_2) + ... + h(y_n) - h(Y) \\ &= h(y_1) + h(y_2) + ... + h(y_n) - log|detW| - h(X) \end{aligned} \tag{3.5}$$

where, $h(X)$ is the joint entropy of data X and is independent of W. The mutual

information of the data matrix $X(t)$ is the same as mutual information of the transformed data $Y(t)$ minus the term including the determinant of W:

$$I(X) = h(x_1) + h(x_2) + ... + h(x_n) - h(X) \tag{3.6}$$

To compare the results of ICA decompositions, the total reduction of mutual information (MIR) when moving from the sensor space (EEG channels) to the source space (ICs) is calculated. The reduction in mutual information is defined by:

$$\begin{aligned} MIR =& I(X) - I(Y) = h(x_1) + h(x_2) + ... + h(x_n) - h(X) \\ & - [h(y_1) + h(y_2) + ... + h(y_n) - log|detW| - h(X)] \\ =& h(x_1) + h(x_2) + ... + h(x_n) - [h(y_1) + h(y_2) + ...+ \\ & h(y_n)] + log|detW| \end{aligned} \tag{3.7}$$

MIR measures the total amount of Mutual Information (MI) reduced in the data when EEG channels are decomposed into ICs. A larger MIR indicates a greater reduction of statistical dependencies between EEG channels and therefore higher independence of the components.

Pair-wise Mutual Information

According to the ICA principals, the estimated sources by ICA are assumed to be statistically mutually independent. It is also known that minimisation of mutual information can be interpreted as maximisation of independence of the components. Therefore, Pair-wise Mutual Information (PMI) between estimated sources by each algorithm can be used as the criterion for assessing the performance of different ICA algorithms. PMI measures the amount of mutual information between each pair of the estimated components' time series (resulting from different ICA algorithms). It considers only the pair-wise dependencies by estimating two dimensional joint densities. The PMI value is always non-negative (unless bias correction is applied) and it is zero only if the variables are independent. In fact,

the highest value of PMI represents more dependencies between the estimated sources by each ICA algorithm.

PMI can be considered as a portion of MIR measurement that considers multicomponent dependencies. Actually, MIR measures the overall mutual information reduced from the set of recorded data channels after applying ICA. Since the components are assumed to be more independent than channels, a big reduction in overall mutual information by applying ICA may result in more independent sources. However, PMI measures the amount of independence of the source pairs and does not include higher order dependence. Therefore, the amount of information each component gives about the others can be obtained using PMI. This information should be zero if components are really independent. However, practically it is not zero but very close to zero; that means the brain and non-brain sources are not perfectly independent. Nevertheless, the lowest PMI value should be better, since it identifies less dependence between the components.

The PMI between two random variables x_i and x_j is defined as a difference between the sum of the individual entropies and the joint entropy of x_i and x_j.

$$[M]_{ij} = I(x_j; x_j) = h(x_i) + h(x_j) - h(x_i, x_j) \tag{3.8}$$

M is a square matrix in which the diagonal values represent the PMI between one source and itself and the off-diagonal values represent the PMI between each source and other sources. Thus, the average of the off-diagonal values in matrix M is calculated as the total PMI between component time courses. The result is reported as an average across subjects for each ICA algorithm. The lower the PMI, the more independent the components. The MI estimation can be inflated by an expected amount, known as bias, which could result in a negative MI value after bias correction (i.e. subtracting the bias value) [168]. In this study, the mutual information for both MIR and PMI estimates is bias-corrected.

3.3.2 Biological Plausibility

The sources estimated by ICA are supposed to be biologically plausible, in addition to being independent. As mentioned in section 2.3, a neuron has a fixed location in the brain and the average of a group of neurons in a small cortical patch can be modelled as an equivalent dipole. The potentials generated by equivalent dipoles are summed linearly on the surface of the head volume conduction. Thus, EEG sources estimated by ICA are expected to be spatially localized and appear dipolar in the far-field at the scalp electrodes' distance.

The estimated sources by ICA are assumed to be temporally independent; that means their scalp maps each should represent only one dipole when it is backprojected to the scalp. The better the dipole fit the less spurious the activity in the component map.

Delorme et al. [104] suggested that dipolarity of ICA decompositions can be assessed by calculating the percentage the returned components that best fit with a single dipole to the scalp with less than 5% residual variance. The spherical four-shell model head is used to localise a best-fitting single equivalent dipole for each component. This involves scanning possible positions and orientations of the dipoles in a 3D grid. Then, an optimisation algorithm is performed to obtain the best position and orientation of a single dipole, which most resembles the observed scalp distribution of a component with a lower amount of residual variance.

In the dipole fitting procedure, the EOG and ECG channels are excluded, as they have non-brain source originations that represent the activity of the eye and heart outside of the brain volume conductor. Delorem et al. [104] demonstrated that, with more independent components, more dipoles can be obtained. Figure 3.7 shows exemplar scalp maps for four components which are estimated by AMICA with the percent of residual variance from the projection of the best-fitting equivalent dipole.

Equivalent dipole modelling

Different source localisation and dipole fitting algorithms exist in the literature [169–

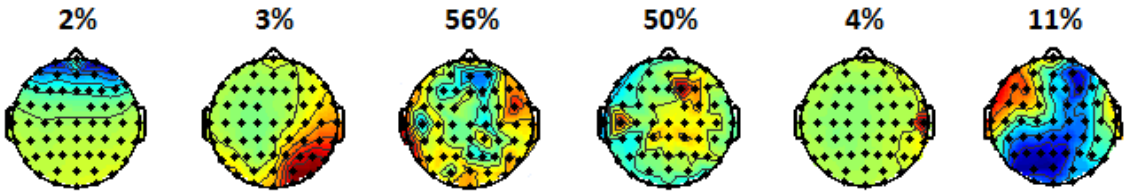

Figure 3.7: Example of component scalp maps resembling the equivalent current dipole, the percentages of residual variance are presented for each IC scalp map.

171]. In this research the state-of-the-art DIPFIT algorithm [172] is employed, as suggested in [104]. For each ICA decomposition of each subject within each pre-processing condition, a best-fitting single equivalent dipole, corresponding to each returned component, is localised using a single equivalent dipole in a best-fitting spherical four-shell model head using the DIPFIT plug-in (version 1.02) in the EEGLAB toolbox (version 4.515) [172]. The DIPFIT plug-in performs source localization by fitting an equivalent current dipole model using a non-linear optimization technique, proposed by Scherg et al. [173] using a 4-shell spherical model described by Kavanagk et al. [174]. The bilateral contribution of ICs is neglected in equivalent dipole fitting.

3.3.3 Statistical Analysis

In order to compare the performances of different ICA algorithms and evaluate the effect of various data pre-processing steps on their performance, a repeated measure analysis of variance (ANOVA) is employed [175].

For each evaluation measure (i.e. MIR, PMI or Dipolarity), a repeated measure ANOVA with within-subject factors of *ICA algorithm* with 4 levels (AMICA/Extended-Infomax/Infomax/fastICA); *bad-channel removal* and *filtering* with 2 levels each (applied/not applied); *segmentation* with 3 levels (continuous/epoched with mean-removal/ epoched with no-mean-removal); and *including ExG* with 2 levels (included/not included) is performed, separately. So the overall ANOVA design for each evaluation measure has 96 within-subject measurements (i.e. $4 \times 2 \times 2 \times 3 \times 2$) for N=10 subjects. The level selected to indicate the statistical significance was at $p < 0.05$. Pairwise comparisons with

Bonferroni correction [176] were performed to find the main factor effects. The outcomes of the ANOVA are reported in terms of p-value, F-value and partial effect size (η^2). The results of the pairwise comparisons are reported in terms of mean difference, standard error (std. error) and p-value. All the statistical analyses were carried out with IBM SPSS Statistics [177].

3.4 Result Analysis

The performance of ICA the algorithms through different pre-processing conditions is evaluated and compared in terms of MIR, PMI and dipolarity of the estimated sources (Figure 3.8). Additionally, the effect of pre-processing conditions on the processing time of the best performing ICA algorithm for source separation is assessed (Figure 3.9).

3.4.1 Pre-processing Conditions, Independence and Dipolarity of Sources

Figure 3.8 illustrates the effect of different pre-processing steps applied to the raw data, on the performance of different ICA algorithms in terms of MIR, PMI and dipolarity; the larger the MIR and dipolarity, and the lower the PMI, the better the ICA decompositions. The repeated measure ANOVA revealed that the effect of the ICA algorithm factor is statistically significant in terms of all the three measures (i.e. MIR [F (3, 27) = 354.402, $p < 0.001$, $\eta^2 = 0.975$]; PMI [F (3, 27) = 73.546, $p < 0.001$, $\eta^2 = 0.891$]; and dipolarity [F (3, 27) = 34.493, $p < 0.001$, $\eta^2 = 0.793$]). The pairwise post test showed that there is a significant difference between the performance of all the pairs of the ICA algorithms for all three evaluation measures, except pair of Infomax and Extended-Infomax ($p = 1$) dipolarity. Also, the difference between the performance of Infomax and FastICA for PMI is marginally significant ($p = 0.052$); the PMI value for Infomax is larger than fastICA (mean difference = 0.006, std. error = 0.002). According to the pairwise comparison, AMICA performed significantly better than the other three algorithms in terms of MIR

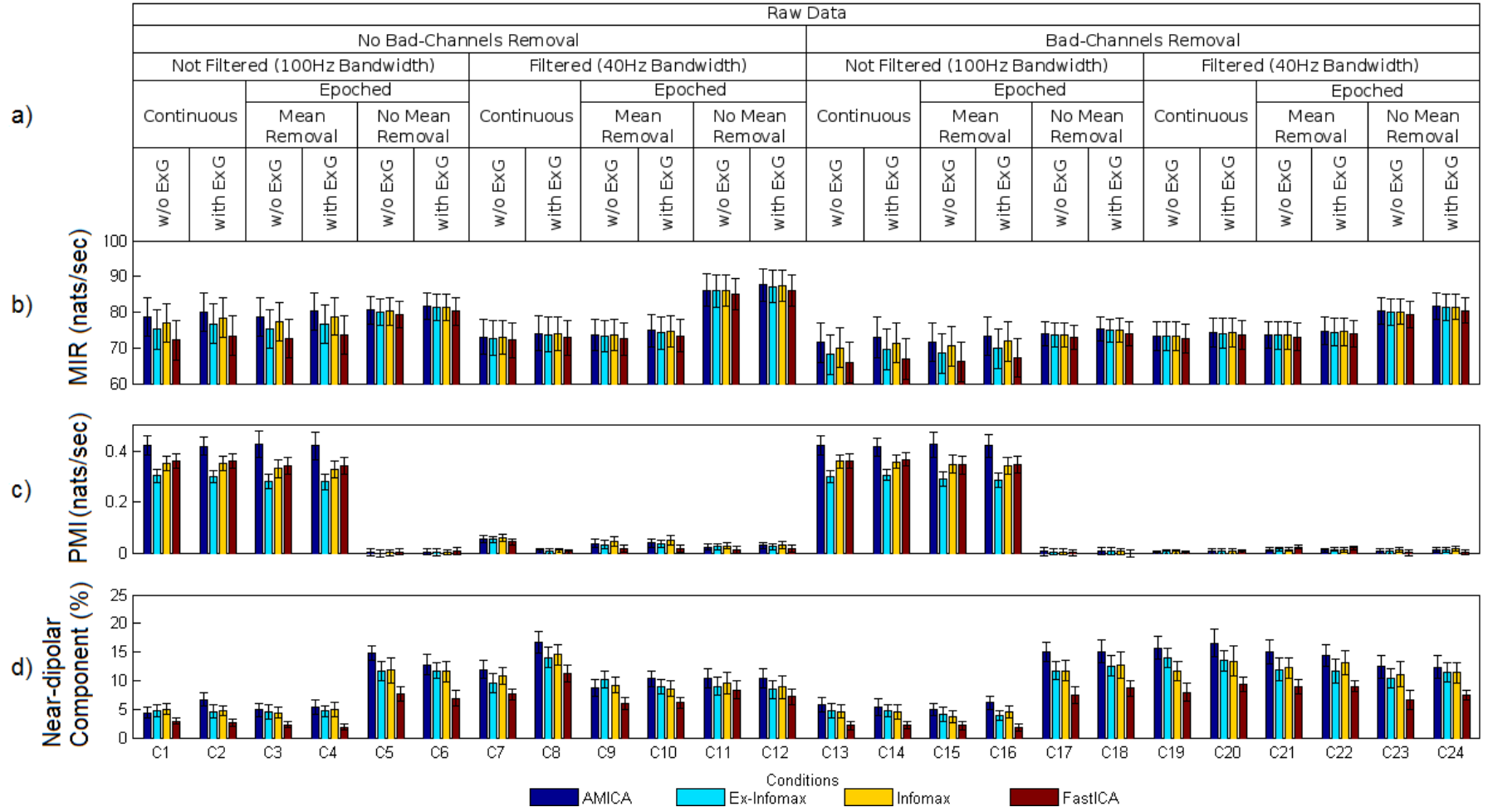

Figure 3.8: The pre-processing hierarchy of the raw EEG data and the performance of ICA algorithms based on MIR, PMI and dipolarity: a) Different types of EEG data pre-processing before running ICA algorithms. The corresponding pre-processing category of each mini bar chart is defined column-wise towards a branch of the hierarchy at the top of the figure (i.e. C5: No-Bad-Channel-Removal\Not-Filtered\Epoched\Mean-Removal\ExG). The mean and standard errors of MIR, PMI and Dipolar sources for each ICA algorithm that were applied on all types of the defined pre-processed data are shown in panels b), c) and d), respectively [114]. The larger the MIR and dipolarity, and the lower the PMI, the better the ICA decompositions.

and dipolarity, while significantly better performance in terms of PMI is obtained by Extended-Infomax. Tables A.1, A.2 and A.3 in Appendix A shows the results of the pairwise comparisons between pairs of ICA algorithms for MIR, PMI and dipolarity, respectively.

When considering the pre-processing factors, removing the bad channels significantly impacts on MIR and dipolarity. The MIR value for bad-channel removal is significantly lower than no-bad-channel removal [F (1, 9) = 11.521, p = 0.008, η^2 = 0.561, mean difference = 4.242, std. error = 1.250]. The reason of this is that the MI of all the EEG channels is lower, resulting in a smaller reduction in MI going from the EEG channel space to the IC space. By itself, this does not necessarily indicate a worse performance and this indication is supported by the universal albeit non-significant decrease in PMI (p = 0.477).

Dipolarity of the bad-channel removal is significantly larger than no-bad-channel removal [F (1, 9) = 30.323, p < 0.001, η^2 = 0.771, mean difference = 1.463, std. error = 0.266]. The reason for this is that bad channels are non-stereotyped and cannot be fitted with a single dipole. The results echo the findings in [104]; which suggest that the more independent the EEG sources, the more they are dipolar.

The pre-processing factor of filtering significantly impacts on PMI and dipolarity, while it fails to become significant in terms of MIR (p = 0.513). PMI and dipolarity for filtering are significantly larger than not filtering; [for PMI: F (1, 9) = 332.193, p < 0.001, η^2 = 0.974, mean difference = 0.223, std. error = 0.012] and [for dipolarity: F (1, 9) = 47.517, p < 0.001, η^2 = 0.841, mean difference = 4.636, std. error = 0.673]. Filtering the data ($0.16 - 40Hz$) can remove the slow drifts and high frequency noise, which can occupy degrees of freedom in ICA space and introduce common information between recovered components. Therefore, the PMI values between estimated sources become higher when the data is not filtered. Consequently, the number of dipolar sources decreases as independence of the sources is decreased.

The segmentation factor significantly impacts on the performance of ICA algorithms

in terms of PMI [F (2, 18) = 284.745, p < 0.001, η^2 = 0.969] and dipolarity [F (2, 18) = 24.005, p < 0.001, η^2 = 0.727] without affecting MIR (p = 0.108). The pairwise post test revealed that the PMI value for epoch no-mean-removal is significantly lower than for continuous (mean difference = 0.180, std. error = 0.008, p < 0.001) and epoch mean-removal (mean difference = 0.166, std. error = 0.009, p < 0.001). However, the difference between continuous and epoch mean-removal is insignificant in terms of PMI (p = 0.331). For dipolarity, the epoch mean-removal is significantly smaller than both continuous (mean difference = 1.926, std. error = 0.211, p < 0.001) and epoch no-mean-removal (mean difference = 3.470, std. error = 0.582, p = 0.001). The difference between continuous and epoch no-mean-removal is insignificant in terms of dipolarity (p = 0.097). The result suggests that in general the performance of ICA algorithms is affected by removing data segments which may be assumed to have non-cerebral information. When the data segments are removed by epoch no-mean-removal, the performance of the ICA algorithms can be improved to extract latent independent components from the EEG data. This may increase the accuracy of the estimated components' activities and scalp topographies [112]. Therefore, the independence criterion and physiological plausibility of the estimated sources improved when non-cerebral segments are removed in the epoch no-mean-removal.

When ECG and EOG channels are included, MIR is significantly larger than when ECG and EOG channels are excluded [F (1, 9) = 22.316, p = 0.001, η^2 = 0.713, mean difference = 1.174, std. error = 249], while PMI and dipolarity have not been affected (p = 0.507 and p = 0.075, respectively). The reason for this is that the extra channels of ECG and EOG can provide more information for characterizing eye movement and heart-beat artefacts in the EEG data; thus improving EEG source separation.

Overall, AMICA performed significantly better than the other algorithms in most cases. Regarding the pre-processing factors of bad-channel removal, filtering, epoching the data and including ECG and EOG channels, considerably improved the performance of the ICA algorithms. However, removing the bad channels and epoching the data may

raise the risk of losing useful information within the removed channels and segments of the data.

3.4.2 Processing Time

In many studies, EEG signal processing delay is taken as an important evaluation measure of a system, especially in the case of real-time applications [178–180]. The aim of this research is to optimally use ICA for EEG signal processing; the pre-processing employed in this research is based on ICA. In section 3.4.1 it was demonstrated that the AMICA algorithm outperformed the other three ICA algorithms in terms of independence and biological plausibility of the estimated sources. Therefore, for further analysis, the effect of different pre-processing conditions on the processing time taken by only the optimum performing ICA algorithm (i.e. AMICA) to estimate the ICs is investigated.

In order to show the computational complexity and time required of the AMICA algorithm, the average CPU time required for the AMICA algorithm for source separation is obtained in all the predefined pre-processing conditions. The reported performance was carried out on a Linux worker machine running Scientific Linux 6.6 equipped with dual-Processor 8-core (16 cores) 64-bit 2.2 GHz Intel Sandy Bridge E5-2660 and 32 GB of memory. The MATLAB process was run as a single process on the worker node and no other applications were loaded on the machine.

To assess the effect of different pre-processing steps on the processing time of AMICA, a repeated measure ANOVA with within-subject factors of *bad-channel removal* and *filtering* with 2 levels each (applied/not applied); *segmentation* with 3 levels (continuous/epoched with mean-removal/ epoched with no mean-removal); and *including ExG* with 2 levels (included/not included) is applied. The overall ANOVA design has 24 within subject measurements (i.e. $2 \times 2 \times 3 \times 2$) for N=10 subjects. The level selected to indicate the statistical significance was at $p < 0.05$. Pairwise comparisons with the Bonferroni correction were performed to find main the factor effects.

Figure 3.9 illustrates the processing time of the AMICA algorithm, across different

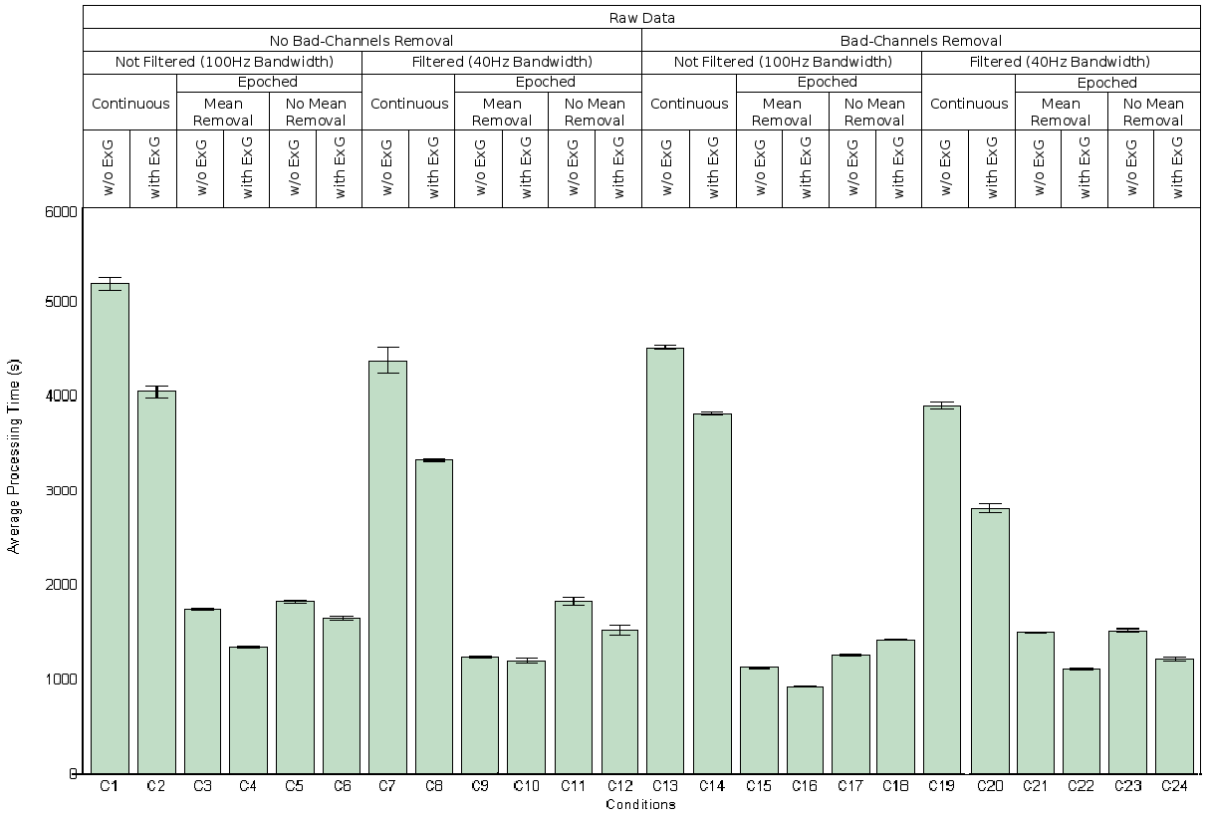

Figure 3.9: Processing time of AMICA algorithms through different pre-processing conditions, which are applied to data prior to ICA.

pre-processing conditions, averaged over 10 subjects. The AMICA processing time ranges from 975 s to 5185 s depending on the pre-processing conditions. The outcome of the ANOVA test revealed that all the pre-processing factors impact on the processing time of AMICA significantly. The AMICA processing time for bad-channel removal is significantly lower than by not removing the bad channels [F (1, 9) = 3797.020, p $<$ 0.001, $\eta^2 = 0.998$, mean difference = 347.988, std. error = 5.647]. The reason for this is that the dimension of the data input to the ICA is reduced by removing the bad channels, thus increasing the speed of the ICA's decomposition.

The AMICA processing time for filtering is significantly lower than when not filtering [F (1, 9) = 5298.359, p $<$ 0.001, $\eta^2 = 0.998$, mean difference = 280.291, std. error = 3.851]. Filtering the data can remove the slow drifts and high frequency noise, which can occupy degrees of freedom in ICA space; thus AMICA can converge faster in source separation.

The segmentation factor has a significant impact on the AMICA processing time [F (2, 18) = 125213.501, p < 0.001, $\eta^2 = 1$]. The outcome of the pairwise post test revealed that the AMICA processing time for epoch mean-removal is significantly lower than both epoch no-mean-removal (mean difference = 257.922, std. error = 4.781, p < 0.001) and continuous (mean difference = 2738.396, std. error = 7.772,p < 0.001). Also, the AMICA processing time for no-mean-removal is significantly lower than continuous (mean difference = 2480.474, std. error = 7.772). The reason is similar to bad-channel removal; where epoching the data decreases the length of the data input to the ICA and leads to faster ICA decomposition. Also, similar to filtering, removing the epoch mean eliminates the DC component (slow drift) in the epoched data and thus increases the speed of ICA decomposition by increasing the degrees of freedom in the ICA space.

Surprisingly, when the two EOG and ECG channels are included and the data dimension is increased, the processing time of the AMICA becomes significantly lower than when ECG and EOG channels are excluded [F (1, 9) = 5316.289, p < 0.001, $\eta^2 = 0.998$, mean difference = 473.815, std. error = 6.498]. This result is in contrast with those obtained for bad-channel removal where the processing time significantly decreased by decreasing the number of EEG channels. However, the result is complementary to the results obtained in section 3.4.1 in which including ECG and EOG channels in the EEG data improved the performance of ICA algorithms by providing more information for characterising eye movement and ECG sources. This suggests that AMICA benefits more from extra sources of information (EOG and ECG channels) from the potential activities which exist in the recording of most EEG channels, rather than from those artefacts which only affect a small number of EEG channels (bad channels).

It can be concluded that removing the bad channels, filtering, epoch mean-removal and including ECG and EOG channels in the data significantly improve the processing time of AMICA for source separation.

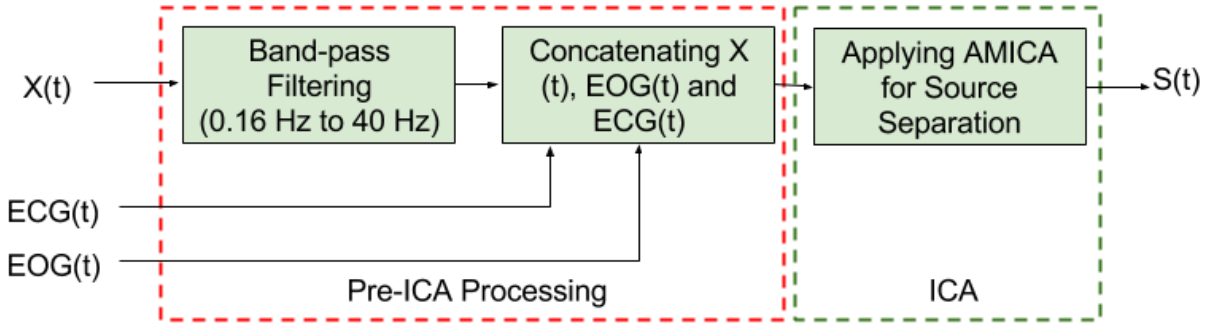

Figure 3.10: Block diagram of the obtained optimum pre-processing steps, where the raw EEG signal $X(t)$ is band-pass filtered at $0.16Hz - 40Hz$, and concatenated with ECG and EOG channels. Then the AMICA algorithm is employed to separate the independent sources, $S(t)$.

3.5 Summary

In this chapter, a pipeline is proposed to effectively select the pre-ICA processing steps and ICA algorithm variant for optimum source separability. Although in most EEG studies selecting the type of ICA algorithm is of concern, in this study it is demonstrated that the reliability of the estimated sources by ICA is considerably dependent on both the type of ICA algorithm and the type of pre-processing of the given data to the ICA algorithms.

Overall, among the algorithms, AMICA significantly performed better than the others in most cases. Regarding the different pre-processing factors, bad channel removal, filtering, epoch no-mean-removal and including ECG and EOG channels in the data improved the performance of the ICA algorithms significantly. However, in considering the entire EEG signal processing chain and the requirement to automatically label ICs for artefact removal, removing bad channels and epoching the data reduce EEG data size and risk data sparsity by potentially reducing the number of training instances for artefact detection. In other words, bad channels and the removed segments may actually be useful for identifying artefact sources and may include either cerebral information or information useful for artefact detection. Thus, in order to prevent information loss, it is preferable to keep bad channels and to not epoch the data (i.e. to use continuous data), in this study. The induced artefacts by bad channels into the EEG data are addressed and detected as

a focal artefact in the next chapter section 4.2.1. Therefore, based on the obtained results and the scope of this study, which is EEG artefact detection, the pre-processing condition $C8$ (Figure 3.10) - ExG, filtered and continuous and no-bad-channel removal is selected as the optimum pre-processing chain to prepare the raw EEG channel mixture for source separation using the ICA variant AMICA. The dataset described in section 3.2.1, under condition $C8$ pre-processing steps and the AMICA algorithm are employed for the rest of this thesis.

"Precision, accuracy and pondering in wisdom and sciences, will nourish and develop a person's brain."

Imam Ja'far al-Sadiq (PBUH)

4

AUTOMATIC ICA-BASED EEG ARTEFACT REMOVAL

4.1 Introduction

In Chapter 3, the performance of the four commonly used ICA algorithms were assessed from the perspective of separating artefactual and non-artefactual sources. Accordingly, the optimum data pre-ICA processing chain (condition 8) and the ICA algorithm variant ($AMICA$) were selected to prepare the recorded raw EEG data for better source separation. Therefore, the EEG datasets underwent the selected pre-processing steps and the 64 EEG channels of each subject were decomposed into 64 ICs. Nonetheless, the estimated

Table 4.1: The automatic ICA-based EEG artefact removal methods in the literature

Author	Year	Type of artefact	Type of feature
Irene Winkler [53]	2011	General artefacts	Frequential, spatial and temporal
Andrea Mognon [1]	2011	Blink, vertical and horizontal eye movement and generic discontinuity	Spatial and temporal
Wanzeng Kong [182]	2013	Blink	Correlation and power distribution
Raymundo Cassani [187]	2014	Ocular, muscle	spectral, amplitude modulation rate of change, coherence, and phase, autocorrelation
Irene Winkler [188]	2014	Ocular, muscle, loose electrodes	Several types of temporal, frequential and spatial features
T. Radüntz [92]	2015	General	Image features
Laura Frolich [189]	2015	Ocular, ECG, muscle	Frequential, spatial and temporal

sources were not yet labelled and specified as artefact and non-artefact sources. One can manually label the ICs, however, artefactual ICs manual identification and labelling can be time-consuming and subjective. Several attempts have been made to automatically detect specific types of artefactual ICs, especially ocular [164,181,182] and muscular artefacts [110, 150, 183]. Artefactual ICs are typically identified by extracting different temporal, spatial or frequential features representing artefact characteristics [1, 99, 184, 185]. Similar to regression methods (described in Chapter2 section 2.5), some studies use reference channels (e.g. simultaneous recording of EOG/ECG along with EEG), and label the IC as an artefact if it highly correlates with the reference channel [162,186]. Table 4.1 lists some other studies that proposed an automatic ICA-based artefact removal method.

The state-of-the-art ICA-based artefact removal method, ADJUST, uses a combination of temporal and spatial features to automatically detect three types of eye-related artefact and a generic discontinuity artefact [1]. However, ADJUST does not detect other prevalent artefacts such as muscle activities and ECG.

In this chapter, all the possible artefacts that can occur in normal EEG recordings are considered: *Blink*, *Saccade*, *ECG*, *Muscle* and *Focal*. It was the intention to automatically detect the highlighted artefacts and remove them from the data based on a two-layered artefact classification algorithm. The EEG datasets first undergo the obtained optimum pre-processing chain (condition 8) and are decomposed by the AMICA algorithm. Then, in the post-ICA processing step, the artefactual segments within each IC are detected by extracting a joint set of temporal, spatial and frequential features representing artefact characteristics. For each artefact type, a binary classification model is implemented to detect it. Finally, based on empirically obtained threshold ranges an entire component is tagged as an artefact and the cleaned EEG can be reconstructed by removing the detected artefacts.

Although ICA algorithms have been introduced in the last two decades and have been applied to EEG to identify artefactual ICs, the existing automatic IC labelling methods can only detect limited artefact types and they consider the whole IC as an artefact. Knowing that in the EEG recording of each subject, the number of artefact ICs (e.g. blink) are considerably less than other activity sources, this may result in wrong detection of neural sources as artefact, due to lack of enough training instances for artefact IC classification. In the proposed method, this issue is addressed, and the number of training samples are increased by dividing each IC into multiple segments and classifying the obtained segments. Therefore, the ICs with the most number of artefactual segments are labelled as the artefact ICs. This way, the extra option of classifying artefactual segments rather than the whole ICs, is also provided. It is known that, the ICA algorithms do not perfectly separate artefact and non-artefact sources and there could be cerebral information in the estimated artefact sources; thus, removing whole artefact ICs could raise the risk of losing useful neural information. The proposed segment classification option may reduce this risk in the desired applications. Additionally, as the system employs a separate binary classifier for each individual IC, there exist an option to only remove the artefacts of interest from the data.

The performance of the proposed method is evaluated and compared with the state-of-the-art ADJUST method in terms of accuracy of the artefact detection based on visual inspection, improvement in Signal-to-Noise Ratio (SNR), percentage of artefacts' energy removed and changes in the ERP classification accuracy.

4.2 Methodology

As mentioned earlier, the AMICA algorithm is used to decompose the 64 EEG channels from each subject into 64 ICs. Each of the decomposed ICs can be either artefact or non-artefact. For each type of artefact, a combination of frequential, temporal and/or spatial features are extracted. A binary classification model utilising a feature set extracted from the segments discriminates individual artefactual sources from cerebral sources.

4.2.1 Feature Extraction

Defining an informative feature set associated with each artefact class plays a crucial role in artefact detection. Different combinations of feature types in temporal, spatial and frequential domains were assessed to detect and discriminate blink, saccade, ECG, muscle and focal artefacts. The highest classification accuracy obtained when a combination of all three types of feature domains were empirically assessed. A knowledge-based approach to the feature selection is followed, based on the characteristics of each artefact type in temporal, frequential and spatial domains [190]. Temporal and frequential features are extracted from the segments; whereas spatial features are obtained via the ICA un-mixing matrix W in equation 2.2. Henceforth, the selected features for each type of artefact can be defined as follows:

Eye related artefacts

In terms of electrical potential, the eye is considered as a single dipole with a positive pole at the cornea and negative pole at the retina. The upward and downward eye

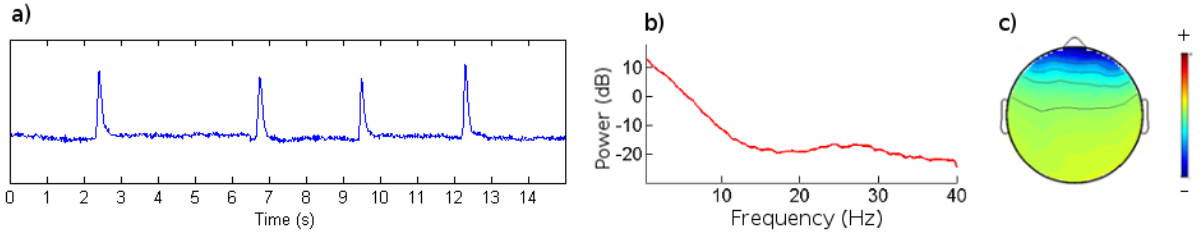

Figure 4.1: A sample of typical blink artefact; the high amplitude voltages generated by blinking over time (a); higher spectral power below $5Hz$ (b); and the effect of blinking on electrodes positioned in frontal area on the scalp (c).

movements produce positive and negative pulses, respectively. Moreover, the left and right eye movements generate a negative and positive potential difference at the outer and inner canthi (corners) of the eye, correspondingly. In addition to eye movements (saccade), eyelid closure (blink) generates potential changes which are described below separately.

- *Blink artefact*: Eye blinks produce rapid and high amplitude voltages, prominently on electrodes positioned in the frontal area of the scalp. The spectrum of the blink artefact is dominated by low frequencies [191].

  Temporal features: Blink ICs have spiky activation patterns over time (Figure 4.1 (a)). The distribution of activation amplitudes is asymmetric having either positive or negative skewness.

  Hence, the absolute value of skewness, that serves as blink's temporal feature, $|S|$, is defined as follows:

$$|S| = \left| E\left[\left(\frac{S - \mu_S}{\sigma_S} \right)^3 \right] \right| \tag{4.1}$$

  where E is the expectation operator; μ_S is the mean; and σ_S is the standard deviation of component S. Figure 4.2 illustrates the distribution of a manually detected blink IC that skews from a normal distribution due to its spiky activation over time.

  Spatial features: The topography of the eye blink IC has a typical projection pattern on electrodes positioned around the eyes and in the frontal sites (Figure 4.1 (c)).

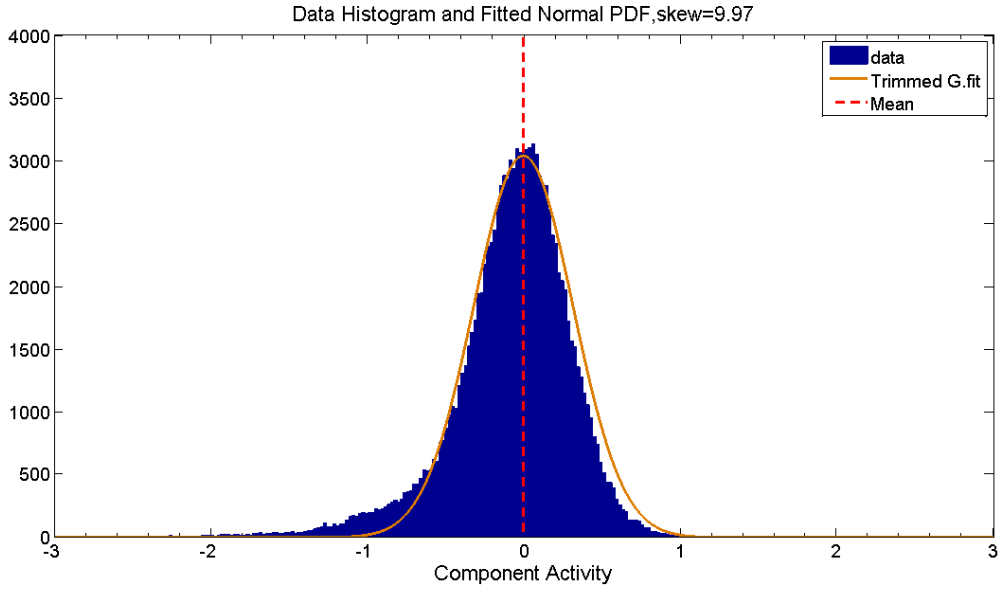

Figure 4.2: Example of a blink IC histogram with a negative skewness of -9.97 compared to the fitted normal distribution which has skewness of 0. The blink IC was manually labelled by two independent experts who visually inspected the datasets employed in this research.

The blink impact decreases from frontal to posterior sites. The spatial distribution of the blink artefact is symmetric in the frontal site with a similar sign of the topography weights across both left and right eye areas. For spatial features, the scalp map is divided into 10 areas corresponding to the brain lobes on the left and right hemisphere of the brain (Figure 4.3) and the averaged topography weights of the electrodes in each area is considered as a feature.

The electrodes located on the vertex (i.e. AFz,Fz,Cz,CPz,Pz,POz,Oz) are considered in both left and right regions in calculating averaged topography weights. For example, FR (i.e. Frontal-Right) is the spatial feature matching the averaged topography weights of the electrodes in the frontal lobe in the right hemisphere of the brain; and is calculated as below:

$$FR = \frac{1}{N}(a_{Fp2} + a_{AFz} + a_{AF4} + a_{AF8} + a_{Fz} + a_{F2} + a_{F4} + a_{F6} + a_{F8} + a_{FC2} + a_{FC4} + a_{FC6} + a_{FT8}) \tag{4.2}$$

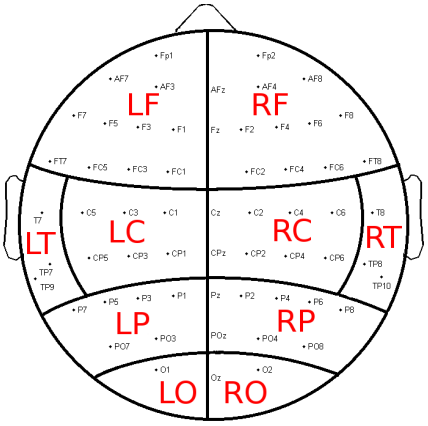

Figure 4.3: The subdivisions of the scalp map according to the brain lobes, to be used for spatial feature extraction to detect artefactual ICs; LF: left frontal, RF: right frontal, LC: left central, RC: right central, LT: left temporal, RT: right temporal, LP: left parietal, RP: right parietal, LO: left occipital, RO: right occipital.

where, $a_{...}$ is the topography weight of the electrodes and N is the number of the electrodes in each of the 10 areas (which is 13 in the example). Since ICA does not provide the original sign of the estimated sources and signs of the weights, the blink topography weights in the frontal area could be either positive or negative. To take this into account, all blink ICs are considered to have a positive sign in this method. If the sign of the ICs' weights in the left frontal site (i.e. FL) are negative, the 10 averaged topography weights are multiplied by -1 and their sign is inverted to positive. Let $A \in \{FR, FL, CR, TR, CL, TL, PR, PL, OR, OL\}$,

$$A = \begin{cases} A & \text{if } \; FL \geq 0 \\ -A & \text{if } \; FL < 0 \end{cases} \tag{4.3}$$

where A is the averaged topography weights of a region of the brain.

Frequential features: Blink artefacts have a high spectral power below $5Hz$ (Figure 4.1 (b)). The power spectral density (PSD) of the ICs, between $0Hz$ and $39Hz$, is estimated using Welch method [192] with $1second$ hamming windows and 25% overlap [193]. The frequency contents of 1 to $39Hz$ in $1Hz$ bins are considered as frequential features.

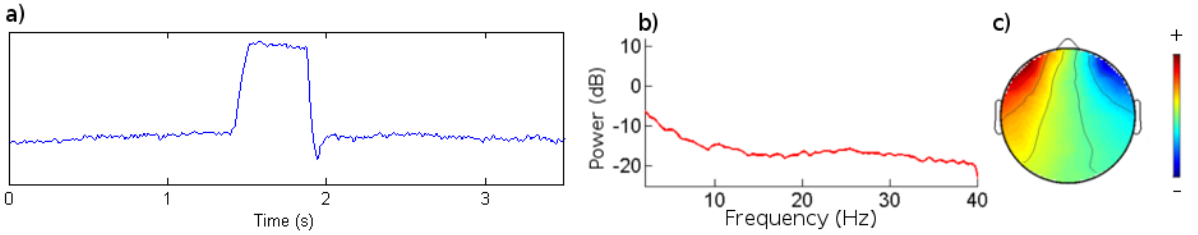

Figure 4.4: A sample of saccade artefact; the high amplitude voltage, produced by horizontal eye movement, over time which decays slowly (a), higher spectral power below $5Hz$ power (b) and the symmetric distribution of saccadic potentials over left and right frontal area (c).

Totally, 1 temporal, 10 spatial and 39 frequential features are concatenated to create a feature vector of 50 features for blink artefact detection.

- *Saccade artefact*: Saccade artefacts generate high amplitude fluctuations in the frontal area, as does the blink artefact. However, the amplitude changes are slower than with the blink artefact (Figure 4.4 (a)). The distribution of saccadic potentials over left and right frontal channels is typically symmetric with different signs (Figure 4.4 (c)). Like the blink artefact, saccade artefacts have a higher spectral power below $5Hz$ than other frequencies (Figure 4.4 (b)). Temporal, spatial and frequential features extracted for saccade component detection are the same as blink components.

Muscular artefacts

Muscle artefacts can be caused by physiological actions such as clenching of jaw muscles, chewing and swallowing which commonly generate muscle activities in temporalis muscles. These artefacts are high frequency activities almost above $20Hz$ and are mostly concentrated around few electrodes [194], which are mostly positioned in temporal regions (Figure 4.5 (c)).

Spatial features: As the muscle sources are mainly concentrated around a few nearby electrodes (Figure 4.5 (b)), in the topography weight matrix, the weights of a few electrodes are significantly higher than other electrodes. Thus, the columns of the topography

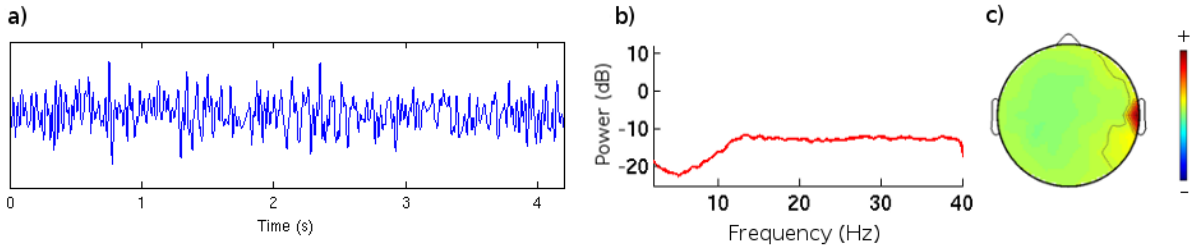

Figure 4.5: A sample of muscle artefact; high frequency activation of muscle IC over time a); higher spectral power above $20Hz$ b); and the concentrated activity of the muscle artefact around a few electrodes on the scalp c).

weight matrix are sorted in descending order and the first 10 maximum weights are selected. Even if the concentration of the muscle activity is spread across 10 electrodes, the method is able to consider those muscle sources. The final spatial feature vector F_{sp} consists of the selected weights, $(a_1, a_2, \ldots, a_{10})$, to the power of 1, 2, 3 and 4:

$$F_{sp} = \Big((a_1^1\ a_2^1\ \ldots\ a_{10}^1)\ (a_1^2\ a_2^2\ \ldots\ a_{10}^2)\ \ldots\ (a_1^4\ a_2^4\ \ldots\ a_{10}^4)\Big) \tag{4.4}$$

The weights are exponentiated to expand the gap between the affected weights by muscle activity and other types of activities. The reason for using different exponentiated weights is to non-linearly increase the dimension of features [195] to increase the performance of the classifier in discriminating the muscle sources from non-muscle sources. When higher powers (greater than 4) are employed, the small weight values in the range of 0 to 1 tend towards zero. Therefore, due to the curse of dimensionality and to prevent loss of information, the higher powers, greater than 4, are not selected. As a common strategy, the optimal number of features is determined by testing the classifier with a different combination of features [196].

Frequential feature: The frequential features of the muscle activity are the same as those for blink.

A single feature vector of 79 features is created by concatenating 40 spatial and 39 frequential features to detect sources associated to the muscle artefact.

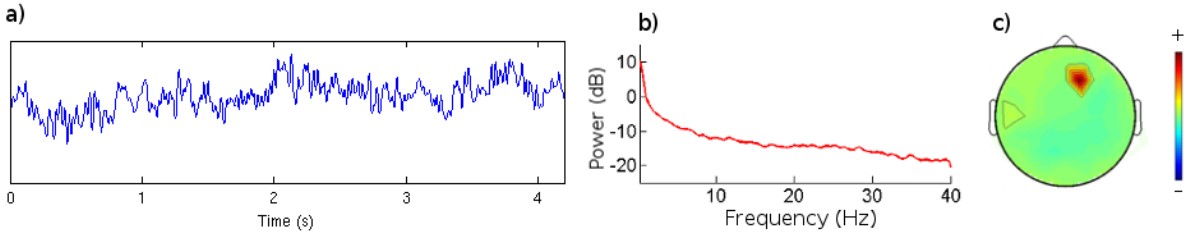

Figure 4.6: A sample of focal artefact; the amplitude fluctuations over time due to displacement of electrodes on the scalp a); the low frequency rhythms b); and topography c).

Focal artefact

Focal artefacts are the components that correspond to the sudden amplitude fluctuations in a single channel (Figure 4.6). This type of artefact can be generated by impedance fluctuations due to the poor contact of electrodes to the scalp, electrode displacement or electronic device interference [197]. Since the scalp map of the brain sources have smooth distributions, the sources with the distribution concentrated over a single channel (Figure 4.6 (a)) are likely to be artefacts [1]. The 40 spatial features of the muscle activity are considered as a feature vector for the focal artefact.

ECG artefact

Being placed on or near a blood vessel, an electrode can pick up an undesirable signal due to the expansion and contraction of the vessel, which is known as an ECG artefact and is normally measured by a cardiograph [95]. ECG artefacts introduce a repeating pattern of peaks conventionally named as QRS complex [198]; this includes a large amplitude peak, R. The impulses repeat about once per second, comparable to a normal resting heart rate of $60-90bpm$. The ECG signal has been reported to have higher power spectrum at lower frequencies (below $50Hz$ - Figure 4.7 (b)) [199].

Temporal features: According to the spiky activation of the ECG component in the time domain (Figure 4.7 (a)), the absolute value of the skewness is calculated as a temporal feature for the ECG artefact. The pattern of the QRS complex in the ECG time series

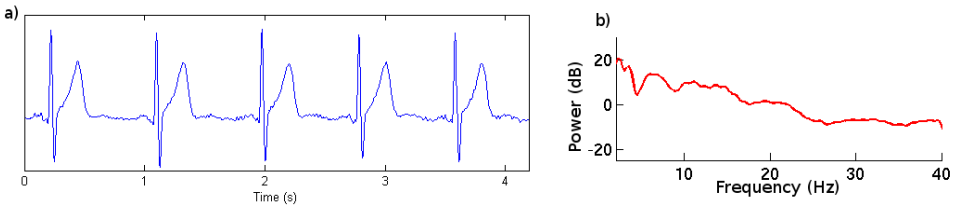

Figure 4.7: A sample of ECG artefact component; a repeating pattern of peaks generated by heart beats over time (a) and higher power spectrum at low frequencies (b).

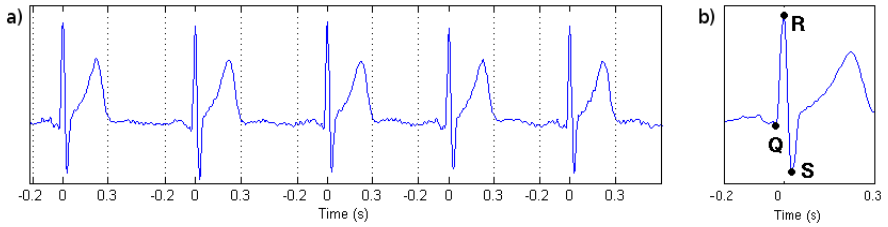

Figure 4.8: The ECG time series segments marked from 200 ms before and 300 ms after the R peaks (a) and a sample of the averaged QRS complex as a temporal feature of the ECG artefact (b).

is considered as another temporal feature. The R peak amplitude and latency, within the QRS complex (Figure 4.8 (b)), are determined using a peak detection procedure proposed by Billauer [200]. According to the method, peaks (local maxima) are detected based on their neighbouring valleys (local minima). The first 5 R peaks within the first 6 seconds of the components' time series are selected and averaged within $200ms$ before and $300ms$ after the QRS peak (Figure 4.8 (a)). In order to reduce dimensionality of the features and generalise the proposed ECG artefact detection method with EEG data recorded at different sampling rates, the averaged QRS complex is resampled from $250Hz$ to $100Hz$ with a rational factor of $2/5$. The obtained 50 sample points are used as features (Figure 4.8 (b)).

Frequential features: the frequential features of the ECG artefact are the same as blink and muscle frequential features.

Altogether, 51 temporal and 39 frequential features are concatenated to form a single feature vector of 90 features for ECG source detection.

4.2.2 Feature Normalisation

In order to eliminate the effect of scaling due to various EEG recording apparatus and the subjects' physiological variability, all feature vectors (extracted from segments) in time, frequency and spatial domains are normalised to a range between 0 and 1. For N dimensional feature vector $F = (f_1, f_2, \ldots, f_N)$, normalisation is done by dividing each feature's value by the magnitude of the feature's vector [201].

$$\|F\| = \sqrt{\sum_{i=1}^{N} f_i^2} \tag{4.5}$$

$$F_{normalisd} = \frac{F}{\|F\|} \tag{4.6}$$

where $F_{normalisd}$ is the normalised feature vector and $\|F\|$ is the Euclidean length of the N dimensional feature vector F.

4.2.3 Artefact Classification

The main objective of this chapter is to detect and remove the ICs associated with specific artefacts. There are two levels of classification performed to achieve this: $segment-level$ and $IC-level$.

Segment Level Classification

In segment-level classification, components are epoched into 30 seconds segments and features are extracted from each segment rather than the whole IC. In this manner, it is possible to only remove the artefactual segments instead of the whole IC, thus retaining potentially valuable EEG information in the system which could be otherwise discarded. This also increases the amount of training data available potentially improving classifier robustness. The average pre-processed data durations are approximately 7 minutes. For each IC, 15 segments each of 30 seconds, are considered with no overlap. The total amount

of segments for each dataset is 960 segments (64 ICs $\times$15 segments). The length of the selected segments, 30 seconds, ensures that in each segment at least one occurrence of the desired artefact is present; for example, the average male and female blinking rate is once every 5 to 6 seconds [202, 203]. The extracted features then serve as the inputs to the Naive Bayes (NB) classifier [204].

The Naive Bayes classifier (NB classifier) is a simple probabilistic generative classifier with the (naive) assumption that features are independent. It assumes that absence or presence of a particular feature of a class does not imply any information about absence or presence of any other feature. An NB classifier is not sensitive to irrelevant features, so can be robust with respect to noise [205]. Also, in contrast to more advanced classifiers such as Support Vector Machines (SVM), it does not need exhaustive parameter optimisation, can be trained quickly and requires a small amount of training data to estimate the class parameters [206–208]. Generally, a Bayesian classifier works in such a way that it assumes the observation feature vector is generative, considering a parametric model whose parameters are estimated from supervised training data. Each class is modelled by a normal distribution using the mean and standard deviation of training instances in that class. The class with highest probability is assigned to a given (test) feature vector sequence. For each of k outcomes, it assigns the class C_k with maximum posterior probability, to a given (test) feature vector sequence $V = (v_1, v_2, ..., v_n)$ representing n features.

$$\begin{aligned} c^* &= \arg \max_i \ P(C_k \mid v_1, v_2, ..., v_n) \\ &= \arg \max_i \ \frac{P(v_1, v_2, ..., v_n \mid C_k)P(C_k)}{P(v_1, v_2, ..., v_n)} \\ &= \arg \max_i \ \prod_{j=1}^{n} P(v_j \mid C_k)P(C_k) \end{aligned} \tag{4.7}$$

where $P(v_j \mid C_k)$ is the probability of the attribute $V = v_h$ given the class C_k and $P(C_k)$ is the number of training samples belonging to class C_k. The described classifier is employed

to distinguish artefactual from non-artefactual segments. Each type of artefact is treated individually with an NB classifier.

Source (IC) Classification

Artefactual ICs are detected based on the outcome of the segment classification. Each of 64 ICs consists of 15 segments with the length of 30 seconds from which, for each type of artefact individually, the features are extracted and classified by NB. The NB classifier allocates two probability values (posterior-probability) to each segment, indicating the likelihood of a segment belonging to artefact or non-artefact classes. For each IC, the probabilities of its corresponding 15 segments belonging to artefacts are added in order to create a score for that IC. The ICs can obtain a score between 0 and 15. ICs scoring higher than a specified threshold are identified as artefacts. Therefore, even if all 15 segments of an artefactual IC are not detected correctly, the whole IC could be detected as an artefact, based on the score obtained for that IC. The optimum value of the threshold is determined empirically by generating a Receiver Operator Curve (ROC) (see section 4.3.3 and Figure 4.10).

Figure 4.11 shows the distribution of IC scores of a subject for different types of artefacts.

4.3 Evaluation Criteria

With the aim of validation and having a ground truth, first, all of the artefactual ICs are manually labelled. Next the proposed artefact classification method is evaluated using several metrics: - True Positive Rate, True Negative Rate, Balanced Accuracy, Receiver Operator Curve (ROC), Signal to Noise Ratio, Relative Variance (RV) and the accuracy of Event Related Potential (ERP) classification.

4.3.1 Visual Inspection

For the ground truth, the ICs were manually labelled in a blind procedure by two independent experts who were familiar with EEG analysis and decomposition by ICA. Each expert visualised a total of 640 ICs by inspecting the IC time series of the average length of 7 minutes, IC topographies and power spectrum, via an EEGLAB software package [172]. Each expert was asked to label the 5 classes of artefact. The *ground truth*, including 202 ICs, was created by considering the 'in-common' voted artefactual ICs between both experts' classification. The level of agreement between classifications performed by the two experts was 97.5% on all artefacts. In total, 10 ECG, 10 blink, 10 saccade, 40 muscle and 132 focal ICs were classified among the 640 ICs presented to the experts.

4.3.2 Balanced Accuracy

To evaluate the proposed artefact classification method, True Positive Rate (TPR) and True Negative Rate (TNR) are selected. TPR and TNR are used, because in addition to the importance of correct artefactual segments/ICs' detection for cleaning EEG data, the accuracy of the method in detecting the non-artefactual segments/ICs is also important. The non-artefactual sources may contain cerebral information, so miss-detection and removal of non-artefactual sources may result in losing useful cerebral information. TPR (sensitivity) and TNR (specificity) are calculated based on the confusion matrix [209]:

$$Sensitivity = \frac{TP}{TP + FN} \tag{4.8}$$

$$Specificity = \frac{TN}{TN + FP} \tag{4.9}$$

where, TP and FP are respectively, the number of true artefacts and non-artefacts identified as an artefact. Also, TN and FN are respectively, the number of true non-artefacts and artefacts identified as a non-artefact. Additionally, due to imbalanced

classes, one can suggest the use of weighted accuracy, where the important class is weighted more than the other class. However, in this experiment the importance level of both the artefact and non-artefact classes is the same (i.e. wrong detection of artefact and non-artefact sources may lead to keeping artefact sources in the data and to losing cerebral information, respectively). Therefore, Balanced Accuracy (BA) is selected as an additional measure, which is the average of sensitivity and specificity and unaffected by class skew [210]:

$$BalancedAccuracy = \frac{(Sensitivity + Specificity)}{2} \tag{4.10}$$

The BA is calculated for each subject and each type of artefact separately. The method's BA for each artefact is obtained by averaging BA over all subjects.

4.3.3 Receiver Operator Curve

The Receiver Operator Curve (ROC) is a plot of TPR against 1−TNR; it indicates the robustness of the binary classifier to changes in its parameters, specifically the threshold value of the classifier's decision boundary. Changing the threshold of the classifier results in various TPR and TNR values which are illustrated as the ROC. The area under the ROC curve (AUC) is an important value as it demonstrates the overall classification accuracy of a binary classifier. The AUC value ranges from 0.5 for an uninformative model to 1 for perfect discriminating ability of the evaluated classifier [211].

4.3.4 Signal-to-Noise Ratio

Signal-to-Noise Ratio (SNR) is calculated using the following method. After removing the artefactual ICs which are labelled as artefacts in the ground truth, the reconstructed cleaned data, EEG_{GT}, is taken as the original signal, $Signal = EEG_{GT}$. Similarly, the identified artefactual ICs by the proposed method are removed from the data and the new cleaned data is obtained, EEG_{sys}. The difference between these two cleaned data

is considered as the noise signal, $Noise = EEG_{GT} - EEG_{sys}$. The power of the signal, P_{Signal}, and noise P_{Noise}, is calculated for each channel;

$$SNR_{sys_i} = \frac{P_{Signal_i}}{P_{Noise_i}} = \frac{P_{(EEG_{GT_i})}}{P_{(EEG_{GT_i} - EEG_{sys_i})}}; \quad i = 1, 2, 3, ..., N \tag{4.11}$$

where, N is the number of EEG channels and SNR_{sys_i} is the SNR obtained for the ith channel after the proposed artefact removal method is applied. In the experiment here there are 62 EEG channels and two ECG and EOG channels; thus, in this case $N = 62$. The system's total SNR, SNR_{sys}, is obtained by calculating the average of the pairwise ratio between the signal and noise of all the EEG channels.

$$SNR_{sys} = \frac{1}{N} \sum_{i=1}^{N} SNR_{sys_i} \tag{4.12}$$

The same procedure is applied when the difference between cleaned (by visual inspection) and raw data is considered as noise (i.e. $Noise = EEG_{GT} - EEG_{raw}$). The obtained new SNR is subtracted from the system SNR and a differential SNR, SNR_{Diff}, is obtained.

$$SNR_{Diff} = SNR_{sys} - SNR_{raw} \tag{4.13}$$

The larger SNR_{Diff} the better the performance of the proposed method. If the value of SNR_{Diff} is less than zero (negative differential SNR), it represents deterioration in the quality of the EEG data.

4.3.5 Relative Variance

The Relative Variance (RV) represents the ratio between the variance of the ICs' time series that are correctly labelled as an artefact by the proposed method and the variance of artefactual ICs labelled in the ground truth. The RV is calculated for each type of artefact separately (e.g. RV of detected eye-related artefacts) and all artefacts together

(i.e. RV of all types of artefacts):

$$RV = \frac{\sum\limits_{i \in CorrectICs} v_i}{\sum\limits_{i \in GT} v_i} \tag{4.14}$$

where, v_i indicates the variance of the time series of the ith component, and $CorrectICs$ is the list of ICs which are labelled correctly by the proposed method. The underlying principle of this RV is that the more the variance is explained by the IC, the more it is important to correctly classify that IC as either artefact or non-artefact. The amount of variance explained by sources which are incorrectly classified as an artefact are also considered, relative to the total variance of all ICs. This indicates the importance of non-artefactual sources, which are detected as an artefact and the amount of information they provide in the data. This measure is similar to that used by Mognon et al. [1] with the difference that it considers the variance accounted for by the labelled artefactual ICs in the ground truth, not all the ICs in the data.

4.3.6 Event-related Potential Classification

Another metric to evaluate the performance of the method for artefactual segment and component removal, is ERP detection accuracy. The efficiency of the method in reconstructing artefact-free EEG data is assessed by calculating the ERP detection accuracy. The method used for single trial ERP detection by Ghaderi [210] is employed to evaluate the performance of the proposed method in detecting and removing the artefactual components. The ERP is calculated for 4 channels by the human-based channel selection method: $O1, O2, P7$ and $P8$, which are manually selected based on the knowledge of the activated brain regions with respect to the visually stimulation paradigm in this research [116].

Pre-processing

For the ERP analysis the datasets are cleaned by removing the artefactual components detected by the proposed artefact removal method. After removing the artefactual components, the cleaned EEG datasets are reconstructed and band-pass filtered at $0.1-4Hz$.

Feature Extraction

The ERP samples $60-500ms$ after the $S1$ stimulus onset are considered as target (ERP). No-target (noERP) samples are extracted from $1060-1500ms$ after $S1$ stimulus onset, in which there is no stimulus response. So 90 ERP and 90 noERP samples with $440ms$ length are extracted for each of the 4 selected channels, the mean of each epoch is subtracted and its variance is normalised to 1. Then, the extracted samples are resampled again from $250Hz$ to $125Hz$ which provides 55 features.

ERP Classification

At this stage, the extracted features are used to train an NB classifier for ERP detection. An NB classifier is allocated for each channel, separately. The posterior probabilities obtained from the NB classifier for each segment are multiplied over all 4 channels for both ERP and noERP classes, individually. Segments are labelled according to the class which has the highest probability.

4.3.7 Cross Validation

A $10-fold$ cross validation, leave-one-out method, is used for evaluating the performance of the method for artefactual segment and IC detection as well as for ERP classification. Under the cross validation assumption, there are 10 iterations (folds); at each iteration the feature vectors of a fold are taken as testing data and all other feature vectors (9 folds) are taken as training data. After the last iteration, the desired performance measures are averaged over all 10 folds.

The dataset used in this study includes EEG recording of 10 individual subjects. For artefactual segment and IC classification, the feature vectors extracted from each subject is taken as a fold. Thus, at each of the 10 iterations, the feature vector of a subject is taken as a test and the feature vector of the other 9 subjects are taken as training data. Therefore, the artefact classification method's BA for each artefact type is obtained by averaging the obtained BAs at all 10 iterations. The $10-fold$ cross validation is used for evaluating the BA of ERP classification for each subject individually. At each fold, the feature vectors of a single subject were used to create the training and testing datasets using the leave-one-out method. Thus, the obtained BAs were averaged over all 10 subjects and the final BA is reported.

4.4 Results Analysis

The accuracies of the method in detecting artefactual segments and ICs, named *Proposed_method_Seg* and *Proposed_method_ICs* respectively, are reported and compared to the state-of-the art ADJUST method, in terms of the BA, SNR, RV and ERP detection accuracy. The statistical significance of the results is obtained by performing simple t-test at $p<0.05$.

4.4.1 Artefact Classification at Segment-Level

Figure 4.9 illustrates the averaged BA of the method in separating artefactual and non-artefactual segments for each type of artefact. The obtained BA values for all types of artefacts are greater than 90% (with low variance), except for saccade. The highest accuracy of the method in the classification of contaminated segments is obtained for ECG artefacts (averaged BA = $98.09 \pm 0.0072\%$). This could be due to the periodic characteristic of the ECG waveform that occurs frequently in each 30 second segment of an ECG IC (Figure 4.7). Therefore, based on the type of the features extracted to detect ECG, the proposed method could successfully discriminate between ECG and non-ECG

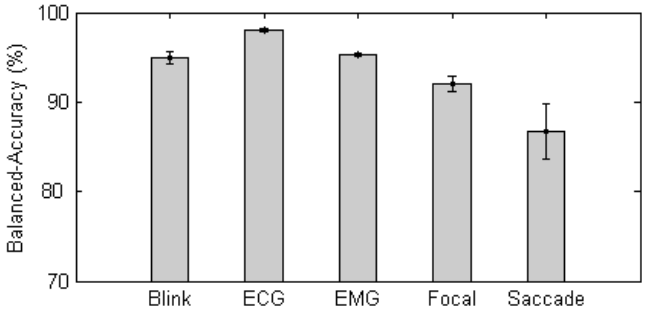

Figure 4.9: The averaged BA of the proposed method in detecting artefactual segments classified as blink, ECG, muscle, focal and saccade. The error bars represent variance across subjects.

segments. The segments contaminated by blink and muscle activities are also detected with high BA (almost 95%). The remarkable characteristics of blink artefact (periodic waveform with strong peaks and specific spectral pattern) and muscle artefact (spectral and spatial topography patterns) and the appropriateness of the extracted features could distinguish between blink and non-blink, muscle and non-muscle segments. The BA for detection of focal segments from non-focal segments in the data is lower than BA for muscle and blink segments. The prevalent characteristics of the focal artefact is its spatial pattern; while blink and muscle artefacts have specific distinguishable patterns in the time and frequency domains. Nevertheless, the proposed method could successfully detect ECG, blink, muscle and focal artefacts with above 90% accuracy and low between-person variations. In contrast, the classification of saccadic segments obtained the lowest BA and highest variance (averaged BA= $86.74 \pm 0.0313\%$) among the other four artefacts. The reason for this could be rare occurrence of saccadic activities in the data (within saccade sources). The experiment was performed under controlled conditions and similarly to common EEG recordings, the participants were asked to avoid eye movements as much as possible during EEG acquisition. However, saccadic eye movements occurred rarely and involuntary in the data. Consequently, all 30 second segments of the saccade ICs do not contain the saccadic peak in the time domain and the BA value and the between subject variation for saccade is lower and higher than for other types of artefacts, respectively. Despite the fact that all contaminated segments by each type of artefact are not detected

Table 4.2: The threshold ranges including the highest value of BA obtained for classification of each type of artefact, according to the ROC curve in Figure 4.10; and the optimum single threshold value associated to the highest BA selected for each type of artefact.

	Blink	ECG	Muscle	Focal	Saccade
Optimum Threshold (%)	50	70	35	75	6
Threshold Range (%)	33.2 to 53.3	60.1 to 73.4	33.1 to 36.7	74.1 to 75.5	5.6 to 6.6
BA Values (%)	100.00 ± 0	99.92 $\pm 6.3 \times 10^{-6}$	97.29 $\pm 5.84 \times 10^{-4}$	96.18 ± 0.001	95.64 ± 0.003

perfectly (100%), the proposed method performs effectively in the separation of artefactual and non-artefactual segments.

4.4.2 Artefact Classification at IC-Level

Figure 4.10 shows the TPR and TNR of IC classification for different values of threshold applied on ICs' scores. As the value of the threshold increases from 0 to 100, TPR decreases gradually while TNR increases. The perfect ROC curve displays 100% TPR and TNR; or $AUC = 1$. The AUC obtained for blink is equal to 1, while for ECG $AUC = 0.99$, close to perfect. The obtained AUC for muscle, focal and saccade are still relatively high, $AUC = 0.98, 0.96, 0.97$, respectively. The graph is produced with no interpolation with a very high density of data point

Table 4.2 shows the optimum classifier threshold values for the highest possible BA obtained. The BA is 100% for blink (while the lowest BA is for saccade (95.64%). All artefact types are detected correctly with BA values above 95% and low between-person variance (instances of the detected artefacts can be found in Appendix B). The threshold range for each type of artefact represents the system's reliability and stability in which the highest BA remains the same. The optimum thresholds are selected based on the ROC curves, with highest values of TPR and TNR.

The results of the BA (Table 4.2) and ROC curves (Figure 4.10) show the improvement of all BA values for artefactual IC detection relative to the artefactual segment

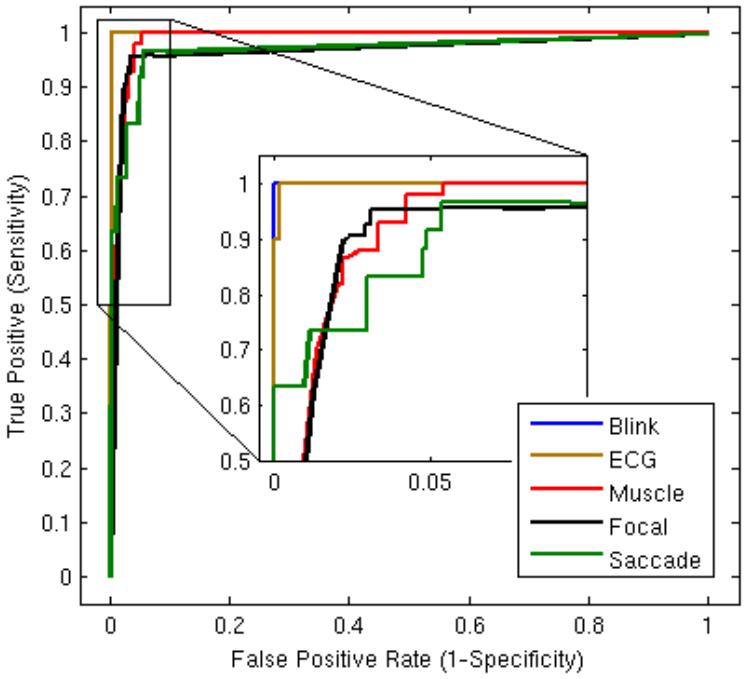

Figure 4.10: ROC curves showing the TPR and TNR of the proposed method in blink, ECG, muscle, focal and saccade IC classification, when different thresholds are used for artefactual IC detection. The threshold values varied between 0 to 1, with 0.001 steps. The ROC curve associated to ECG artefact superimposed on the blink ROC curve.

classification.

Figure 4.11 shows the distribution of IC scores of all 10 subjects for the blink artefact. The red line represents a specific threshold value for blink IC detection. The ICs whose scores are above the threshold (to the right side of the red line) are detected as an artefact. The distribution of IC scores for other types of artefacts can be found in Appendix C.

Generally, the proposed method could identify the artefactual ICs associated with each type of artefact with high BA (above 95%) and AUC (above 0.96). The between-subject variation for each type of artefact is negligible, which shows the method's stability for artefact detection.

Despite other ICA-based artefact removal methods that have used only a single threshold for separating artefacts and non-artefacts, the proposed method also introduced a threshold range in which the highest BA values remain the same. This may refer to the reliability of the method when applied to other datasets. It also suggests easier estimation

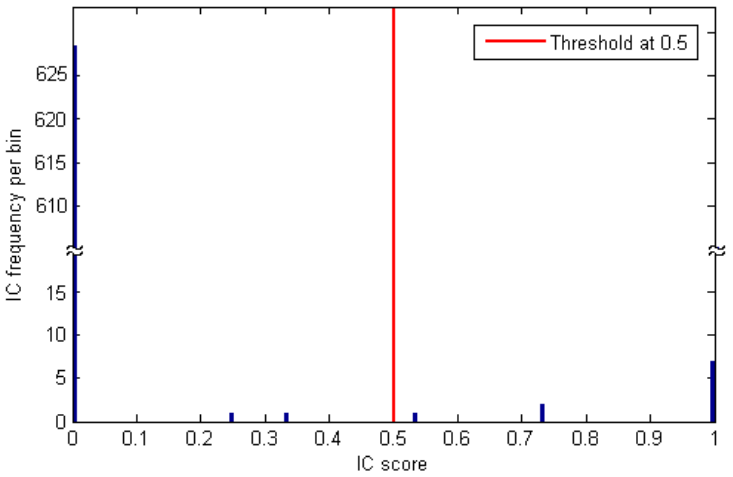

Figure 4.11: The distribution of IC scores for all subjects are shown for blink artefact. The ICs are labelled and classified as an artefact if their scores are above the threshold value (red solid line).

of a threshold that has near optimum performance for a wide range of values. It is shown that the artefact type with a higher BA has a larger threshold range, representing more stability of the method in detecting the corresponding artefact type.

4.4.3 Comparison with ADJUST

Figure 4.12 illustrates the BA for the three artefact types (blink, saccade and focal artefacts) held in common, individually, all types of artefacts in each method and all the three communal artefacts together. In this experiment there is only one blink component in each subject's recording, which are detected by the proposed method successfully. Similarly, the ADJUST method detected most of the blink artefacts (BA= 99.28%). For saccade ICs, the ADJUST BA is 4.85% lower (statistically insignificant) than the proposed method's BA with a larger between-person variation. This refers to the weakness of ADJUST method in detection of some saccade ICs, where there exists more than one saccade IC in the data of a single subject. There are several components associated to focal artefacts in each data which are relatively more than blink and saccade ICs. Some focal ICs are not detected by ADJUST and it achieved 34.46% lower BA than the proposed method for focal artefacts, which is statistically significant ($p = 0.0001$). The between-

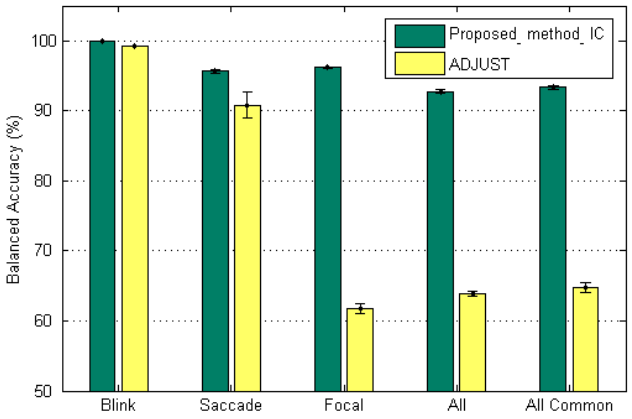

Figure 4.12: BA of the proposed method (Proposed_method_IC) in detecting the artefactual components compared with ADJUST; individual artefacts held in common by the proposed method and ADJUST, all types of artefacts in each method, and all communal artefactual components in both methods.

Table 4.3: Comparing the proposed method (Proposed_method_IC) and ADJUST based on the explained variance by the true detected artefactual ICs, relative to the ground truth (True Acceptance - TA) and the percentage of the variance thrown away by removing the detected ICs as an artefact from the data using the proposed method and ADJUST (False Acceptance - FA). The best results are highlighted in bold.

	Blink		ECG		Muscle		Focal		Saccade		All Artefacts	
	TA	FA	TA	FA	TA	FA	TA	FA	TA	FA	TA	FA
Proposed_method_IC (RV%)	**100**	**0**	**100**	**2.70**	**100**	**3.01**	**95.31**	**2.69**	**98.58**	3.83	**97.39**	**4.36**
ADJUST (RV %)	**100**	13.62	—	—	—	—	30.31	3.09	86.38	**0.84**	54.38	4.86

subject variation obtained by ADJUST is larger than the proposed method in most cases except for blink detection. The performance of the ADJUST method decreased when the number of artefactual sources is increased in the data. In the case of all types of artefacts and communal artefacts, the ADJUST BA is significantly lower than the proposed method ($p = 0.0001$). This could be due to the unsuccessful detection of focal artefacts by the ADJUST method.

Table 4.3 represents the averaged percentage of the variance accounted for (RV) by the artefacts labelled by this method and ADJUST relative to the ground truth, for each individual type of artefact and all artefacts together. It is more important to correctly classify ICs with larger RV (contribution). On one hand, if the ICs with large RV are

artefacts, they contaminate the data, so they should be correctly labelled and their effect should be removed from the data. On the other hand, if the ICs with large RV are non-artefact or cerebral, keeping these sources in the data is crucial in order to prevent information loss.

The aim of comparing both methods is to assess their ability and performance in detecting all defined types of artefact. The proposed method obtains 100% of the explained variance by blink, ECG and muscle sources; 98% of the explained variance by saccade; and 95% by focal artefacts, relative to the ground truth's sources. ADJUST detects 100% of the explained variance by blink sources. However, the explained variance by the saccade sources correctly labelled (True Acceptance - TA) by ADJUST is significantly lower (almost 12%, $p = 0.02$) than by the proposed method (98.58%). The RV obtained for the true focal sources detected by ADJUST is the lowest (30%), which is significantly lower than the proposed method ($p = 0.0001$). When considering all types of artefacts together, the explained variance of the correctly labelled artefactual sources detected by the proposed method is 97.39%; which is significantly higher than ADJUST (43%, $p = 0.0001$). The proposed method detected almost all the artefactual ICs and the ICs with a high level of contribution (RV) correctly, in both cases of the individual artefact types and all artefacts which are labelled in the ground truth. However, the explained variance of the artefactual ICs detected by the ADJUST method is significantly lower than by the proposed method ($p = 0.0001$), relative to the ground truth in cases of saccade, focal and all artefacts; as all these artefact sources could not be detected by ADJUST and their variance remained in the data.

Regarding the non-artefactual sources which are classified as an artefact (False Acceptance) by the proposed method and by ADJUST, the explained variance obtained for both methods is almost the same (approximately 4%) for all artefacts together. However, different RVs are obtained when individual artefacts are considered. Using the proposed method, the largest amount of information loss is attained for incorrectly detected saccade sources (about 4%) and then for muscle and focal sources (about 3%). The residual

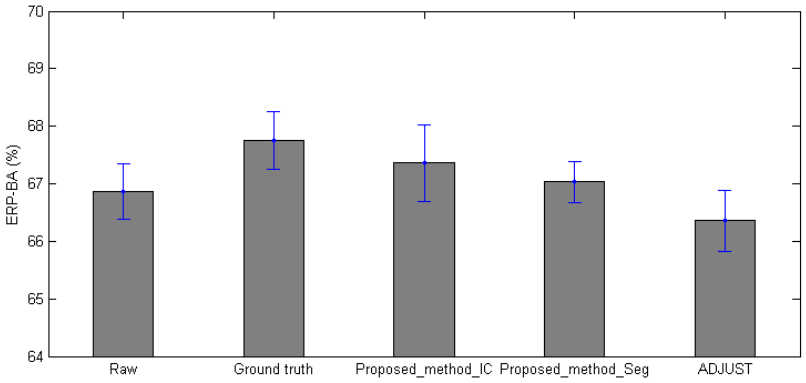

Figure 4.13: The averaged BA of the ERP classification for the *Raw*, cleaned data when removing artefacts labelled in the ground truth (*Ground truth*), by the proposed method (*Proposed_method_IC* and *Proposed_method_Seg*) and *ADJUST* method.

variance accounted for by the incorrectly detected ECG sources by the proposed method is less than 3%, which is unlikely removed from the data by removing those sources. However, the residual variance for incorrectly detected blink sources is zero as there were no non-blink sources detected as blink by the proposed method.

When ADJUST is applied, about 13% of data information would be lost for incorrect blink detection. The RV for incorrectly detected saccade sources by ADJUST is about 3% less than by the proposed method; while for focal artefact it is similar (approximately 3%). Figure 4.13 depicts the BA of ERP detection for no artefact removal (Raw), in contrast with the same results using the ground truth, ADJUST, and the proposed method (i.e. segment removal and IC removal). Removing artefacts in the ground truth resulted in the highest ERP detection rate (67.98%), as shown in the figure; which can confirm the valid labelling of artefactual ICs in the ground truth. The ERP classification BA obtained by removing the whole artefactual ICs detected by the proposed method (67.37%) is improved insignificantly compared to the raw data, but lower than the ground truth ($p>0.05$). The reason is that although artefactual ICs, detected by the proposed method, are removed from the data some artefacts are not detected correctly and remained in the data. There is a negligible difference in the performance of the proposed method when only artefactual segments are removed (67.03%), compared to when whole ICs are removed. This may

refer to the artefactual segments remaining in the data which were not detected by the proposed method. The ADJUST method achieved 66.36%, which is insignificantly lower ($p>0.05$) than the raw data. This might be due to the remaining artefactual ICs and incorrectly removed cerebral information from the data. This is not elicited in the BA values obtained in artefactual IC detection, because the number of non-artefactual ICs is more than the artefactual ICs in these experiments. However, it can be confirmed by the obtained result in the SNR evaluation. The SNR is increased by 8.60 dB when removing the artefacts detected by the proposed method; while it is reduced by 9.96 dB when detected artefacts by the ADJUST method are removed from the data.

Generally, the differences between BA values of the ERP classification calculated from the cleaned data by removing artefacts labelled in the ground truth, the proposed method and ADJUST, presented in Figure 4.13, are statistically insignificant.

4.5 Summary

In this chapter, a fully automated EEG artefact labelling method is proposed to maximise the performance of the EEG signal processing chain. The proposed method (Figure 4.14) detects the common artefact types in EEG data (blink, saccade, muscle, ECG and focal) with balanced accuracies above 95% and low between-person variation. The method identifies not only the artefactual components but also the segments contaminated by artefacts. Whilst other ICA-based artefact removal methods determine a single linear threshold for artefact classification, a range of thresholds with high BA are introduced to cover all artefact types, which can suggest the reliability of the method. This may potentially assist in generalising the proposed method with other EEG applications. Although the proposed artefact removal method showed a good performance in the classification of artefactual segments and improved ERP classification rate, compared to the ADJUST, it did not performed as well as the whole IC classification. This could be due to the imperfect labelling of the artefactual segments in the gold standard. In the gold standard, the

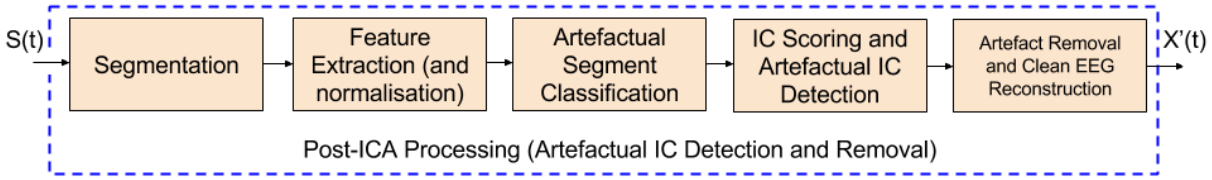

Figure 4.14: Block diagram of the proposed automatic artefact detection method. First, the ICs are segmented and the features (described in section 4.2.1) are extracted from each segment. Then, the segments are classified into artefact and non-artefact. Based on the result of this classification, artefact ICs are scored and detected. Finally, the detected artefact ICs are removed and the cleaned EEG, X', is reconstructed.

label of all segments within each artefact IC is the same as the corresponding artefact IC. However, in the case some artefacts such as saccade, there could be only a few saccadic segment and all the other segments are non-saccade. Thus, considering all the segments as saccade could misguide the artefact segment classifier, and decrease the reliability of artefact segment classification.

Overall, the proposed method compares favourably with the state-of-the-art ADJUST method in terms of percentage of correctly classified artefactual ICs, removing the variance explained by artefacts from the data, the SNR of the cleaned data and ERP classification. The main reason for the good performance is the consideration of data pre-processing conditions on the ICA source decomposition and artefact detection, coupled with the knowledge driven from the feature selection method with artefact features in time, frequency and spatial domains proposed.

"There is no knowledge and science like pondering and thought; and there is no prosperity and advancement like knowledge and science."

Imam Ali ibn Abi Talib (PBUH)

5

ENHANCED BLINK ARTEFACT REMOVAL VIA SPARSE SIGNAL COMPONENT ANALYSIS

5.1 Introduction

In Chapter 4, the common EEG artefacts, including blink, were automatically detected using ICA. Then, according to the conventional use of ICA, the entire ICs which identified as artefacts were removed to obtain the cleaned EEG data. Among the EEG artefacts, blink has been reported to be considerably more significant than the others [1,50,212–217],

and some studies are mainly targeted at blink artefact removal from the EEG data [162, 218–223]. This is due to the fact that, eyelids can be considered as one of the closest muscles to the scalp and, as mentioned in section 4.2.1, eyelid closure (i.e. blinking) produces tremendous amplitude in the EEG signal [224]. Additionally, the occurrence of the blinks in the EEG recordings is inevitable and subjects could not completely avoid blinking.

Conventional artefact removal methods were discussed in Chapter 2 section 2.5 and their advantages and disadvantages were outlined. Among those methods, ICA has been successfully employed to remove the blink artefact. However, its performance is not impeccable due to bidirectional interference of blink IC and EEG [185, 214], which leads to the loss of some useful cerebral information when the whole artefactual sources are removed.

The epoch-based method, as a basic approach to remove artefacts, has been used in several studies [225–229] to reject the epochs of multichannel EEG data that are contaminated by blink artefacts, by setting a predefined threshold value [224, 230]. The epoch-based method requires the detection of epochs contaminated by blink artefacts by calculating either some statistical measures such as kurtosis [143, 231] or correlation between EEG channels and the reference EOG channel [232,233]. However, a major drawback of epoch-based methods is the great loss of brain information which are buried in the rejected epochs.

Recently, Sameni et al. [2] demonstrated the separation of the ocular artefact was improved based on generalised eigenvalue decomposition in an iterative procedure. In this method, named DEFL, the EOG reference channel is used to detect the EOG and non-EOG segments in the EEG data by calculating the power of the signal within a moving window. Using generalised eigenvalue decomposition and wavelet denoising, the effect of blinking is reduced in an iterative procedure up to a satisfactory level.

In this chapter, the proposed artefact removal method (presented in Chapter 4) is further improved when targeting only blink as a major artefact contaminating the EEG

data. In contrast to the conventional use of ICA, where it is desirable to detect and remove the whole artefactual sources, only the blink segments of the blink ICs need to be removed for the blink artefact enhancement. Inspired by the DEFL method and by combining ICA and the epoch-based method mentioned in section 2.5, two methods are proposed to further enhance the blink artefact removal. As a consequence, the information loss both by ICA, due to the bidirectional interference of the blink IC and EEG, and by the epoch-based method, due to the rejection of the contaminated segments of multichannel EEG, is minimised. To this aim, first the blink ICs are detected automatically by the method proposed in Chapter 4. Then, in contrast to the conventional epoch-based method which is applied to multichannel EEG, the epochs including blinking are detected within the blink IC. Finally, the effect of blinking in the detected epochs is eliminated by means of two methods: time masking, and regression-based Sparse Component Analysis (SCA); then the cleaned EEG data is reconstructed. Two sets of simulated and real data are used to evaluate the proposed artefact removal approaches. The results of both proposed methods are compared to the DEFL method in terms of the normalised residual variance and BA of the ERP classification.

5.2 Methodology

In this section, two methods for blink artefact removal are presented. In both the proposed methods, first the AMICA ICA algorithm is applied to the EEG data to separate sources corresponding to the blink artefact from non-blink sources. The blink ICs are then detected by the automated artefact removal method proposed in Chapter 4, which was called *Proposed_method_IC*. Within the blink ICs, the data segments in which blinks occurred are detected by estimating the signal power within a sliding window. According to the first method, called *Time Masking*, the sample points of the blink segments in the blink ICs are set to zero and all other samples are kept intact. The cleaned EEG data is then reconstructed. In the second method, the blink signals estimated by SCA

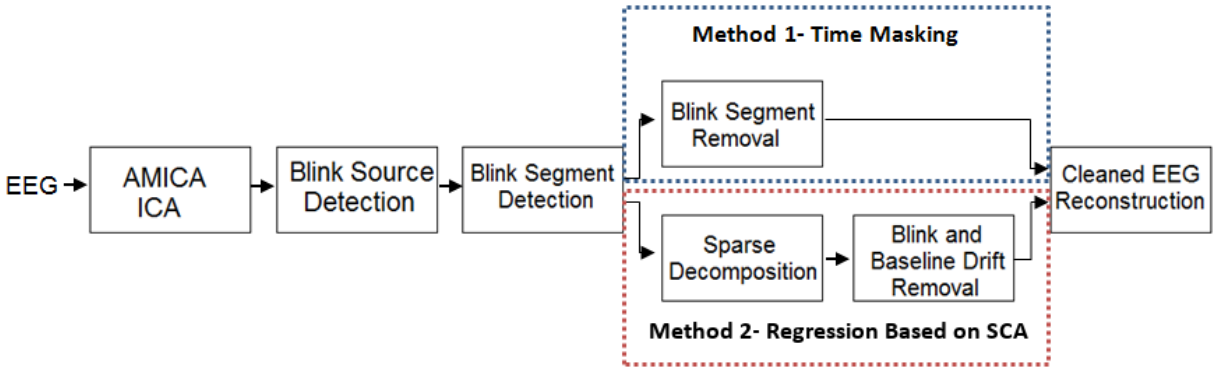

Figure 5.1: Diagram of the proposed methods for removing the blink artefact from the data.

are regressed out from the blink segments. Finally, the obtained results are reported and compared with the employed DEFL method. The proposed methods are overviewed as a digram in Figure 5.1.

5.2.1 Blink Segment Detection

According to the previous studies [162,234,235], blinking produces large amplitude peaks in the data with a duration of less than $500ms$ [220,236]. In order to detect blink segments (i.e. the intervals that blinks occurred in the data), the average power of the blink ICs' samples is calculated over a $500ms$ moving window, which is shifted over a sample at a time, after removing the mean of the signal. This method is similar to that in the DEFL method:

$$P(t) = \frac{1}{L} \sum_{l=-\frac{L}{2}}^{\frac{L}{2}} blink(t+l)^2 \tag{5.1}$$

Where L is the discretised length of the moving window defined as:

$$L = window\,length \times sampling\,frequency \tag{5.2}$$

The lower boundary of the blink segments is considered as the time that the calculated power, $P(t)$, exceeds a predefined threshold. Similarly, the upper boundary is when $P(t)$

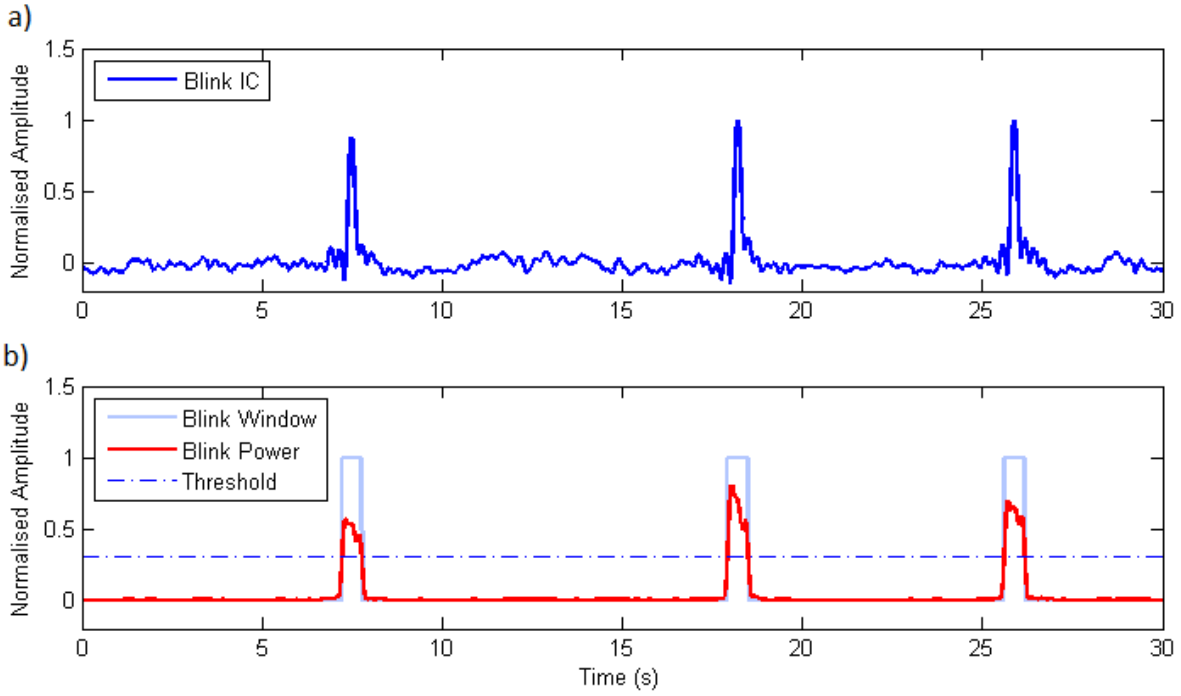

Figure 5.2: Sample of blink IC time series a), and the averaged power of the blink IC, red signal, to detect blink segments, blue squares b). The dashed line represents the threshold to separate blink and non-blink segments.

drops below the threshold value. The optimum threshold value is selected to be $50\mu V$ as previous studies have shown that the blink has a minimum amplitude of $55\mu V$ [237]. As a measure of percussion, any detected segments smaller than $50ms$ are not recognised as blink regarding the fact that typical blink duration is normally longer than $50ms$ [220,236].

Figure 5.2 shows a sample of a blink IC time series (Figure 5.2 (a)) and the averaged power calculated to detect the segments including blink (Figure 5.2 (b)).

5.2.2 Method-1: Time Masking

In the epoch-based method, rejecting the contaminated epochs of data result in considerable loss in the amount of data available for analysis, especially when the blinks occur frequently in the data [238, 239]. Time masking works in a similar way; however, instead of rejecting EEG channels, the contaminated segments of the blink IC are nullified. The motivation comes from the fact that, on the one hand, EEG is a sum of the weighted

source signals of the brain which is collected at each electrode site on the scalp. Therefore, rejecting a segment of the multichannel EEG data can be regarded as the loss of a mixture of source signals of the brain. On the other hand, the BSS and ICA algorithms are aimed to separate the constitutive EEG sources. Thus, rejecting a segment of an IC (e.g. blink IC) may leads to nullifying the specific source signal of interest in that IC. However, the source separation by the BSS and ICA is reported to be imperfect [240,241], which implies that the sources identified as artefacts (i.e. blink) may include both cerebral and non-cerebral information. Accordingly, in contrast to the typical application of ICA, where the entire blink ICs are being removed, it is suggested to only remove the blink segments and the EEG activity in all other segments, which may include cerebral information, is kept intact.

The time masking procedure is applied as follows:

$$S_i(t) = \begin{cases} 0 & \text{if } t = t_{blink} \\ S_i(t) & \text{otherwise} \end{cases} \tag{5.3}$$

Where, $S_i(t)$ is the ith source identified as blink, and t_{blink} is the time samples (within blink segments) where blinking occurred in the data.

5.2.3 Method-2: Regression-Based SCA

In the time masking method, the blink segments were completely removed by setting the samples to zero. Here, the blink artefact removal is further developed by only removing the effect of artefacts arising by blinking within the blink segments.

In this method, SCA is applied on the detected blink segments, described in section 5.2.1, to decompose the signals in the blink segment into blink and non-blink waveforms (signals). Then, the effect of blinking is removed by regressing out the SCA estimated blink waveform. In this section, first the principles of SCA are given followed by its implementation in this study.

Sparse Component Analysis

SCA belongs to the BSS family which utilises sparse representation to decompose the observation signals into multiple sources [242,243]. The concept of SCA was first introduced by Lewicki and Sejnowski [82], since then SCA has become a research hotspot.

Despite ICA, the main advantage of SCA is that it can deal with the under-determined problem, where the number of sources is more than the sensors [244–246]. Also, if underlying sources have Gaussian distribution or are dependent, they can be estimated by the SCA method. Therefore, in this study SCA can be used to decompose the blink segment in to blink and non-blink waveforms.

Based on the BSS equation outlined in section 2.1, the aim of SCA is to estimate the mixing matrix A and to extract sources S under the sparsity condition of the sources; which implies most samples in the source signals are nearly zero and just a few samples have significant values. Several definitions have been made on the sparsity of a vector; such as the *iteration optimisation approach* [247] that iteratively finds an optimal solution. Based on this approach, the source matrix S of the SCA model $X = AS$, is assumed as a linear mixture of a small set of predetermined signals from a much larger set of signals, called a *dictionary* [248, 249]:

$$\Phi = (\phi_\gamma : \gamma \in \Gamma) \tag{5.4}$$

Where Φ represents the dictionary and ϕ_γ is an individual waveform in that dictionary. Using this dictionary, the decomposition of a signal S of length N can be expressed as follows:

$$S = \sum_{\gamma \in \Gamma} \alpha_\gamma \phi_\gamma \tag{5.5}$$

Where α_γ is an unknown weight and ϕ_γ is a waveform in the dictionary.

In practice the SCA algorithm may not decompose the original signal precisely [250]. Therefore, an approximate decomposition, by considering a noise R, can be defined as

follows:

$$S = \sum_{\gamma \in \Gamma} \alpha_\gamma \phi_\gamma + R = \Phi\alpha + R \tag{5.6}$$

Where R represents some residual error vector for the decomposition process and it should be as small as possible or below a specified threshold.

To measure the sparsity of the signal, the $l1$ norm, $\|...\|_1$, is employed in this study [251]:

$$\|\alpha\|_1 = \sum_{i=1}^{N} |\alpha_i| \tag{5.7}$$

The principle of the method is to find the source waveforms, which lead to the sparsest solution (i.e. the lowest $l1$ norm), by an optimisation process such that the residual error is minimised:

$$\min \|\alpha\|_1 \text{ subject to } \|\Phi\alpha - S\|_2 \leq \varepsilon \tag{5.8}$$

Where ε is a user specified parameter (minimum error).

Artefact Removal

For sparse decomposition, the source signals contributing to the mixed signal within the blink IC should be predetermined and modelled. It is assumed that the signals within the blink segments are blink and non-blink (e.g. cerebral) sources which are linearly mixed. A DC drift is also considered for the mixed signal within the blink segment, which causes it to be shifted. The shape of the blink signal (peak) is similar to a Gaussian distribution and so it can be modelled by a set of Gaussian waveforms [252].

DC drift is characterised with a low frequency dominance, and can be modelled by a set of low-frequency sine and cosine waveforms [253]. The non-blink signal (cerebral) can be considered as an additive noise to the blink signal, and can be modelled by an identity matrix to reflect and fit to the remaining data. Therefore, the mixed signal within the blink segments can be decomposed into three types of parameterised waveforms.

The above predetermined source signals, ϕ_γ, form the dictionary Φ (Equation 5.4). At

each iteration a sum of the weighted source signals in the dictionary is obtained and the residual error in Equation 5.4 is calculated. The optimum estimation of the sources is achieved when the sparsest solution leads to the minimum error.

Once the sources are estimated, the blink signal waveform is regressed out, by subtracting the Gaussian model of the blink from the blink segments. The blink artefact-free data is then obtained by backprojecting the remaining signals. In this manner, the EEG activity within the blink segments is preserved.

5.3 Evaluation

The performance of the proposed blink artefact removal methods, time masking and regression-based SCA, are evaluated by means of the simulated and real data. The evaluating performance measures are described in section 5.3.3.

5.3.1 Simulated Data

The simulated data contains both normal ongoing EEG activity and the blink artefact. First, the normal EEG is generated based on Multivariate Autoregressive model (MVAR) [254] as employed in [2]. Then, the EOG signal, which contains blink peaks, is simulated by mixing a set of Gaussian waveforms. Finally, the normal EEG and blink waveform are combined to generate the simulated EEG contaminated with the blink artefact. Details of the generating normal EEG and blink artefacts are given in the following sections.

Ongoing EEG Activity

Using the MVAR model, the ongoing EEG activity can be represented as the weighted linear combination of a previous EEG observation plus a random uncorrelated input:

$$EEG(t) = -\sum_{i=1}^{p} A_i EEG(t-i) + e(t) \tag{5.9}$$

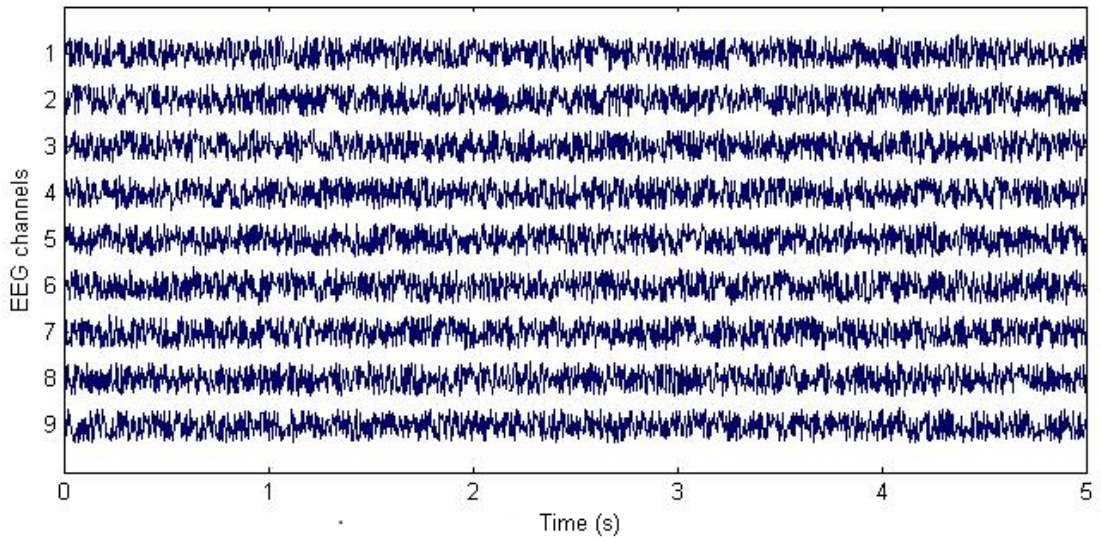

Figure 5.3: A sample of 9 channel EEG data generated by MVAR model with order of $p = 8$, within $5s$ time interval.

Where, $EEG(t)$ is a n-dimensional discrete (sampled) EEG signal, recorded at n channels, at time t, and $e(t)$ is a n-dimensional vector of unknown uncorrelated random variables with mean of zero, randomly selected from the uniform distribution $U(-1, +1)$.

$A(i)$, for $i = 1, ..., p$ is the $n \times n$ matrix of auto-regression coefficients, which are randomly selected from the uniform distribution $U(-0.25, +0.25)$ (i.e for all i, $A(i) \sim U(-0.25, +0.25)$) [255]. The value of p represents the order of the MVAR model, which refers to the number of preceding EEG samples to be combined to generate each sample of the ongoing EEG activity. The output of the MVAR model is assumed to be artefact-free normal EEG data.

Figure 5.3 depicts an instance of $5s$ of EEG data with 9 channels ($n = 9$) outputted from an 8 order ($p = 8$) MVAR model with $250Hz$ sampling rate. The output of MVAR is considered as being similar to normal ongoing EEG data. The real EEG recording is a mixture of different activities originating from cerebral and non-cerebral sources, which can be separated by ICA. However, as the main focus of this experiment is to remove the effect of only the blink artefact segments within the blink IC estimated by ICA, it is not

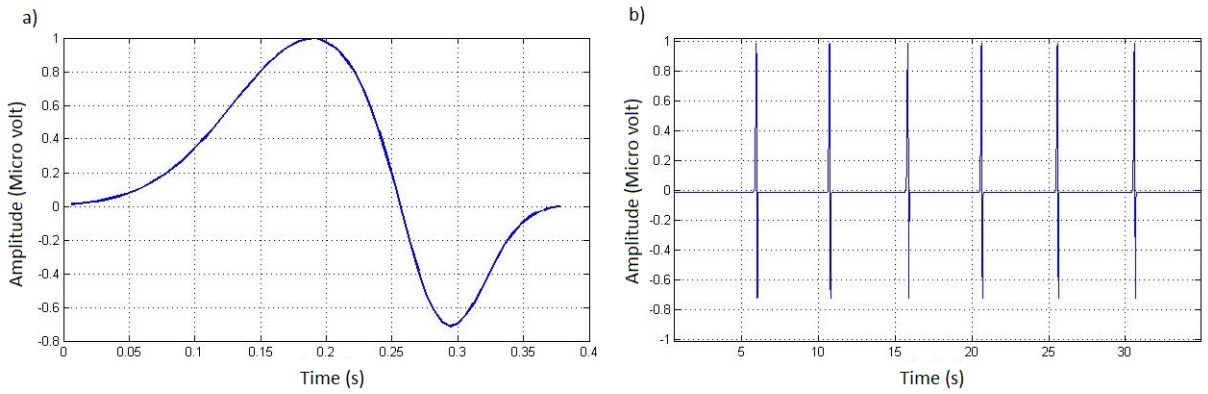

Figure 5.4: The simulated blink modelled by two Gaussian waveforms a); and the repetition of blinking every 5 seconds to generate a blink signal b).

necessary to consider all other possible sources of activities of the real EEG data in the simulated EEG. The sampling rate and order of the MVAR model is selected according to the suggestions in [2].

Blink Artefact Signal

A mixture of two Gaussian waveforms is used to model the blink peak with unity amplitude and a duration of about $400ms$ (Figure 5.4 (a)), as the typical blink duration is reported to be less than $500ms$ [236]. The simulated blinking is then repeated every 5 seconds (based on the normal blinking rate reported in section 4.2.3) to generate a blink signal (Figure 5.4 (b)). In real EEG data the changes in the blink amplitude may be more abrupt which may not be perfectly fitted by a Guassian waveform, or there may be cases where there are large temporal variations to the periods of the repeated blinks. In the simulated blink model of this study, those cases are neglected.

The amplitude of a typical blink artefact could be several times larger than the brain scalp potentials [213]. However, the amplitude of the real eye blink usually varies due to factors such as eye dryness and fatigue [48]. Therefore, a scale parameter, β, is also needed to adjust the blink amplitude relative to the EEG amplitude. Hence, the parameter β is tuned in a way that the ratio of the power of the artefact-free EEG signal to the power

of the blink artefact signal varies between $-50dB$ and $0dB$ with $5dB$ step [2]:

$$SNR = 10 \log \left(\frac{EEG}{\beta \times blink} \right) \tag{5.10}$$

Where *blink* is the simulated blink signal. The $0dB$ SNR refers to the case where the amplitudes of the EEG and blink signal are similar, while the $50dB$ SNR represents the largest blink amplitude relative to the EEG.

Multichannel EEG Contaminated with Blink Artefact

In order to mix the blink artefact and EEG and to generate a simulated multichannel EEG contaminated with blink artefact, a set of weights are required to show the effect of blink on the EEG channels. The blink artefact affects the EEG channels with regards to the distance between EEG channels and eyes (i.e. the frontal channels are impacted most by eye blinks). The weights are generated based on the method proposed by Gouy-Pailler [256]. For EEG data with n channels, n weights, k_i $(i = 1 \cdots n)$, are randomly extracted from the normal distribution $N(1, 0.3)$ (i.e. for all i, $k_i \sim N(1, 0.3)$). Therefore, the simulated EEG and blink signals are mixed, and artificial EEG contaminated by the blink artefact is generated, as follows:

$$x(t) = \text{EEG}(t) + \beta(k_1 ... k_n)^T \, \text{EOG(t)}. \tag{5.11}$$

Where EEG(t) is the normal artefact-free EEG generated by the MVAR model, β is the parameter to tune the power ratio between blink and EEG between $-50dB$ and $0dB$, and EOG(t) is the simulated blink segment.

Figure 5.5 shows the simulated 9 channel EEG data, $x(t)$; the normal EEG data, (i.e. $EEG(t)$) is generated by an 8-order MVAR model and the blink artefact is added to the EEG data with SNR values equal to $0dB$ (Figure 5.5 (a)) and $-30dB$ (Figure 5.5 (b)), respectively. As evident from the figure, when SNR= $0dB$ the amplitude of the blink artefact signal is very small and the effect of the blink artefact is not strong compared to

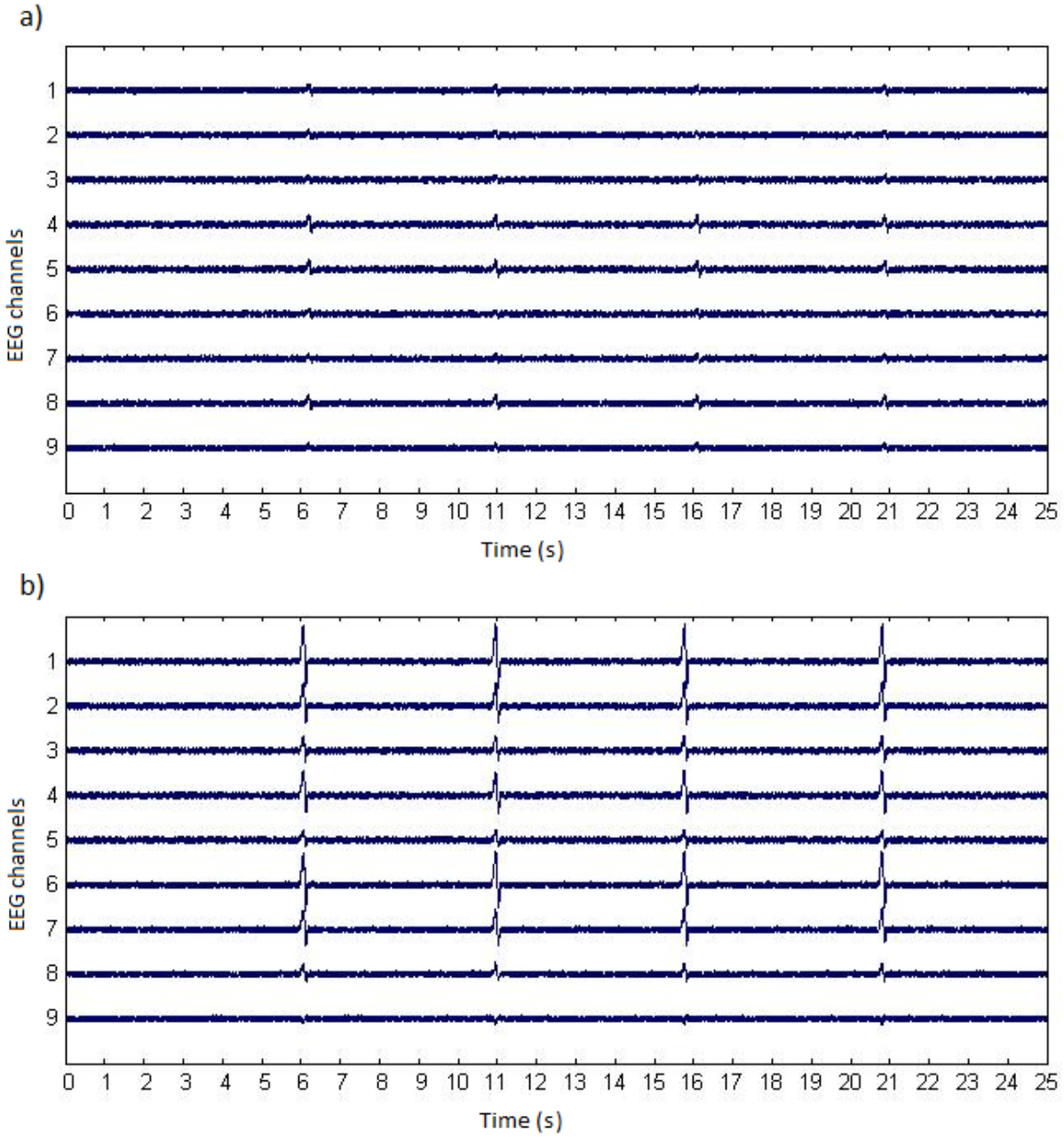

Figure 5.5: The effect of the blink artefact on the EEG channels, with SNR equal to: a) $0dB$ and b) $-30dB$.

the $-30dB$ SNR, where the blink artefact had a large affect on the EEG.

5.3.2 Real Data

As in the previous chapters, the same data described in section 3.2.1 is used to evaluate the proposed artefact removal method.

5.3.3 Evaluation Measures

To assess the performance of the proposed methods using the simulated data, the measure of normalised residual variance on each channel [2] is used;

$$\eta = \frac{var(\epsilon(t))}{var(EEG(t))} \tag{5.12}$$

where,

$$\epsilon(t) = EEG(t) - EEG_c(t) \tag{5.13}$$

Where $var(.)$ denotes variance; $EEG(t)$ is the artefact-free EEG signal; $EEG_c(t)$ is the EEG signal cleaned by the proposed methods and $\epsilon(t)$ is the cleaning error.

The objective is to make the value of $\epsilon(t)$ as small as possible. Therefore, the lower the η, the better the artefact removal is performed. In order to obtain the normalised residual variance of a multichannel EEG data, the normalised residual variance is calculated for each channel and added together.

In order to evaluate the performance of the proposed methods using the real EEG data, the ERP classification rate is calculated based on the method employed in section 4.3.6.

5.4 Results Analysis

In this section, the two proposed methods for removing blink artefacts from EEG data are applied to real and simulated data. The obtained results are then compared to the results of when the DEFL method and the proposed artefact removal method proposed in Chapter 4 (Proposed_method_IC), has been applied to the data. The statistical significance of the results is obtained by performing simple t-test at $p<0.05$.

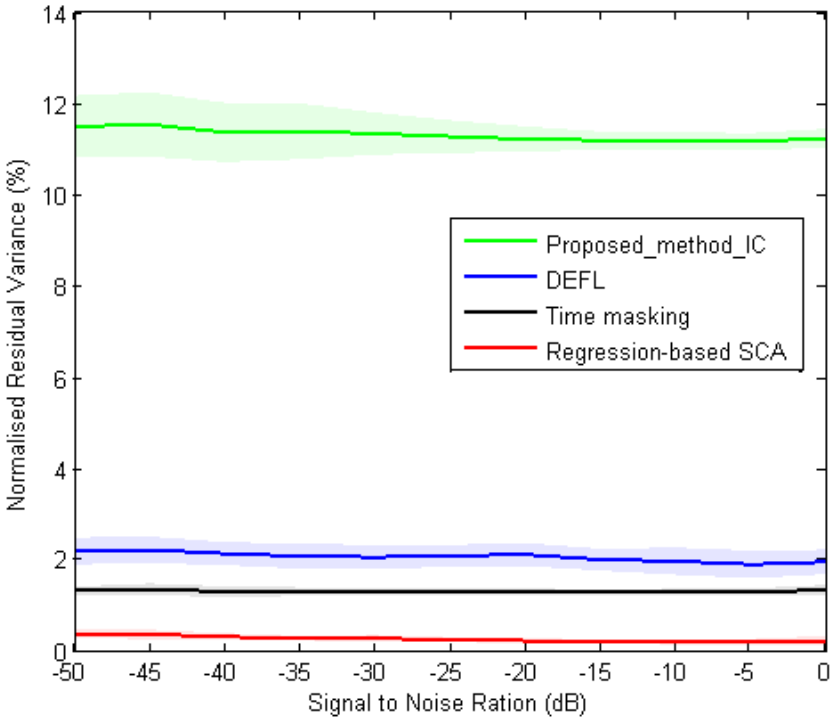

Figure 5.6: The normalised residual variance obtained for time masking, regression-based SCA, DEFL and the Proposed_method_IC blink artefact removal methods, for different SNR values. The shaded area around the graph lines represents the error bars of the averaged normalised residual variance across subjects.

5.4.1 Simulated Data

Figure 5.6 shows the residual variance obtained by four different approaches: removing the whole blink IC using the Proposed_method_IC, removing the blink segments by time masking and the regression-based SCA methods, and eliminating the blink artefact from the EEG channels using the DEFL method.

For each method, the residual variances are plotted versus different SNR values from which the simulated data is generated. For each SNR value, 100 different 9-channel simulated EEG data are randomly generated and the average residual variance is reported.

As shown in the figure, when the entire blink IC is removed by means of the Proposed_method_IC, the average residual variance obtained is approximately 11% associated with removing one IC from the 9 channel EEG data, which is equal to $\frac{1}{9}$ of the

total energy of the simulated data. It is also notable that the variance in this technique is significantly higher compared to the other techniques. This shows the uncertainty of the ICA in removing the simulated blinks with small amplitude from the data. As the blinking does not occur continuously at all times in the EEG data, removing the whole blink IC may result in non-blink information loss. Therefore, a large amount of signal energy is lost. This can be confirmed by comparing it to the result obtained by the time masking method in which only blink segments are removed from the blink IC. On average the outcome is significantly improved by 10% to 1.09% ($p = 0.01$).

The result is a further improvement from less than 1% to 0.35% by the regression-based SCA where only the impact of the blink artefacts are removed from blink segments within blink ICs, compared to the time masking method. The reason for the poor performance of the time masking method compared to the regression-based SCA is that there are still some EEG data combined with the blink signal in the blink segments; by removing the whole blink segment those EEG data are also lost.

However, the obtained results of both proposed methods are improved compared to the DEFL method. This might have happened because of the ability of ICA in source separation, in that most blink activities could be separated in the blink sources. Thus, by considering the blink segments in only blink ICs, more blink signal can be thrown away from the data, while more non-blink signals in the data can be saved.

The best performance is achieved by the regression-based SCA method, as evident from the results; in which the effect of the blink artefact is regressed out from automatically detected blink segments of the blink ICs. This is followed by the time masking method in which the amplitude of the blink segments within the blink ICs is set to zero. The worst results are obtained by the conventional method in which the amplitude of the whole blink IC (or its corresponding weights in the weight matrix) is set to zero.

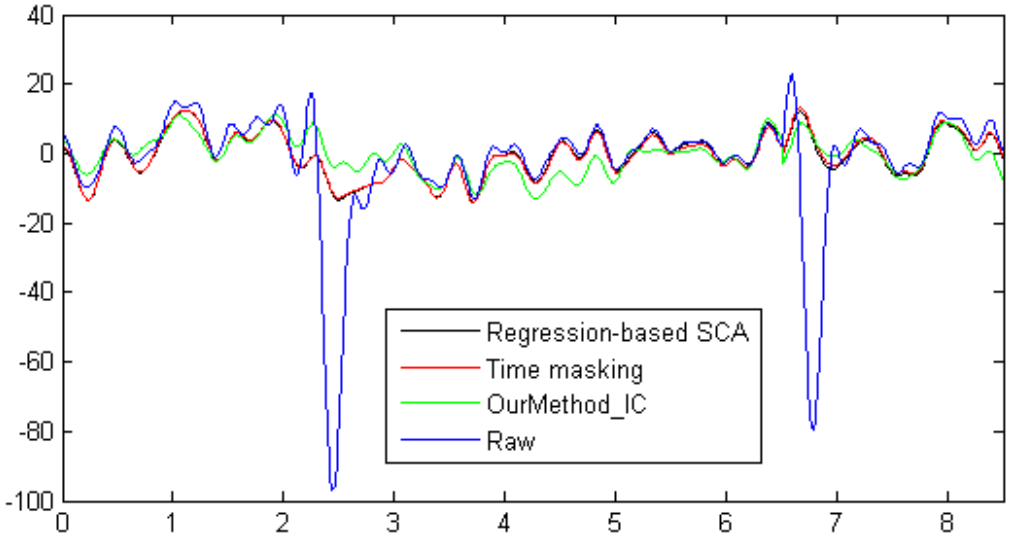

Figure 5.7: Blink artefact correction by the time masking, the regression-based SCA and Proposed_method_IC methods are compared at a frontal channel of the raw EEG, which includes blinking (Raw).

5.4.2 Real Data

Figure 5.7 shows the effect of the blink artefact on a frontal channel of the raw EEG, compared to the associated cleaned channel by the proposed blink correction methods: time masking, regression-based SCA, and Proposed_method_IC where the whole blink IC is removed.

As illustrated in the figure, all three methods removed the effect of blinking with relatively good performance. However, outside the blink peak, the cleaned data by the time masking and regression-based SCA methods are more similar to the original raw data, than the cleaned data by the Proposed_method_IC. This proves more EEG data preservation by the first two methods than by removing the whole blink IC. There exist a difference between the cleaned data by time masking and regression-based SCA methods, however this difference is not obvious in the figure.

Figure 5.8 shows a fragment of multichannel EEG data including the EOG channel, which is contaminated by blink artefact; and Figure 5.9 illustrates the same segment of data, in which the effect of blink artefact is eliminated by the regression-based SCA

method.

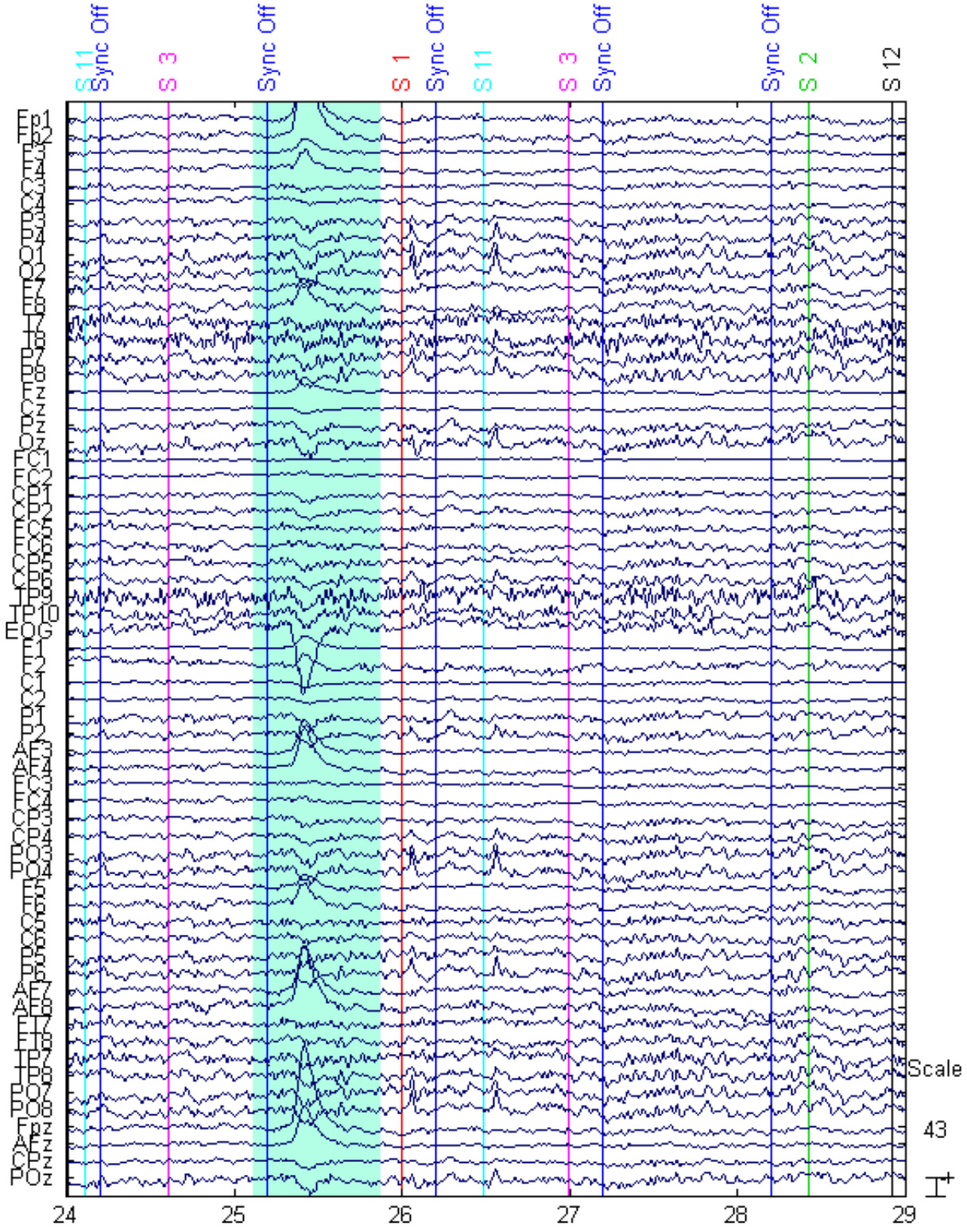

Figure 5.8: A fragment of multichannel EEG data contaminated by blink artefact. The highlighted segment of data shows the effect of blinking within EOG channel, on other channels of data.

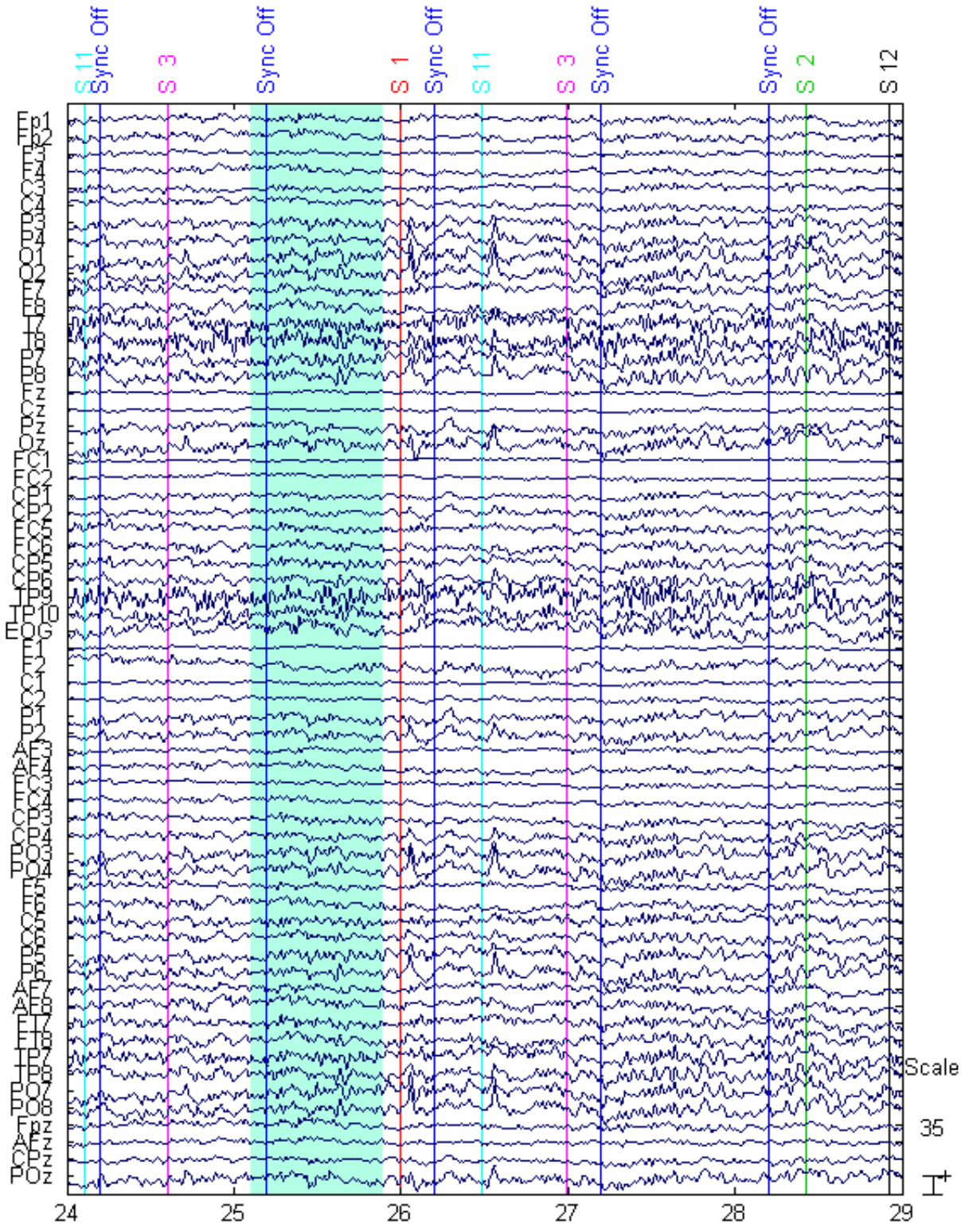

Figure 5.9: A fragment of multichannel EEG data cleaned by the regression-based SCA method. The highlighted segment of data shows the effect of blinking within EOG channel, on other channels of data, after performing regression-based SCA to remove blink artefatcs.

Table 5.1: Comparison of the blink artefact correction methods: the proposed automated artefact removal method 'Proposed_method_IC', time masking, regression-based SCA and DEFL methods, in terms of balanced accuracy and standard deviation calculated for ERP classification.

	Proposed_method_IC	Time masking	regression-based SCA	DEFL
BA (%)	66.32 ± 0.61	68.36 ± 0.65	68.36 ± 0.65	67.88 ± 0.51

Table 5.1 shows the accuracy of ERP classification for the real cleaned data after removing the blink artefact by different methods. Based on the results, the time masking and regression-based SCA methods performed the same and achieved the highest results ($BA = 68.36\%$), followed by the DEFL method ($BA = 67.88\%$). The worst performance was obtained when the whole blink IC was removed from the data. However, the obtained ERP classification BAs are almost similar and their difference is not statistically significant ($P > 0.05$). The reason is that based on the datasets used in this research, almost none of the blinks occurred within the ERP target segments. Therefore, the ERP classification rate may not be affected significantly by the existence or the removing of the blink artefacts. This can be confirmed by the results presented in Figure 4.13, where the difference between the raw and other artefact-free datasets is statistically insignificant in terms of ERP classification accuracy. Therefore, ERP may not be a good evaluation criterion here for comparing the performance of various artefact removal methods employed in this study. However, they can be compared in terms of the residual variance reported in section 5.3.3.

Generally, the proposed ICA-based methods improved the SNR and ERP classification results when compared to the conventional ICA-based artefact removal methods, which remove the whole artefactual ICs. Additionally, the proposed methods outperformed the DEFL method (however statistically insignificant) in terms of residual variance for simulated data and ERP classification BA for real data.

5.5 Summary

Following on from the proposed ICA-based artefact removal method in the previous chapter, the blink artefact removal is further improved by proposing a SCA-based method in this chapter. The aim was to remove blinking from the blink IC and within the preselected segments. As the blink IC separated by ICA is not a pure blink source and contained other source signals, the amount of non-blink signal discarded from the data is minimised resulting in a higher residual variance. However, this improvement was not achieved in terms of ERP classification, as the employed datasets in this research mostly do not include blinking within the ERP target intervals. Accordingly, the ERP classification rate is not affected significantly by removing blinking. The performances of the proposed methods were compared to the recently related study that claimed to enhance blink artefact detection. Based on the results obtained in terms of the residual variance, the proposed methods performed better and the blink artefact removal was further improved.

"Knowledge and science are the fruit of paradise; in times of threat it is one's ally, in exile it keeps one company, and in solitude it is one's intimate friend and companion."

Imam Muhammad al-Baqir
(PBUH)

6

ICA-BASED EVENT-RELATED POTENTIAL CLASSIFICATION

6.1 Introduction

Prior to this point of the research, with the purpose of getting a better interpretation of the brain's responses and underlying neuronal processes, the artefact-contaminated EEG, recorded during an ERP stimulation paradigm, underwent a pre- and post-ICA processing chain. In Chapter 4, an EEG artefact removal method was proposed and the ERP features were extracted from the cleaned EEG data. In Chapter 5, the proposed artefact removal method was further improved by means of the optimised blink artefact removal method,

resulting in a larger SNR. However, it did not affect the ERP classification rate.

As mentioned in Chapter 2, ERPs are electric potentials produced in the brain in response to a particular internal or external stimuli [257]. Based on the type of stimulus, various regions of the brain are activated and respond to that specific stimulus. These brain responses can be collected during EEG recordings to understand the underlying brain function.

As a result of the volume conduction of different layers of the brain, including the scalp and skull, the EEG signal is attenuated and spread over the scalp (section 2.4). This may suggest that more channels placed on the scalp can provide more ERP information. However, using an excessive number of channels causes an issue known as "the curse of dimensionality" that leads to poor performance of the ERP classification [258]. Thus, optimum channel selection can play a crucial role in ERP studies. Several studies have reported that optimised channel selection can improve the ERP classification rate [258–264].

Conventionally, the ERP features are extracted from the relevant EEG channels located on a certain region of the scalp relative to the type of stimuli, by human-based methods. This mainly relies on prior knowledge about the type of stimuli in the experimental paradigm or in the empirical findings in the previous literature. However, this leads to a fixed subset of channels that can endanger the performance of the ERP classification, as the optimal ERP channel subset is highly subject dependant and can vary between subjects [260, 265]. Also, Blankertz et al. [266] reported that it does not necessarily yield optimum ERP classification rate compared to using all EEG channels.

More advanced methods assess individual channel effectiveness in a discriminative manner such as recursive backward channel elimination [263], which is derived from the recursive feature elimination method proposed by Guyon et al. [267]. These techniques suffer from expensive computational cost and are time-consuming. Besides, other common methods for channel selection are established based on a spatial filter [268, 269]. The state-of-the-art xDAWN algorithm [3, 270] reported an enhancement in the ERP response

using a spatial filter, yielding better ERP classification accuracy. However, the xDAWN algorithm has one main drawback: it requires some prior knowledge about the stimuli and subjective configuration of the filter dimension itself.

In this chapter, ERP response classification is enhanced; first, an iterative backward channel elimination method is employed to select the informative EEG channels containing more ERP information. The result is compared to the human-based channel selection method used in Chapter 4 section 4.3.6. Then, an ICA-based approach is proposed to further improve the ERP classification rate. In contrast to the conventional ICA-based methods, where ICA is used for separation and removal of the artefactual sources contaminating the EEG data, an ICA-based method is proposed here to automatically detect the sources with most ERP information (ERP task-related ICs) based on their temporal, spatial and frequential characteristics. The detected task-related ICs are considered as the observation vectors for ERP analysis and all other ICs are discarded. In this approach, the task-related ICs are used for ERP feature extraction; and discarding all non-task-related ICs leads to a considerable reduction in the dimensionality of the ERP features.

The proposed method is used for classification of ERP responses within the data described in Chapter 3 section 3.2.1. The reliability of the ERP classification accuracy, obtained by the proposed ICA-based method, is compared with that obtained by means of the state-of-the-art algorithm, xDAWN.

6.2 Methodology

This section first presents the channel selection method "recursive channel elimination", which iteratively eliminates channels with the least ERP information and selects the optimum set of channels leading to the highest ERP classification accuracy. The aim of using "recursive channel elimination" method is to demonstrate the importance of employing a channel selection method and to show how the appropriate channel selection impacts ERP classification result.

Secondly, an ICA-based ERP classification method is proposed, which employs the AMICA algorithm to decompose EEG data into sources containing ERP responses (task-related ICs) and the sources without ERP responses (non-task-related ICs). The task-related ICs are automatically detected based on the two layered source classification algorithm employed in Chapter 4 section 4.2.3. Then, the ERP features (described in section 4.3.6) are extracted from the detected task-related ICs, which are a new representation of the most relevant ERP response sources. Next, the extracted features are entered into an NB classifier for ERP classification. With this method, applying an optimum channel selection algorithm and employing an efficient artefact removal method are no longer needed. Additionally, the dimensionality of the data is significantly reduced.

6.2.1 Recursive Backward Channel Elimination

In order to select the optimum set of task-relevant channels with the largest amount of ERP information, first all the EEG artefacts are cleaned using the ground truth described in section 4.3.1, then the recursive backward channel elimination method is employed. The recursive backward elimination is a prominent approach to single out k channels of n channels. The algorithm was initially introduced as a feature selection strategy in the same frame of reference as recursive feature elimination [267] and can easily be applied to channel selection situation [271].

It starts with a complete set of n EEG channels input to the ERP classification method. The idea is to evaluate the ERP classification accuracy of all possible combinations of channels' subsets of size $n-1$. It is assumed that the subset with most amount of ERP information leads to the maximum ERP classification accuracy. Therefore, the channel subset with highest ERP classification accuracy is considered as the input for the next iteration and the nth excluded channel in that subset is eliminated for the rest of the evaluation. The excluded channel in each iteration represents the least contribution to the ERP; thus introducing the minimum impact on ERP classification accuracy. This process is performed continually until all the n channels are eliminated. Then, among all

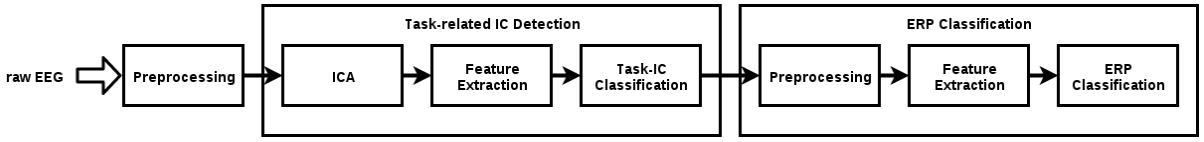

Figure 6.1: Block diagram of the proposed two-stage ICA-based ERP classification method.

iterations a channel subset associated with the highest ERP classification is considered as the optimum channel subset.

6.2.2 ICA-based ERP Classification

In this section, an ERP classification method is proposed which is based on extracting features from the task-related sources estimated by ICA. In the previous section 6.2.1, the recursive backward channel elimination method was used to select the optimum EEG channels encompassing most ERP information from the artefact-free data. However, in the current proposed method, ICA is used to separate task-related sources from all other sources of activity within the EEG observations; and the sources encompassing most ERP information are selected, prior to the ERP feature extraction [272]. Figure 6.1 illustrates the proposed ICA-based ERP classification approach. It consists of two classification stages; *Automatic task-related IC detection* and *ERP classification*. In the first stage, the task-related ICs are obtained by automatically labelling ICA decomposition according to their characteristics in time, frequency and spatial domains. In the second stage, a feature vector is extracted from the labelled task-related ICs and used as an input for ERP classification.

6.2.3 Stage 1: Automatic Task-related IC Detection

In the first stage, the full-length EEG channel signals are decomposed into ICs by the ICA algorithm variant AMICA [65], which has been reported to give better performance over other ICA algorithms for separating EEG sources [104, 114]. A knowledge-based approach to the feature selection is followed, based on the characteristics of the expected

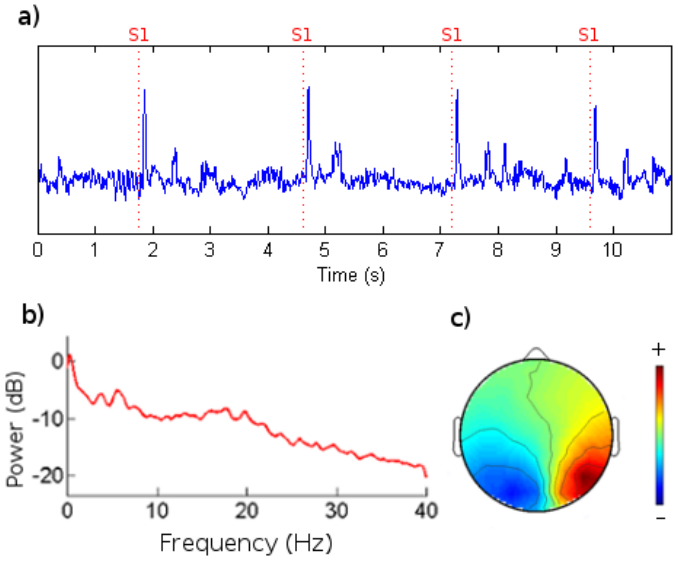

Figure 6.2: An example of spiky activation of a task-related IC over time (a), higher spectral power in low frequency contents (b) and the activated region of scalp, occipital lobe, in response to the stimulus (c).

task-related components in temporal, frequential and spatial domains. For example, based on the visual stimulation used in this research, large amplitude deflection is expected to occur in EEG channels placed over the visual cortex, after stimulation. Therefore, ICs with spiky activation in time and prominent activation in the occipital lobe can be considered as task-related components in this experiment. The task-related ICs are distinguished from all other ICs using the following classification procedure:

1) A set of temporal, spatial and frequential features are extracted from 7 seconds epochs of all the ICs' time series. The length of the selected segments, 7 seconds, is selected regarding the experimental paradigm of the data and ensures that in each segment at least one occurrence of a full stimulus response period is presented. Within each IC of an approximate length of 7 minutes, 60 segments are considered, each of the length of 7 seconds, with no overlaps. The total amount of segments for each dataset is 3840 segments (64 ICs $\times$ 60 segments).

- *Temporal features*: The task-related IC has a spiky activation over time, $100ms$ after $S1$ stimuli onset (Figure 6.2 (a)). Therefore, the distribution of task-related ICs does not follow a Gaussian distribution. Because ICA does not guarantee signs

of the estimated ICs, the absolute values of the skewness and kurtosis are considered as temporal features.

- *Spatial features*: The topography of the task-related IC has a projection pattern on the electrodes positioned in the occipitoparietal lobes (Figure 6.2 (c)). The averaged topography weights of the electrodes, estimated by ICA decomposition, placed in frontal, central, temporal and occipitoparietal lobes, are exponentiated to the power of 1, 2 and 3 and used as spatial features, representing the spatial characteristic of the task-related sources. Similarly to the muscle artefact detection described in Chapter 4 section 4.2.1, the number of features is increased non-linearly by using the combination of different exponentiated weights which can enhance the performance of a classifier in discriminating the task-related sources from non-task-related sources. The topography weights are exponentiated to expand the gap between the affected weights by task-related cerebral activity and other types of activities. When higher powers (greater than 3) are employed, the small weight values in the range 0 to 1 are inclined to be zero. Therefore, due to the curse of dimensionality and to prevent the loss of information, the higher powers, greater than 3, are not selected.

- *Frequential features*: Based on the stimulus paradigm in this research, the higher spectral power of the task-related IC is observed in low frequency contents (Figure 6.2 (b)). The power spectrum of ICs is estimated by the Welch method [192]. The estimated frequency contents from $1Hz$ to $39Hz$ are considered as spectral features.

2) The extracted features are then served as the input to the NB classifier to detect task-related segments within the task-related sources. Consequently, similar to section 4.2.3, task-related sources are detected based on the outcome of the segment classification. First, the ICs' scores are obtained by the summation of the probabilities of corresponding 60 segments belonging to a task-related class. Secondly, the ICs scoring

higher than a specified threshold (determined empirically) are labelled as task-related sources.

6.2.4 Stage 2: ERP Classification

The ERP classification method is similar to that described in section 4.3.6. Once task-related ICs are detected, the amplitude of their samples is considered as an ERP feature. The samples from $60 - 500ms$ after the $S1$ stimuli onset are considered as target (ERP) instances. No-target (noERP) instances are extracted from $1060 - 1500ms$ after $S1$ stimulus onset, in which there is no stimulus response. The extracted samples are resampled from $250Hz$ to $125Hz$, to reduce processing and storage cost, which provides 55 features. Feature vectors are generated by concatenating the extracted 55 samples of ERP and no-ERP from each channel and used to train the classifier models for ERP detection.

6.2.5 xDAWN Algorithm

The spatial filtering algorithm advanced by Rivet et al. [270], namely xDAWN, attempts to define an estimation of the subspace of pseudo channels which contains ERPs. It employs a Bayesian linear discriminant analysis and attempts to maximize the Signal to Signal plus Noise Ratio (SSNR) to enhance the quality of the estimated signals [270].

In order to apply the xDAWN algorithm to the data, OpenVibe software which is developed by Renard et al. [273] is employed in this study. The xDAWN algorithm should first be trained by defining the stimulus response interval. For this purpose, EEG data fragments from $70ms$ to $500ms$ after stimulus onset (S1) are given. Then, the optimum number of output channels has to be set. In the original research by Cecotti et al. [260], xDAWN succeeded in reducing the number of channels from 32 to 10 with nearly the same classification success rate of 94%; and to 5 channels with a similar performance of 92%. In this experiment, the EEG is recorded using 62 scalp electrodes. Therefore, a similar dimension reduction evaluation by xDAWN is carried out in this training.

6.3 Evaluation

The proposed task-IC detection method is validated by comparing it to the ground truth, which is created by manual labelling of the task-related ICs by two experts. The performance measures of sensitivity, specificity and BA (described in section 4.3.2) are used to evaluate the performance of the task-related IC detection and ERP classification methods.

The EEG recordings of 10 individual subjects used in Chapter 3 section 3.2.1 and the $10-fold$ cross validation technique explained in section 4.3.7, are also employed in this chapter. For task-related IC classification, the feature vectors extracted from each subject are taken as a fold. Thus, at each of the 10 iterations, the feature vector of a subject are taken as a test and the feature vector of the other 9 subjects are taken as training data. Therefore, the task-related IC classification system's BA for each artefact type is obtained by averaging the obtained BAs at all 10 iterations. For ERP classification, the 10-fold cross validation is used for evaluating the BA of ERP classification for each subject individually. Therefore, the obtained BAs are averaged over all 10 subjects and the final BA is reported.

6.3.1 Visual Inspection

A ground truth for task-related ICs is created. All ICs were manually labelled as task-related or non-task-related by visualising IC time courses, topographies and the power spectrum, using the EEGLAB software package [172]. ICs were labelled in a blind procedure, by two independent experts who were familiar with EEG analysis and ICA decompositions. The ground truth (GT), including 20 task-related ICs, was created by considering the in common voted task-related ICs between both experts' classification. The level of agreement between classifications performed by the two experts was 100.00%.

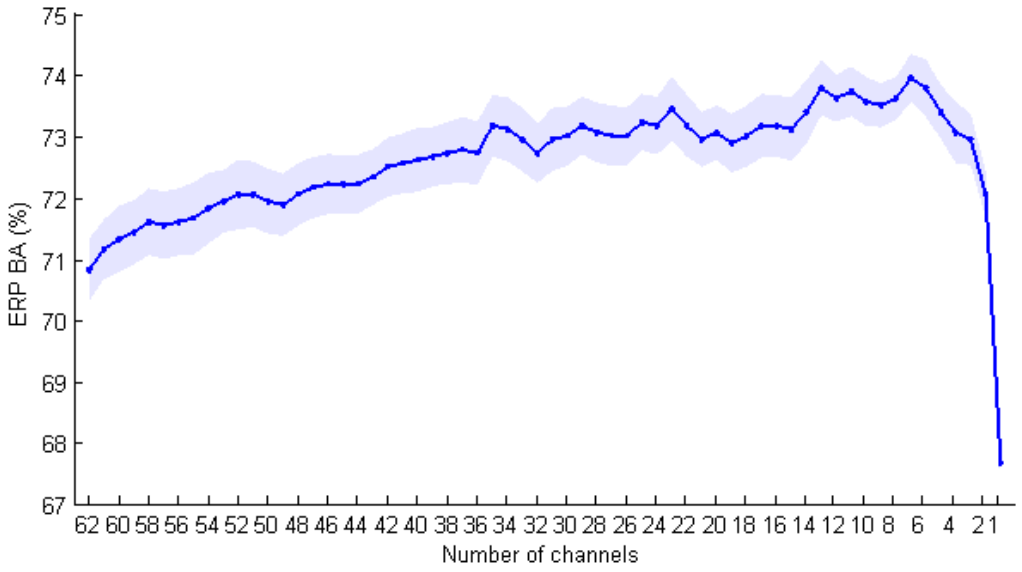

Figure 6.3: The ERP classification rates obtained by the recursive backward elimination method for each set of channels at each iteration. The cleaned data is obtained by removing the artefacts labelled in the ground truth. The shaded area around the graph line represents the error bars of the averaged ERP classification accuracy across subjects.

6.4 Results Analysis

The recursive channel elimination method is employed to enhance the ERP classification accuracy. The result is then compared to the human-based channel selection used for ERP classification in section 4.4.3. Also, the accuracy of the proposed ICA-based ERP classification method is compared with the state-of-the-art channel selection algorithm, xDAWN and the outcome is reported in terms of BA. The statistical significance of the results is obtained by performing simple t-test at $p<0.05$.

6.4.1 Recursive Backward Channel Elimination

Figure 6.3 illustrates the averaged BA of the ERP classification obtained from all possible channel combinations, selected by the recursive channel elimination method. The method is applied on the cleaned (artefact-free) EEG data.

The ERP classification accuracy obtained by using all 62 EEG channels is shown in the figure (left side). The number of used channels for the ERP classification is reduced

by one when moving from left to right until it reaches the last channel.

As shown in the figure, the ERP classification accuracy is improved when the irrelevant ERP channels are removed from the data in each iteration. This can confirm the improvement of the ERP classification accuracy by selecting the most relevant ERP channels, thus, avoiding the curse of dimensionality. However, there is a significant reduction ($p = 0.0001$) in ERP classification accuracy when the iteration reached the last few remaining channels in the data (right side). This is due to removing the highly informative channels to the ERP, which leads to poor performance of the ERP classification. Therefore, selecting all the highly informative channels contributing to the ERP is desirable. According to the obtained results, the highest ERP classification accuracy is achieved when 7 channels are used (BA = $73.94\% \pm 0.39$). For the aim of comparison between the human-based and the recursive backward elimination methods, in addition to the optimum 7 channels, the 4 best channels were used as well, on the grounds that the human-based channel selection method (in section 4.3.6) used 4 channels for the ERP classification.

Figure 6.4 compares the results of the ERP classification accuracy obtained from the 4 channel subsets selected by the human-based method with those obtained from 4 and 7 channels by the recursive backward elimination method; when applied to the raw data, cleaned data by removing artefacts in the ground truth and by the Proposed_method_IC. As illustrated in the figure, the ERP classification accuracy obtained by the recursive backward elimination method is improved by approximately 5% and 4% using the optimum 7 and 4 channels, respectively, compared to the human-based method for the raw and cleaned data by the ground truth and the Proposed_method_IC. The results confirm the benefit of using the channel selection method, for improving the ERP classification rate, over the human-based method, in which using a fixed subset of channels may raise an error due to the inter-subject variations. However, there can be a potential risk of inflated false positive rates (Type-1 error rates) in the recursive backward channel elimination method as; after each iteration the channels are selected based on the result of the ERP classification.

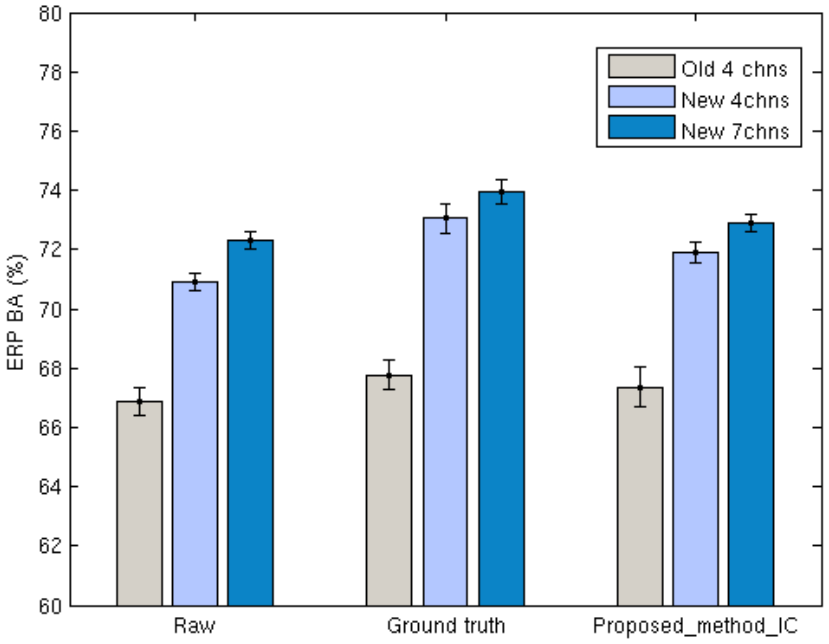

Figure 6.4: Comparison of ERP classification rates calculated using channels selected by different channel selection methods; human-based (Old 4chns), recursive backward elimination method (New 4chns and New 7chns), for the raw, and cleaned data by removing artefacts in ground truth and by Proposed_method_IC.

6.4.2 Task IC Classification

Regarding the task-related IC classification stages, first the task-related segments are classified. Based on the extracted features for detecting task-related segments, the averaged BA value of $90.94\% \pm 0.0413$ is obtained. Then, similar to section 4.2.3 the optimum threshold value for the highest possible BA is obtained for task IC classification. The averaged highest BA value of $95.6\% \pm 5.3$ within the threshold range of 58.2 to 73.1 is obtained for task-related IC classification. Figure 6.5 shows the number of task-related ICs detected for each participant. At least one task-related IC is detected in all cases enabling ERP classification for each dataset.

Table 6.1 represents the sensitivity, specificity and BA of task-related IC classification. The averaged obtained sensitivity is 96.6%. Only one task-related IC of a single subject (subject 7) is not detected correctly. The averaged specificity over all subjects

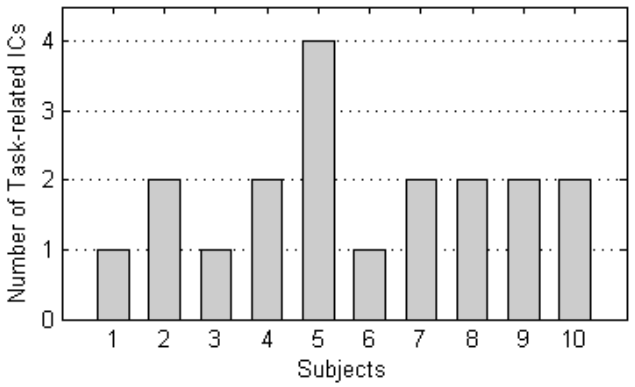

Figure 6.5: Number of task-related ICs, for each participant, detected automatically by the proposed method.

Subjects	Sensitivity(%)	Specificity(%)	BA(%)
1	100	85.7	92.8
2	100	96.8	98.4
3	100	98.4	99.2
4	100	91.9	95.9
5	100	96.7	98.4
6	100	95.3	97.6
7	66.7	96.7	81.7
8	100	90.5	95.2
9	100	98.4	99.2
10	100	95.2	97.6
Mean	**96.6**	**94.6**	**95.6**
std	10.5	4.1	5.3

Table 6.1: Performance of task-related IC classification for all participants, measured by sensitivity, specificity and balanced accuracy (BA).

(94.6%) and the imperfect individual specificity associated to each subject indicate the incorrect detection of at least one non-task IC as a task IC for each single subject's dataset (Appendix D). The obtained averaged BA of 95.6% across all participants indicates the reliability of the proposed system in task-related IC detection.

Subjects	GroundTaskIC-ERP(%)	AutoTaskIC-ERP(%)
1	96.1	97.2
2	93.9	93.9
3	82.8	81.7
4	72.2	75.0
5	88.8	88.2
6	89.3	89.4
7	76.7	70.0
8	62.8	73.9
9	86.1	86.1
10	87.8	88.9
Mean	**83.6**	**84.4**
Std	10.3	9.0

Table 6.2: Accuracy of ERP classification for the cleaned data obtained by the proposed automated task-IC detection (AutoTaskIC-ERP) compared with the cleaned data by the task-ICs in the ground truths (GroundTaskIC-ERP).

6.4.3 ERP Classification from Task ICs

Table 6.2 summarises the obtained ERP classification accuracies when ERP features are extracted from the task-related ICs labelled in the ground truth (GroundTaskIC-ERP) and compares them by the extraction of ERP features from the task-ICs automatically detected using the proposed IC labelling method (AutoTaskIC-ERP). As the table illustrates, the averaged and individual ERP information detected by both AutoTaskIC-ERP and GroundTaskIC-ERP are almost the same. However, GroundTaskIC-ERP outperformed AutoTaskIC-ERP for subject 7; this is due to one out of three task-related ICs in this data not being detected correctly by AutoTaskIC-ERP. Therefore, the ERP information associated to this non-detected task-related IC is missed. Also, the obtained ERP classification accuracy by GroundTaskIC-ERP for subject 8 decreased compared to by AutoTaskIC-ERP. This might be due to the task-related ICs which are not detected visually by experts in the ground truth, whereas they are detected by the proposed automatic task-related IC detection method.

Although the proposed method could not perfectly detect task-related ICs (aver-

aged BA= 95.6%), it achieved approximately the same ERP classification BA as the GroundTaskIC-ERP.

Overall, the accuracy of ERP classification obtained from task-related ICs is significantly improved (p=0.0023) by almost 11%, compared to that obtained by using the ERP relevant channels selected either by human-based or by the recursive backward channel elimination methods (Figure 6.4). This ERP enhancement could be due to losing some ERP information in the cleaned EEG data, when the artefactual sources are completely removed. Also, there could be an error in the selection of the ERP channels by the human-based technique, because there are variations between subjects and the channels containing ERP information may vary from subject to subject. Additionally, due to the volume conduction of the scalp and spread of the potentials, there might be other channels located close to the expected channels on the scalp that may include ERP information as well.

6.4.4 Comparison with xDAWN

The performance of the proposed ICA-based ERP classification method has been compared to the state-of-the-art xDAWN algorithm which is used to project the data channels into estimated signal subspace. First, the ERP classification by the NB classifier was assessed using the xDAWN algorithm with different dimensions (channels). Then, the optimum number of channels associated with the best performance of the NB classifier was selected and compared to the task-related IC ERP classification in terms of BA.

Figure 6.6 represents the performance of the NB classifier in ERP classification, when a different number of channels are used in xDAWN algorithm.

The variation of ERP classification rates by reducing the number of xDAWN channels from 62 to 2 is statistically insignificant. However, the ERP classification rate drops significantly (p=0.0019) by approximately 20%, in the case of a single channel. The best ERP classification rate is obtained when 8 channels are selected (BA = 82.46%). However, with the aim of obtaining a high performance of the ERP classification rate with the least

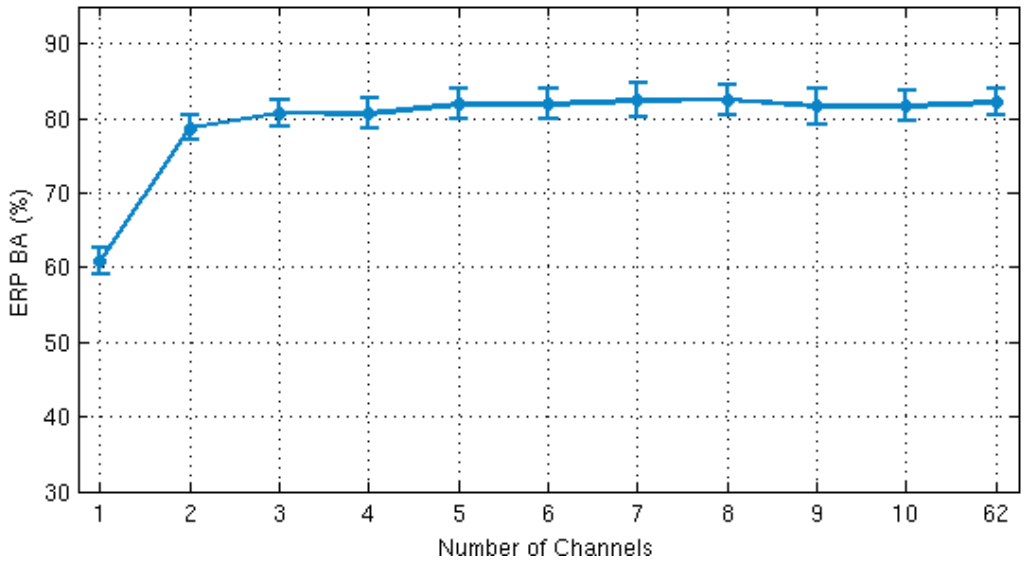

Figure 6.6: ERP classification rate (BA) for different number of channels selected by the xDAWN algorithm.

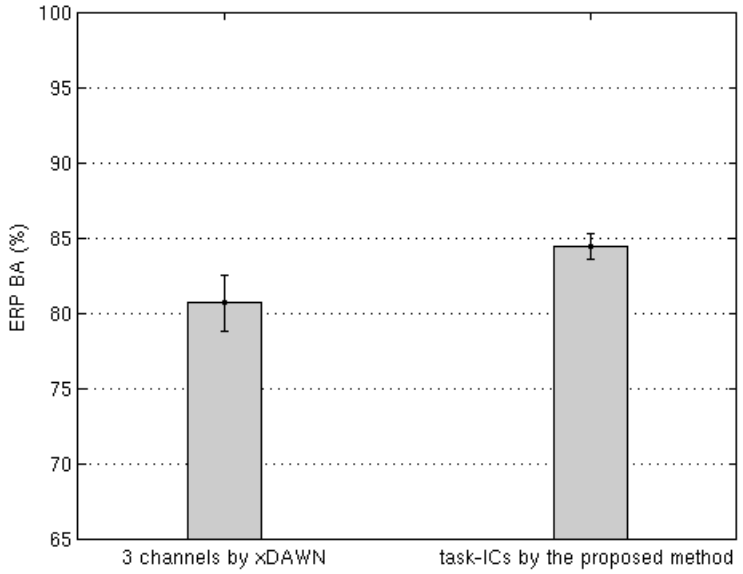

Figure 6.7: Comparison of the ERP classification rate (BA) using the 3 channels selected by xDAWN algorithm and task-related ICs.

number of channels, selecting 3 xDAWN channels is a safe choice, where the accuracy is insignificantly reduced by only about 1.7% compared to 8 channels.

Figure 6.7 shows the averaged ERP classification BA (averaged over 10 subjects) obtained by three xDAWN channels and the task-related ICs detected by the proposed

ICA-based method. Comparing the obtained results, the proposed method outperformed xDAWN and achieved a 3.72% higher ERP classification rate (BA=84.4%), albeit statistically insignificant. The reason may be attributed to the performance of ICA in source separation, in which most of the ERP response information are estimated and decomposed into task-related sources. Therefore, the task-related sources can be considered as a new representation of the most relevant ERP information.

6.5 Summary

In this chapter, an automatic ICA-based ERP detection method, called AutoTaskIC-ERP is proposed which utilises temporal, spatial and frequential features from task related ICs for ERP detection rather than features extracted from the cleaned EEG signal channels. Using the proposed method, rejecting the artefactual ICs that may contain EEG information is no longer required and the detected task-ICs are directly fed into the ERP classifier.

The performance of the ERP classification is enhanced using an iterative backward channel elimination method, compared to the classical human-based channel selection for ERP classification. Both the state-of-the-art method xDAWN and the proposed ICA-based method improved the accuracy of ERP classification significantly, compared to the classical or iterative backward channel elimination techniques; while the proposed method scored the highest accuracy with the value of 84.4%.

In conclusion, using both the proposed method and the-state-of-art xDAWN shows that by projecting the data into a spatial subspace, either ICs or pseudo channels, provide more reliable ERP classification compared to the EEG channel space. Meanwhile, the proposed ICA-based method out performed the xDAWN algorithm and further improved the accuracy of ERP classification. It is also confirmed that cleaning the data by removing the artefacts cannot compete with these techniques.

"Human experiences have no end and the knowledge of a wise man always increases through his experiences."

Imam Ali ibn Abi Talib (PBUH)

7

CONCLUSION

This thesis intends to propose an EEG signal processing chain, based on ICA, to improve the SNR of artefact contaminated EEG data and effectively extract ERP information. On the path to this goal, several research questions were formed. In order to answer these questions, first, the performance of the most commonly used ICA algorithms were systematically assessed over a range of pre-processing conditions applied to the data. The reliability of ICA decompositions was determined as highly dependent on the data pre-processing steps applied to the data in addition to the choice of the ICA algorithm. AMICA applied to the bandpass filtered continuous EEG data was shown to be the most effective combination of pre-processing conditions and ICA algorithm, for this study. Additionally, it was demonstrated that including extra sources of information about ECG

and EOG activities can improve the quality of ICA source separation and significantly decrease the processing time of AMICA algorithm.

Afterwards, a fully automated ICA-based artefact removal method was proposed to detect and remove all the common EEG artefacts, including blink, saccade, heartbeat, muscle and focal artefacts. A set of temporal, spatial and frequential features, representing artefact characteristics, is extracted to distinguish ICs corresponding to the artefacts from all other EEG activities. Then, the desired artefacts are detected and removed, based on a two-layered artefact classification algorithm. The proposed method successfully detected the common EEG artefacts with balanced-accuracy above 95%.

In the next step, the artefact removal process was further improved, by only removing the effect of blinking from the parts of the detected blink ICs, where blinking occurs. This process was performed by means of two methods; zeroing the blink segments and regressing out the blinking effect which was estimated by SCA. Both of the methods were shown to be successful in removing the effect of blink artefacts from real and simulated EEG data.

Finally, in contrast to the previous works, where the ERP classification rate and the SNR of the EEG signals were improved by detecting and removing artefactual ICs, an ICA-based method was proposed to improve the accuracy of ERP classification by detecting the ICs corresponding to the subject's response to the stimulation tasks. The task-related ICs were used as the sources of ERP information and feature extraction. Consequently, the channel selection and artefact removal issues are addressed. Using the proposed method, the task-related ICs were accurately detected, and the ERP classification accuracy was significantly improved.

The performance of all the proposed methods in this thesis were compared to the associated state-of-art methods at each step; and the results showed a better performance by means of the proposed methods in this thesis. The validity and reliability of all the proposed methods in this research are assessed by performing the statistical test on the reported findings.

This research might be of interest to clinicians, neurologists or researchers dealing with EEG data. As the EEG data is usually contaminated with different types of artefacts, the proposed pre-processing chain, the ICA-based automated artefact removal and ERP classification methods can be beneficial as a guideline to prepare the recorded raw EEG signal for extracting the latent cerebral activities present in the EEG data.

7.1 Summary of Findings

In this study, first the reliability of the ICA decompositions, estimated by various ICA algorithms was assessed, when 24 different data preparation steps were introduced and performed prior to ICA. It is showed that in addition to the choice of the ICA algorithm the reliability of the estimated sources by ICA is highly dependent on the type of pre-processing conditions applied to the data before ICA. Overall, the AMICA algorithm applied to the filtered and continuous EEG data integrated with EOG and ECG channels, was suggested as the most effective ICA-based processing chain to remove EEG artefacts. By employing the most effective combination of the pre-processing conditions and the ICA algorithm, a fully automated method was proposed to detect and remove segments and ICs corresponding to the most common EEG artefacts. The proposed method could correctly identify the common EEG artefacts with balanced accuracy above 95% and low between-person variations. When the results were compared to the state-of-the-art artefact removal method (ADJUST), the improvement in the performance of the proposed method in terms of SNR and ERP classification rate was shown.

Among all EEG artefacts, blink is the main source of artefact as it is characterised by a large amplitude that inevitably occurs and introduces serious distortion in the data. Therefore, in the next step of this research, the proposed artefact removal method was further improved, by optimising removal of the blink artefact. The blink artefacts were removed by regressing out the blink segments using a hybrid of ICA and SCA. According to the obtained results, the proposed method performed well in removing blink artefacts,

while keeping the ongoing EEG data intact. Using the simulated data, there was 10% improvement in the obtained residual variance when only blink segments were removed from the blink IC rather than the whole IC. The method was also compared to the recently proposed method (DEFL) and showed favourably better performance. Finally, it was demonstrated that the ERP classification rate is highly dependent on, artefact removal, channel selection procedure and dimensionality of the ERP features. These aspects were addressed by proposing an automated method, based on ICA, to reliably detect ICs corresponding to the ERP responses; and extract ERP features from those ICs. Using the proposed method, the ERP classification rate is further improved by 16%, to 84.4%. Additionally, the proposed method showed better performance when it was compared to the advanced channel selection method xDAWN. This way, it was also demonstrated that ICA could be more beneficial for ERP classification, when it is used to extract ERP features rather than to remove artefacts.

7.2 Future Research Directions

This work mainly focused on improving the quality and usability of EEG data by reducing the noise level via optimised use of the BSS method ICA, and introducing the optimum pre- and post-ICA processing methods to improve ERP classification rate and SNR of EEG data. At the same time, the research outlined in this thesis raises further developments that future work can address; some of which are pointed out in the following:

- Expanding the proposed pre-processing pipeline, prior to source separation, to compare the performance of all ICA and BSS algorithms.
- Generalising the proposed artefact classification, blink artefact removal, task-related IC detection and ERP classification methods to other types of EEG datasets recorded with various EEG apparatus and experimental paradigms, collected from different subjects.

- Using larger data pool size from more subjects in order to assess consistency of the proposed methods.
- Improving the performance of artefact segment classification by labelling the segments of all ICs in which the specific artefact occurs, rather than labelling all segments within their corresponding IC as artefact.
- Requesting more experts to label the segments and ICs for the ground truth.
- Detecting the gradient and ballistocardiogram (BCG) artefacts for EEG data recorded inside MRI scanner.
- Improving the performance of artefact and task-related IC detection by using more advanced classification methods such as Support Vector Machines (SVM).
- Developing the regression-based SCA method proposed in Chapter 5, to detect and reduce the effect of all common EEG artefacts occurred at specific time intervals.
- Improving the ERP classification rate by employing more advanced feature sets and classifier.
- Using Deep Neural Networks to learn suitable features rather than rely on the knowledge-driven approach outlined in the research.
- Optimising algorithm and implementation of the proposed methods for real-time applications.
- Using the eye movement and heartbeat information coming from ECG and EOG channels, to optimise the ICA source estimation and proposing an ICA algorithm constraint to ECG and EOG information.

The ultimate goal of all the above works is to improve the accuracy of ERP classification and SNR of EEG data and increase the usability of the information within EEG recordings, either for clinical applications or brain-computer interactions.

Appendices

"There is no capital more useful than intellect and wisdom, and there is no indigence more injurious than ignorance and unawareness."

Imam Ali ibn Abi Talib (PBUH)

A

Pairwise comparison of the ICA algorithms in terms MIR, PMI and dipolarity

The performances of the ICA algorithms are compared pairwise. The outcomes are reported in terms of mean difference, std. error and p-value for MIR, PMI and dipolarity, separately.

Table A.1: Pairwise comparison of the ICA algorithms in terms of MIR.

I	J	Mean Difference (I-J)	Standard Error (Std. Error)	p-value
AMICA	Extended-Infomax	1.351	0.077	p<0.001
AMICA	Infomax	0.620	0.043	p<0.001
AMICA	FastICA	2.795	0.128	p<0.001
Extended-Infomax	Infomax	-0.731	0.70	p<0.001
Extended-Infomax	FastICA	1.443	0.094	p<0.001
Infomax	FastICA	2.175	0.106	p<0.001

Table A.2: Pairwise comparison of the ICA algorithms in terms of PMI.

I	J	Mean Difference (I-J)	Standard Error (Std. Error)	p-value
AMICA	Extended-Infomax	0.044	0.004	p<0.001
AMICA	Infomax	0.024	0.003	p<0.001
AMICA	FastICA	0.030	0.004	p<0.001
Extended-Infomax	Infomax	-0.020	0.002	p<0.001
Extended-Infomax	FastICA	-0.14	0.001	p<0.001
Infomax	FastICA	0.006	0.002	p=0.052

Table A.3: Pairwise comparison of the ICA algorithms in terms of the mean percentage of dipolar sources.

I	J	Mean Difference (I-J)	Standard Error (Std. Error)	p-value
AMICA	Extended-Infomax	1.658	0.206	p<0.001
AMICA	Infomax	1.575	0.242	p=0.001
AMICA	FastICA	4.664	0.683	p<0.001
Extended-Infomax	Infomax	-0.084	0.208	p=0.99
Extended-Infomax	FastICA	3.006	0.582	p=0.004
Infomax	FastICA	3.089	0.610	p=0.004

"Increase of experiences, increases the wisdom of mankind."

Imam Hussain ibn Ali (PBUH)

B

Automatic Artefact Detection

Figure B.1 shows the scalp map of artefactual sources of a typical multichannel EEG data, which are estimated by AMICA algorithm and are automatically labelled as artefacts by the proposed system. The detected artefacts are as follow: ECG (a), blink (b), saccade (c), muscle (f, g,k,l) and focal (d,e,h,i,j,m).

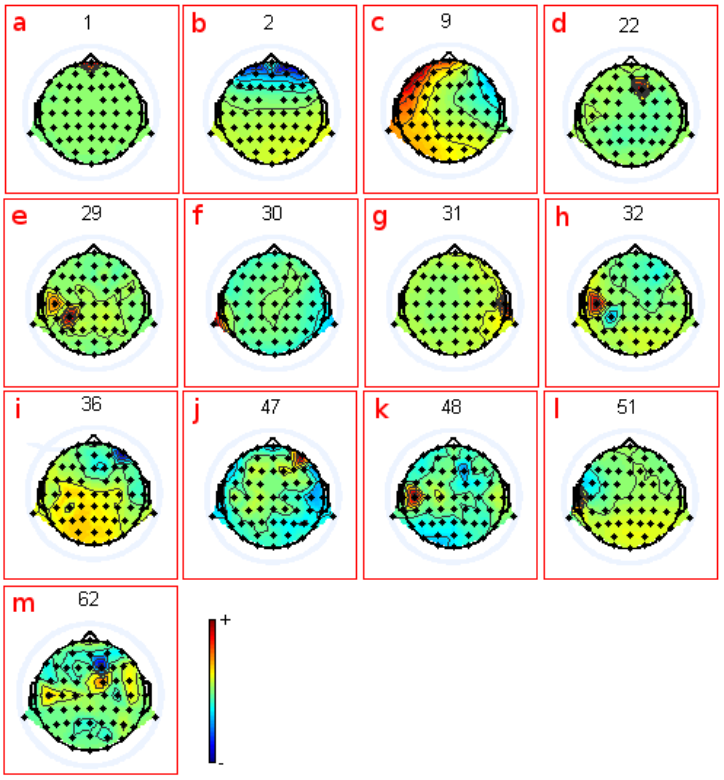

Figure B.1: Artefact ICs, automatically labelled by the proposed method in Chapter 4.

"Receiving education nurtures human wisdom."

Imam Hussain ibn Ali (PBUH)

C

Distribution of Artefactual ICs

Figure C.1 illustrates the distribution of IC scores of all 10 subjects for different types of artefacts. The red lines represent a specific threshold value, for each type of artefact separately. The ICs whose scores are above the threshold (to the right side of the red line) are detected as an artefact.

a) ECG

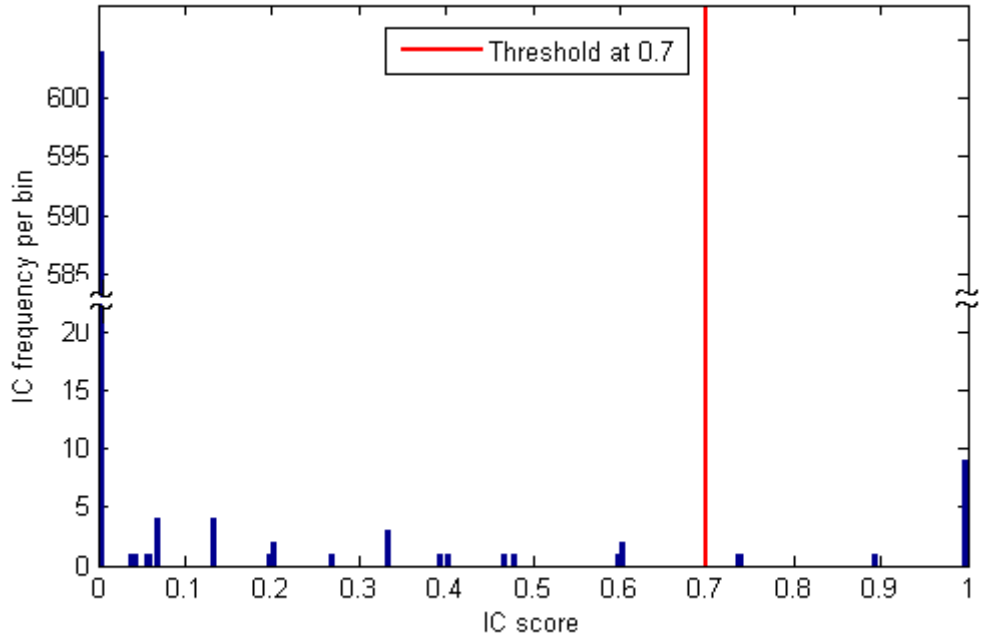

b) Muscle

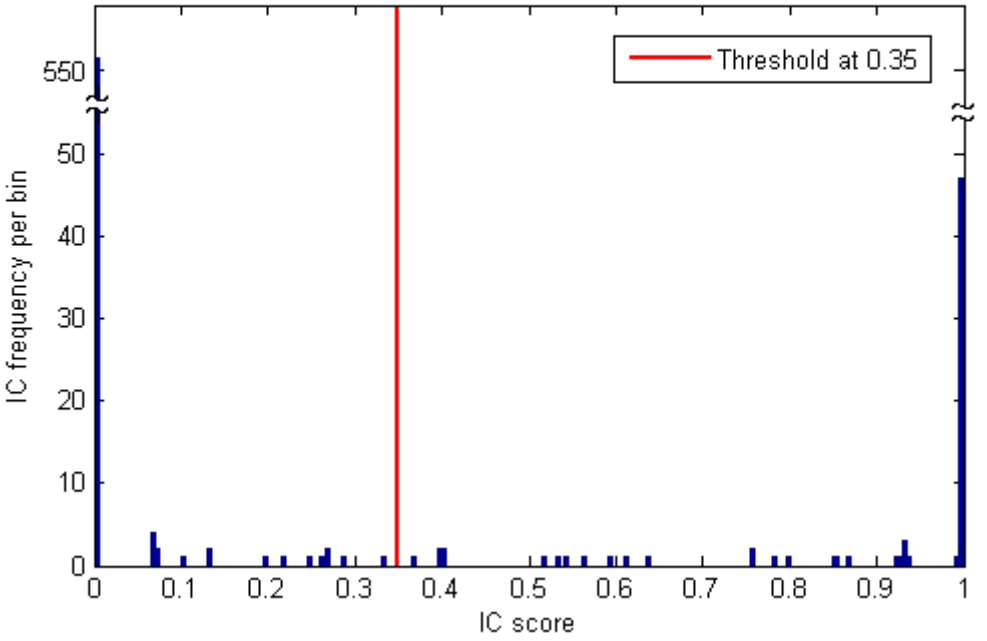

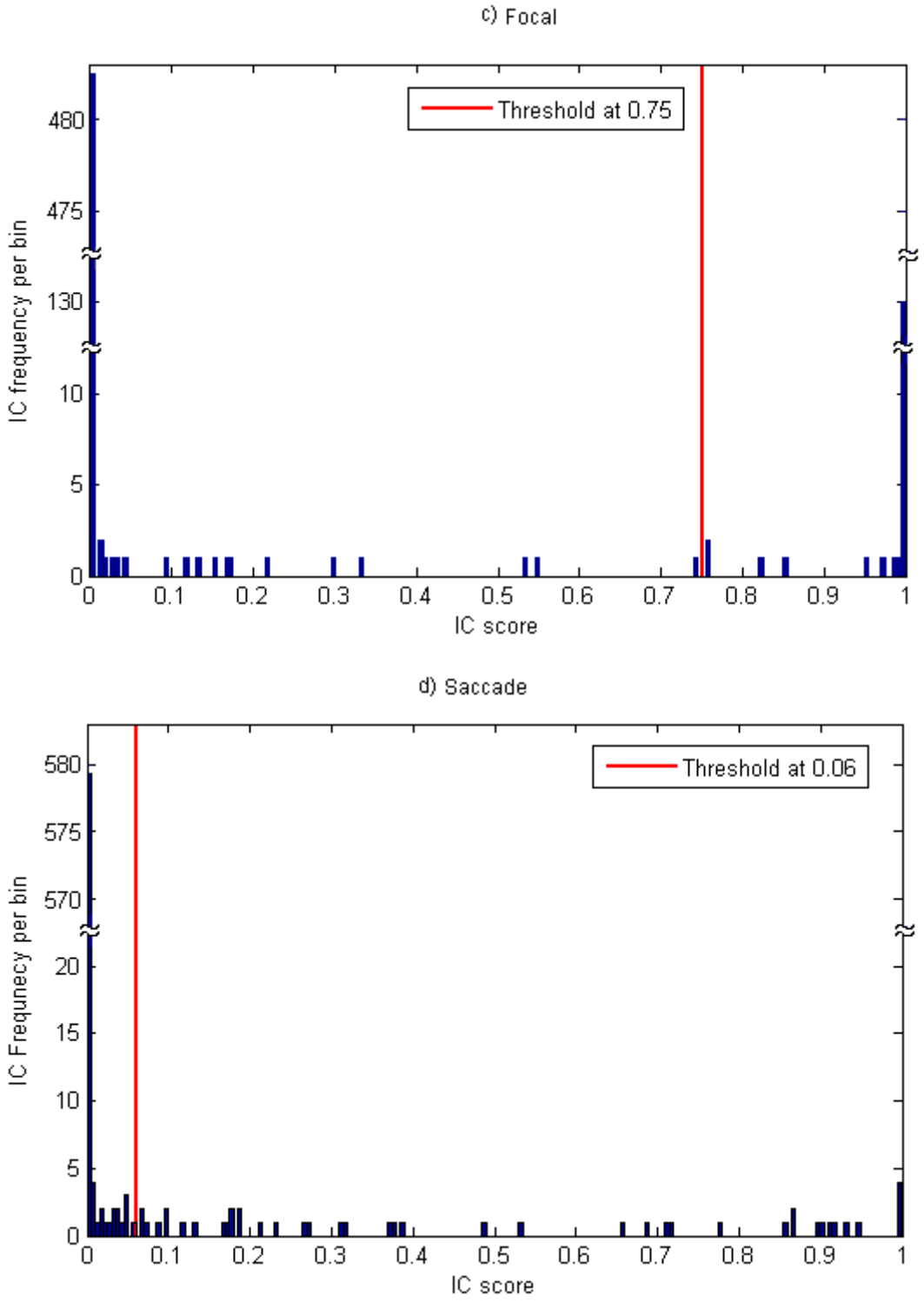

Figure C.1: The distribution of IC scores for all subjects are shown for a) ECG, b)Muscle, c)Focal and d)Saccade artefacts.

"To whatever extent a person's knowledge increases, his attention will be turned more towards his soul."

Imam Ali ibn Abi Talib (PBUH)

D

Task-Related IC Detection

Figure D.1 illustrates the fragment of the multichannel EEG data decomposed into ICs by AMICA algorithm. The task-related IC is detected by the ICA-based proposed method in Chapter 6 correctly (red signal). The green signals are the EEG sources which are detected as task-related ICs incorrectly, by the proposed method.

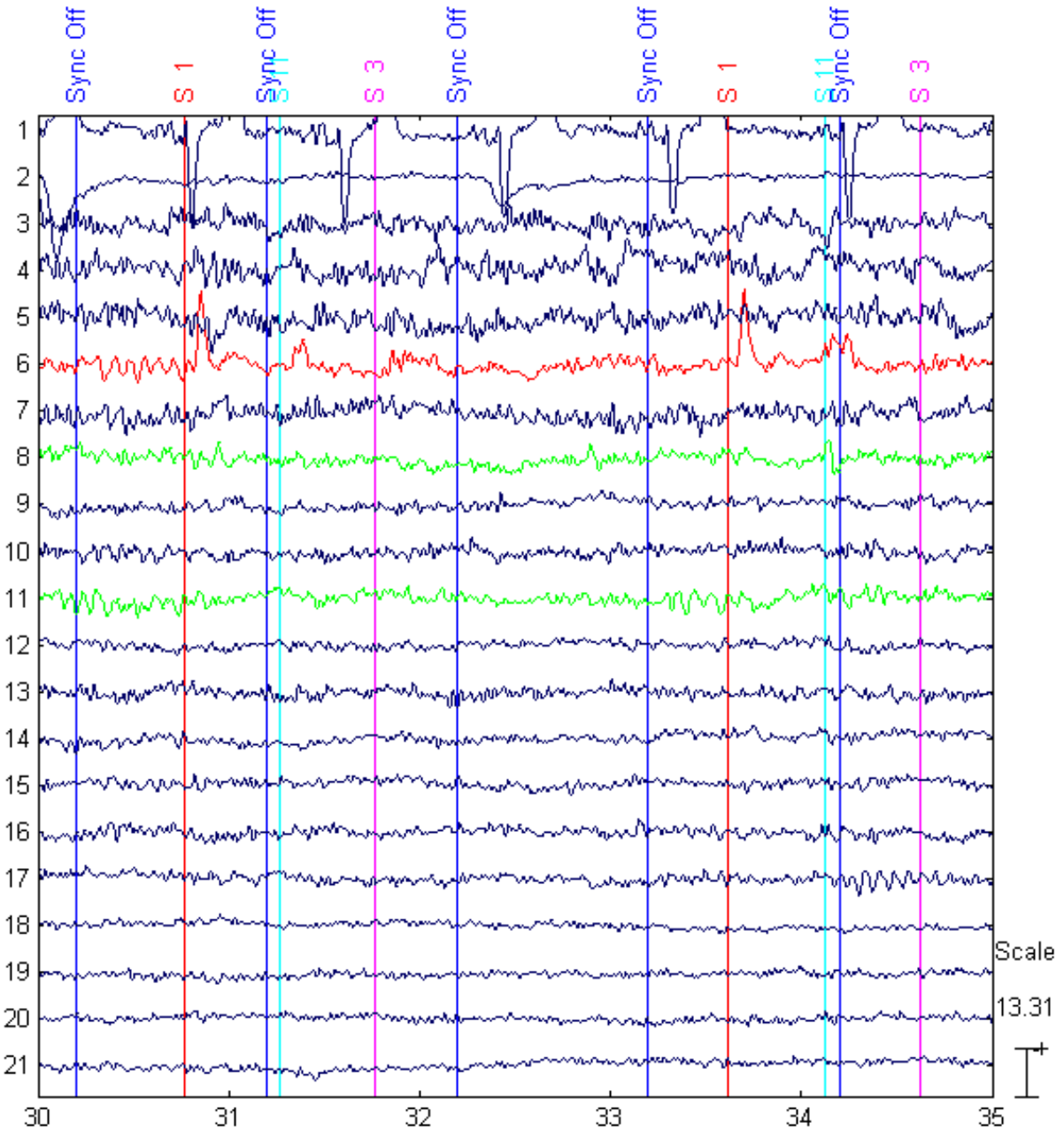

Figure D.1: The time series of the multichannel EEG data decomposed by AMICA algorithm, including the correctly and incorrectly detected task-related ICs, red signal and green signals, respectively.

List of References

[1] Mognon A, Jovicich J, Bruzzone L, Buiatti M. ADJUST: An automatic EEG artifact detector based on the joint use of spatial and temporal features. Psychophysiology. 2011;48(2):229–240.

[2] Sameni R, Gouy-Pailler C. An iterative subspace denoising algorithm for removing electroencephalogram ocular artifacts. Journal of neuroscience methods. 2014;225:97–105.

[3] Rivet B, Souloumiac A, Gibert G, Attina V. "P300 speller" Brain-Computer Interface: Enhancement of P300 evoked potential by spatial filters. In: Signal Processing Conference, 2008 16th European. IEEE; 2008. p. 1–5.

[4] The work of Hans Berger : P. Gloor (Montreal, Canada). Electroencephalography and Clinical Neurophysiology. 1969;27(7):649 –. {VIIth} International Congress of Electroencephalography and Clinical Neurophysiology. Available from: `http://www.sciencedirect.com/science/article/pii/0013469469912073`.

[5] Nunez PL, Srinivasan R. Electric fields of the brain: the neurophysics of EEG. Oxford university press; 2006.

[6] Niedermeyer E. 9. The normal EEG of the waking adult. Electroencephalography: Basic principles, clinical applications, and related fields. 2005;p. 167.

[7] Luck SJ. An introduction to the event-related potential technique. MIT press; 2014.

[8] Odom JV, Bach M, Barber C, Brigell M, Marmor MF, Tormene AP, et al. Visual evoked potentials standard (2004). Documenta ophthalmologica. 2004;108(2):115–123.

[9] Nicolas-Alonso LF, Gomez-Gil J. Brain computer interfaces, a review. Sensors. 2012;12(2):1211–1279.

[10] Kaplan A, Shishkin S, Ganin I, Basyul I, Zhigalov A. Adapting the P300-based brain–computer interface for gaming: a review. Computational Intelligence and AI in Games, IEEE Transactions on. 2013;5(2):141–149.

[11] Sanei S, Chambers JA. EEG signal processing. John Wiley & Sons; 2013.

[12] Jung TP, Makeig S, Humphries C, Lee TW, Mckeown MJ, Iragui V, et al. Removing electroencephalographic artifacts by blind source separation. Psychophysiology. 2000;37(02):163–178.

[13] Papadelis C, Chen Z, Kourtidou-Papadeli C, Bamidis PD, Chouvarda I, Bekiaris E, et al. Monitoring sleepiness with on-board electrophysiological recordings for preventing sleep-deprived traffic accidents. Clinical Neurophysiology. 2007;118(9):1906–1922.

[14] Hyvärinen A, Karhunen J, Oja E. Independent component analysis. vol. 46. John Wiley & Sons; 2004.

[15] Debener S, Kranczioch C, Gutberlet I. EEG Quality: origin and reduction of the EEG cardiac-related artefact. In: EEG-fMRI. Springer; 2010. p. 135–151.

[16] Collura TF. History and evolution of electroencephalographic instruments and techniques. Journal of clinical neurophysiology. 1993;10(4):476–504.

[17] Swartza BE, Goldensohnb ES. Erratum to:"Timeline of the history of EEG and associated fields"[Electroencephalography and clinical Neurophysiology 106 (1998) 173±176] q. Electroencephalography and clinical Neurophysiology. 1998;106:173–176.

[18] Fuller GD. Biofeedback: Methods and procedures in clinical practice. Biofeedback Press; 1977.

[19] Gibbs FA, Davis H, Lennox WG. The electro encephalogram in epilepsy and in conditions of impaired consciousness. American Journal of EEG Technology. 1968;8(2):59–73.

[20] GIBBS FA, LENNOX WG, Gibbs EL. The electro-encephalogram in diagnosis and in localization of epileptic seizures. Archives of Neurology & Psychiatry. 1936;36(6):1225–1235.

[21] Jasper HH. Cortical excitatory state and synchronism in the control of bioelectric autonomous rhythms. In: Cold Spring Harbor Symposia on Quantitative Biology. vol. 4. Cold Spring Harbor Laboratory Press; 1936. p. 320–338.

[22] Jutten C, Herault J. Blind separation of sources, part I: An adaptive algorithm based on neuromimetic architecture. Signal processing. 1991;24(1):1–10.

[23] Bell AJ, Sejnowski TJ. An information-maximization approach to blind separation and blind deconvolution. Neural computation. 1995;7(6):1129–1159.

[24] Belouchrani A, Abed-Meraim K, Cardoso JF, Moulines E. A blind source separation technique using second-order statistics. Signal Processing, IEEE Transactions on. 1997;45(2):434–444.

[25] Tang AC, Liu JY, Sutherland MT. Recovery of correlated neuronal sources from EEG: the good and bad ways of using SOBI. Neuroimage. 2005;28(2):507–519.

[26] Fitzgibbon SP, Powers DM, Pope KJ, Clark CR. Removal of EEG noise and artifact using blind source separation. Journal of Clinical Neurophysiology. 2007;24(3):232–243.

[27] Naraharisetti K. Removal of ocular artifacts from EEG signal using Joint Approximate Diagonalization of Eigen Matrices (JADE) and wavelet transform. Can J Biomed Eng Technol. 2010;1:56–60.

[28] Cardoso JF. High-order contrasts for independent component analysis. Neural computation. 1999;11(1):157–192.

[29] Hyvarinen A. Survey on independent component analysis. Neural computing surveys. 1999;2(4):94–128.

[30] Ce J, Yang Y, Peng Y. Improved algorithm for independent component analysis. In: Future Computer and Communication (ICFCC), 2010 2nd International Conference on. vol. 2. IEEE; 2010. p. V2–467.

[31] Kumar PS, Arumuganathan R, Sivakumar K, Vimal C. Removal of artifacts from EEG signals using adaptive filter through wavelet transform. In: Signal Processing, 2008. ICSP 2008. 9th International Conference on. IEEE; 2008. p. 2138–2141.

[32] Stangor C. Introduction to psychology. 2010;.

[33] Amthor F. Neuroscience For Dummies. Wiley; 2012. Available from: `https://books.google.co.uk/books?id=QeN5OIWUL7UC`.

[34] Lacatus E, Savulescu AF. Nano-Bio-Cogno Model of Acoustic Patterning for Molecular Neurostimulation. In: ASME 2013 Conference on Frontiers in Medical Devices: Applications of Computer Modeling and Simulation. American Society of Mechanical Engineers; 2013. p. V001T10A047–V001T10A047.

[35] Esiri MM, Lee VMY, Trojanowski JQ. The Neuropathology of Dementia. Cambridge University Press; 2004. Available from: `https://books.google.co.uk/books?id=axQ3PERykzoC`.

[36] De Munck JC, Van Dijk BW, Spekreijse H. Mathematical dipoles are adequate to describe realistic generators of human brain activity. Biomedical Engineering, IEEE Transactions on. 1988;35(11):960–966.

[37] Niedermeyer E, da Silva FL. Electroencephalography: basic principles, clinical applications, and related fields. Lippincott Williams & Wilkins; 2005.

[38] JASPER HH. The ten twenty electrode system of the international federation. Electroencephalography and clinical neurophysiology. 1958;10:371–375.

[39] Fisch BJ, Spehlmann R. Fisch and Spehlmann's EEG primer: basic principles of digital and analog EEG. Elsevier Health Sciences; 1999.

[40] Ball T, Kern M, Mutschler I, Aertsen A, Schulze-Bonhage A. Signal quality of simultaneously recorded invasive and non-invasive EEG. Neuroimage. 2009;46(3):708–716.

[41] Hüsing B, Jäncke L, Tag B. Impact assessment of neuroimaging: final report. vdf Hochschulverlag AG; 2006.

[42] Nyquist H. Thermal agitation of electric charge in conductors. Physical review. 1928;32(1):110.

[43] Bashashati A, Fatourechi M, Ward RK, Birch GE. A survey of signal processing algorithms in brain–computer interfaces based on electrical brain signals. Journal of Neural engineering. 2007;4(2):R32.

[44] Smith SW, et al. The scientist and engineer's guide to digital signal processing. 1997;.

[45] Oppenheim AV, Schafer RW, Buck JR, et al. Discrete-time signal processing. vol. 2. Prentice-hall Englewood Cliffs; 1989.

[46] Ebersole JS, Pedley TA. Current practice of clinical electroencephalography. Lippincott Williams & Wilkins; 2003.

[47] Ochoa CJ, Polich J. P300 and blink instructions. Clinical Neurophysiology. 2000;111(1):93–98.

[48] Hoffmann S, Falkenstein M. The correction of eye blink artefacts in the EEG: a comparison of two prominent methods. PLoS One. 2008;3(8):e3004.

[49] Gasser T, Möcks J, et al. Correction of EOG Artifacts in Event-Related Potentials of the EEG: Aspects of Reliability and Validity. Psychophysiology. 1982;19(4):472–480.

[50] Gratton G, Coles MG, Donchin E. A new method for off-line removal of ocular artifact. Electroencephalography and clinical neurophysiology. 1983;55(4):468–484.

[51] Whitton JL, Lue F, Moldofsky H. A spectral method for removing eye movement artifacts from the EEG. Electroencephalography and clinical neurophysiology. 1978;44(6):735–741.

[52] Woestenburg J, Verbaten M, Slangen J. The removal of the eye-movement artifact from the EEG by regression analysis in the frequency domain. Biological psychology. 1983;16(1):127–147.

[53] Winkler I, Haufe S, Tangermann M. Automatic classification of artifactual ICA-components for artifact removal in EEG signals. Behavioral and Brain Functions. 2011;7(1):30.

[54] Zeng H, Song A, Yan R, Qin H. EOG artifact correction from EEG recording using stationary subspace analysis and empirical mode decomposition. Sensors. 2013;13(11):14839–14859.

[55] Rajapakse JC, Cichocki A, et al. Independent component analysis and beyond in brain imaging: EEG, MEG, fMRI, and PET. In: Neural Information Processing, 2002. ICONIP'02. Proceedings of the 9th International Conference on. vol. 1. IEEE; 2002. p. 404–412.

[56] Vigário R, Särelä J, Jousmiki V, Hämäläinen M, Oja E. Independent component approach to the analysis of EEG and MEG recordings. Biomedical Engineering, IEEE Transactions on. 2000;47(5):589–593.

[57] Wisbeck JO, Barros AK, Yy AKB, Ojeda RG. Application of ICA in the separation of breathing artifacts in ECG signals. 1998;.

[58] Comon P, Jutten C. Handbook of Blind Source Separation: Independent component analysis and applications. Academic press; 2010.

[59] Hérault J, Jutten C, Ans B. Détection de grandeurs primitives dans un message composite par une architecture de calcul neuromimétique en apprentissage non supervisé. In: 10Âř Colloque sur le traitement du signal et des images, FRA, 1985. GRETSI, Groupe d'Etudes du Traitement du Signal et des Images; 1985. .

[60] Comon P. Independent component analysis, a new concept? Signal processing. 1994;36(3):287–314.

[61] Amarai S, Cichoki A, Chen T. A new learning algorithm for blind source separation. Advances in Neural Information Processing Systems;8:757–763.

[62] Amari SI. Natural gradient works efficiently in learning. Neural computation. 1998;10(2):251–276.

[63] Lee TW, Girolami M, Sejnowski TJ. Independent component analysis using an extended infomax algorithm for mixed subgaussian and supergaussian sources. Neural computation. 1999;11(2):417–441.

[64] Hyvärinen A, Oja E. A fast fixed-point algorithm for independent component analysis. Neural computation. 1997;9(7):1483–1492.

[65] Palmer JA, Kreutz-Delgado K, Rao BD, Makeig S. Modeling and estimation of dependent subspaces with non-radially symmetric and skewed densities. In: Independent Component Analysis and Signal Separation. Springer; 2007. p. 97–104.

[66] Stone JV. Independent component analysis: an introduction. Trends in cognitive sciences. 2002;6(2):59–64.

[67] Pedersen MS, Larsen J, Kjems U, Parra LC. A survey of convolutive blind source separation methods. Multichannel Speech Processing Handbook. 2007;p. 1065–1084.

[68] Dauwels J, Vialatte F, Cichocki A. Diagnosis of Alzheimer's disease from EEG signals: where are we standing? Current Alzheimer Research. 2010;7(6):487–505.

[69] Makeig S, Onton J, et al. ERP features and EEG dynamics: an ICA perspective. Oxford Handbook of Event-Related Potential Components New York, NY: Oxford. 2009;.

[70] Le Cam L, et al. The central limit theorem around 1935. Statistical science. 1986;1(1):78–91.

[71] Castañeda-Villa N, Calderón-Ríos E, Jiménez-González A. On the identification of an ICA Algorithm for Auditory Evoked Potentials extraction: A Study on Synthetic Data. Revista Mexicana de Ingeniería Biomédica. 2015;36(2).

[72] Jung TP, Humphries C, Lee TW, Makeig S, McKeown MJ, Iragui V, et al. Extended ICA removes artifacts from electroencephalographic recordings. Advances in neural information processing systems. 1998;p. 894–900.

[73] Lee TW, Lewicki MS. The generalized Gaussian mixture model using ICA. In: International Workshop on Independent Component Analysis (ICA); 2000. p. 239–244.

[74] Elishakoff I, Soize C. Nondeterministic mechanics. vol. 539. Springer Science & Business Media; 2013.

[75] Hyvärinen A, Oja E. Independent component analysis: algorithms and applications. Neural networks. 2000;13(4):411–430.

[76] Cover TM, Thomas JA. Elements of information theory. John Wiley & Sons; 2012.

[77] Hall P, Morton SC. On the estimation of entropy. Annals of the Institute of Statistical Mathematics. 1993;45(1):69–88.

[78] Joe H. Estimation of entropy and other functionals of a multivariate density. Annals of the Institute of Statistical Mathematics. 1989;41(4):683–697.

[79] Jones MC, Sibson R. What is projection pursuit? Journal of the Royal Statistical Society Series A (General). 1987;p. 1–37.

[80] Lee TW, Lewicki MS, Girolami M, Sejnowski TJ. Blind source separation of more sources than mixtures using overcomplete representations. Signal Processing Letters, IEEE. 1999;6(4):87–90.

[81] Palmer JA, Makeig S, Kreutz-Delgado K, Rao BD. Newton method for the ICA mixture model.;. .

[82] Lewicki MS, Sejnowski TJ. Learning overcomplete representations. Neural computation. 2000;12(2):337–365.

[83] Palmer JA, Kreutz-Delgado K, Makeig S. Super-Gaussian mixture source model for ICA. In: Independent Component Analysis and Blind Signal Separation. Springer; 2006. p. 854–861.

[84] Benesty J, Huang Y. Adaptive signal processing: applications to real-world problems. Springer Science & Business Media; 2013.

[85] Hartley H. Maximum likelihood estimation from incomplete data. Biometrics. 1958;14(2):174–194.

[86] Dempster AP, Laird NM, Rubin DB. Maximum likelihood from incomplete data via the EM algorithm. Journal of the royal statistical society Series B (methodological). 1977;p. 1–38.

[87] Palmer JA, Kreutz-Delgado K, Makeig S. AMICA: An adaptive mixture of independent component analyzers with shared components. San Diego, CA: Technical report, Swartz Center for Computational Neuroscience; 2011.

[88] Debener S, Hine J, Bleeck S, Eyles J. Source localization of auditory evoked potentials after cochlear implantation. Psychophysiology. 2008;45(1):20–24.

[89] Gilley PM, Sharma A, Dorman M, Finley CC, Panch AS, Martin K. Minimization of cochlear implant stimulus artifact in cortical auditory evoked potentials. Clinical Neurophysiology. 2006;117(8):1772–1782.

[90] Zhang F, Benson C, Fu QJ. Cortical encoding of pitch contour changes in cochlear implant users: a mismatch negativity study. Audiology and Neurotology. 2013;18(5):275–288.

[91] Zhang F, Hammer T, Banks HL, Benson C, Xiang J, Fu QJ. Mismatch negativity and adaptation measures of the late auditory evoked potential in cochlear implant users. Hearing research. 2011;275(1):17–29.

[92] Radüntz T, Scouten J, Hochmuth O, Meffert B. EEG artifact elimination by extraction of ICA-component features using image processing algorithms. Journal of neuroscience methods. 2015;243:84–93.

[93] Makeig S, Bell AJ, Jung TP, Sejnowski TJ, et al. Independent component analysis of electroencephalographic data. Advances in neural information processing systems. 1996;p. 145–151.

[94] Vigário RN. Extraction of ocular artefacts from EEG using independent component analysis. Electroencephalography and clinical neurophysiology. 1997;103(3):395–404.

[95] Maggioni E, Arrubla J, Warbrick T, Dammers J, Bianchi AM, Reni G, et al. Removal of Pulse Artefact from EEG Data Recorded in MR Environment at 3T. Setting of ICA Parameters for Marking Artefactual Components: Application to Resting-State Data. 2014;.

[96] Kusumandari DE, Fakhrurroja H, Turnip A, Hutagalung SS, Kumbara B, Simarmata J. Removal of EOG artifacts: Comparison of ICA algorithm from recording EEG. In: Technology, Informatics, Management, Engineering, and Environment (TIME-E), 2014 2nd International Conference on. IEEE; 2014. p. 335–339.

[97] Mayeli A, Zotev V, Refai H, Bodurka J. An automatic ICA-based method for removing artifacts from EEG data acquired during fMRI in real time. In: Biomedical Engineering Conference (NEBEC), 2015 41st Annual Northeast. IEEE; 2015. p. 1–2.

[98] Solé-Casals J, Vialatte FB, Chen Z, Cichocki A, et al. Investigation of ica algorithms for feature extraction of eeg signals in discrimination of alzheimer disease. 2008;.

[99] LeVan P, Urrestarazu E, Gotman J. A system for automatic artifact removal in ictal scalp EEG based on independent component analysis and Bayesian classification. Clinical Neurophysiology. 2006;117(4):912–927.

[100] De Lucia M, Fritschy J, Dayan P, Holder DS. A novel method for automated classification of epileptiform activity in the human electroencephalogram-based on independent component analysis. Medical & biological engineering & computing. 2008;46(3):263–272.

[101] Assecondi S. Automated Subject-Specific Peak Identification andBallistocardiographic Artifact Correction in EEG-fMRI. Ghent University; 2009.

[102] Luck SJ. Ten simple rules for designing ERP experiments. Event-related potentials: A methods handbook. 2005;262083337.

[103] Jung TP, Humphries C, Lee TW, Makeig S, McKeown MJ, Iragui V, et al. Removing electroencephalographic artifacts: comparison between ICA and PCA. In: Neural Networks for Signal Processing VIII, 1998. Proceedings of the 1998 IEEE Signal Processing Society Workshop. IEEE; 1998. p. 63–72.

[104] Delorme A, Palmer J, Onton J, Oostenveld R, Makeig S. Independent EEG sources are dipolar. PloS one. 2012;7(2):e30135.

[105] Albazzaz H, Wang XZ. Statistical process control charts for batch operations based on independent component analysis. Industrial & engineering chemistry research. 2004;43(21):6731–6741.

[106] Stone JV. Independent component analysis. Wiley Online Library; 2004.

[107] Krishnaveni V, Jayaraman S, Kumar PM, Shivakumar K, Ramadoss K. Comparison of independent component analysis algorithms for removal of ocular artifacts from electroencephalogram. Meas Sci Rev J. 2005;5(2):67–78.

[108] Matic V, Deburchgraeve W, Van Huffel S. Comparison of ICA algorithms for ECG artifact removal from EEG signals. In: Proc. of the 4th Annual symposium of the IEEE-EMBS Benelux Chapter.(IEEE-EMBS); 2009. p. 137–140.

[109] Mutihac R, Mutihac RC. A comparative study of independent component analysis algorithms for electroencephalography. Romanian reports in physics. 2007;59(3):827–853.

[110] Delorme A, Sejnowski T, Makeig S. Enhanced detection of artifacts in EEG data using higher-order statistics and independent component analysis. Neuroimage. 2007;34(4):1443–1449.

[111] Ilavennila BP, Saravanakumar JJR. Comparative Evaluation of Various Independent Components (ICA) Tech for the removal of artifacts of EEG Signals. IJCSNS. 2010;10(3):226.

[112] Groppe DM, Makeig S, Kutas M. Identifying reliable independent components via split-half comparisons. NeuroImage. 2009;45(4):1199–1211.

[113] Korats G, Le Cam S, Ranta R. Impact of Window Length and Decorrelation Step on ICA Algorithms for EEG Blind Source Separation. In: BIOSIGNALS; 2012. p. 55–60.

[114] Zakeri Z, Assecondi S, Bagshaw A, Arvanitis T. Influence of Signal Preprocessing on ICA-Based EEG Decomposition. In: XIII Mediterranean Conference on Medical and Biological Engineering and Computing 2013. Springer; 2014. p. 734–737.

[115] Sharpless S, Jasper H. Habituation of the arousal reaction. Brain. 1956;79(4):655–680.

[116] Ostwald D. An information theoretic approach to EEG-fMRI integration. University of Birmingham; 2010.

[117] Gupta P, Gupta PK, Muppidi S, Modur P, et al. Clinical Neurophysiology Board Review Q&A. Demos Medical Publishing; 2014.

[118] Splinter R. Handbook of Physics in Medicine and Biology. CRC Press; 2010.

[119] Sullivan TJ, Deiss SR, Cauwenberghs G, Jung TP. A low-noise low-power EEG acquisition node for scalable brain-machine interfaces. In: Microtechnologies for the New Millennium. International Society for Optics and Photonics; 2007. p. 659203–659203.

[120] Jellinger K. Reading EEGs: A Practical Approach. European Journal of Neurology. 2010;17(4):e34–e34.

[121] Varsavsky A, Mareels I, Cook M. Epileptic seizures and the EEG: measurement, models, detection and prediction. CRC Press; 2010.

[122] Bajaj V, Pachori RB. EEG signal classification using empirical mode decomposition and support vector machine. In: Proceedings of the International Conference on Soft Computing for Problem Solving (SocProS 2011) December 20-22, 2011. Springer; 2012. p. 623–635.

[123] Von Bünau P, Meinecke FC, Scholler S, Müller KR. Finding stationary brain sources in EEG data. In: Engineering in Medicine and Biology Society (EMBC), 2010 Annual International Conference of the IEEE. IEEE; 2010. p. 2810–2813.

[124] Tcheslavski GV, Gonen FF. Alcoholism-related alterations in spectrum, coherence, and phase synchrony of topical electroencephalogram. Computers in biology and medicine. 2012;42(4):394–401.

[125] Wong L, Abdulla W. Time-frequency evaluation of segmentation methods for neonatal EEG signals. In: Engineering in Medicine and Biology Society, 2006. EMBS'06. 28th Annual International Conference of the IEEE. IEEE; 2006. p. 1303–1306.

[126] De Tollenaere J, Deburchgraeve W, De Vos M, Van Huffel S. New Approaches for the Adaptive Segmentation of Neonatal EEG Signals. In: Proc. of the 4th Annual Symposium of the IEEE-EMBS Benelux Chapter; 2009. p. 141–144.

[127] Azami H, Mohammadi K, Bozorgtabar B. An improved signal segmentation using moving average and Savitzky-Golay filter. 2012;.

[128] Mariani S, Grassi A, Mendez MO, Milioli G, Parrino L, Terzano MG, et al. EEG segmentation for improving automatic CAP detection. Clinical Neurophysiology. 2013;124(9):1815–1823.

[129] Jordan K. Nonconvulsive seizures (NCS) and nonconvulsive status epilepticus (NCSE) detected by continuous EEG monitoring in the neuro ICU. Neurology. 1992;42(Suppl 1):194.

[130] Hirsch LJ. Continuous EEG monitoring in the intensive care unit: an overview. Journal of clinical neurophysiology. 2004;21(5):332–340.

[131] Claassen J, Mayer S, Kowalski R, Emerson R, Hirsch L. Detection of electrographic seizures with continuous EEG monitoring in critically ill patients. Neurology. 2004;62(10):1743–1748.

[132] Sutter R, Fuhr P, Grize L, Marsch S, Rüegg S. Continuous video-EEG monitoring increases detection rate of nonconvulsive status epilepticus in the ICU. Epilepsia. 2011;52(3):453–457.

[133] Duncan H, Spillane K, Morrison I. Electroencephalography–An Overview. 2014;.

[134] André-Obadia N, Parain D, Szurhaj W. Continuous EEG monitoring in adults in the intensive care unit (ICU). Neurophysiologie Clinique/Clinical Neurophysiology. 2015;.

[135] Debener S, Makeig S, Delorme A, Engel AK. What is novel in the novelty oddball paradigm? Functional significance of the novelty P3 event-related potential as revealed by independent component analysis. Cognitive Brain Research. 2005;22(3):309–321.

[136] Makeig S, Delorme A, Westerfield M, Jung TP, Townsend J, Courchesne E, et al. Electroencephalographic brain dynamics following manually responded visual targets. PLoS biology. 2004;2(6):e176.

[137] Kropotov J. Quantitative EEG, event-related potentials and neurotherapy. Academic Press; 2010.

[138] Kluetsch R, Ros T, Théberge J, Frewen P, Calhoun V, Schmahl C, et al. Plastic modulation of PTSD resting-state networks and subjective wellbeing by EEG neurofeedback. Acta Psychiatrica Scandinavica. 2014;130(2):123–136.

[139] Mohamed A, Marwala T, John L. Single-trial EEG discrimination between wrist and finger movement imagery and execution in a sensorimotor BCI. In: Engineering in Medicine and Biology Society, EMBC, 2011 Annual International Conference of the IEEE. IEEE; 2011. p. 6289–6293.

[140] Ahn M, Ahn S, Hong JH, Cho H, Kim K, Kim BS, et al. Gamma band activity associated with BCI performance: simultaneous MEG/EEG study. Frontiers in human neuroscience. 2013;7.

[141] Wang J, Barstein J, Ethridge LE, Mosconi MW, Takarae Y, Sweeney JA. Resting state EEG abnormalities in autism spectrum disorders. J Neurodev Disord. 2013;5(1):1–14.

[142] Zhou B, Wu X, Zhang L, Lv Z, Guo X. Robust Spatial Filters on Three-Class Motor Imagery EEG Data Using Independent Component Analysis. Journal of Biosciences and Medicines. 2014;2(02):43.

[143] Delorme A, Makeig S, Sejnowski T. Automatic artifact rejection for EEG data using high-order statistics and independent component analysis. In: International workshop on ICA (San Diego, CA); 2001. .

[144] Castermans T, Duvinage M, Petieau M, Hoellinger T, Saedeleer C, Seetharaman K, et al. Optimizing the performances of a p300-based brain–computer interface in ambulatory conditions. Emerging and Selected Topics in Circuits and Systems, IEEE Journal on. 2011;1(4):566–577.

[145] Lau TM, Gwin JT, McDowell KG, Ferris DP. Weighted phase lag index stability as an artifact resistant measure to detect cognitive EEG activity during locomotion. J Neuroeng Rehabil. 2012;9(1):1–9.

[146] Duvinage M, Castermans T, Petieau M, Cheron G, Dutoit T. Are current gait-related artifact removal techniques useful for low-complexity BCIs? In: Neural Networks (IJCNN), The 2012 International Joint Conference on. IEEE; 2012. p. 1–7.

[147] van Vugt MK, Simen P, Nystrom L, Holmes P, Cohen JD. Lateralized readiness potentials reveal properties of a neural mechanism for implementing a decision threshold. PloS one. 2014;9(3):e90943.

[148] Makeig S, Gramann K, Jung TP, Sejnowski TJ, Poizner H. Linking brain, mind and behavior. International Journal of Psychophysiology. 2009;73(2):95–100.

[149] Ullsperger M, Debener S. Simultaneous EEG and fMRI: recording, analysis, and application. Oxford University Press; 2010.

[150] Nolan H, Whelan R, Reilly R. FASTER: fully automated statistical thresholding for EEG artifact rejection. Journal of neuroscience methods. 2010;192(1):152–162.

[151] Rogasch NC, Thomson RH, Farzan F, Fitzgibbon BM, Bailey NW, Hernandez-Pavon JC, et al. Removing artefacts from TMS-EEG recordings using independent component analysis: Importance for assessing prefrontal and motor cortex network properties. NeuroImage. 2014;101:425–439.

[152] MacLean SE, Ward LM. Temporo-frontal phase synchronization supports hierarchical network for mismatch negativity. Clinical Neurophysiology. 2014;125(8):1604–1617.

[153] Lenartowicz A, Delorme A, Walshaw PD, Cho AL, Bilder RM, McGough JJ, et al. Electroencephalography correlates of spatial working memory deficits in attention-deficit/hyperactivity disorder: vigilance, encoding, and maintenance. The Journal of Neuroscience. 2014;34(4):1171–1182.

[154] Liversedge SP, Findlay JM. Saccadic eye movements and cognition. Trends in cognitive sciences. 2000;4(1):6–14.

[155] Prinsloo GE, Rauch H, Lambert MI, Muench F, Noakes TD, Derman WE. The effect of short duration heart rate variability (HRV) biofeedback on cognitive performance during laboratory induced cognitive stress. Applied Cognitive Psychology. 2011;25(5):792–801.

[156] Elliot AJ, Payen V, Brisswalter J, Cury F, Thayer JF. A subtle threat cue, heart rate variability, and cognitive performance. Psychophysiology. 2011;48(10):1340–1345.

[157] Vine SJ, Wilson MR. Quiet eye training: effects on learning and performance under pressure. Journal of Applied Sport Psychology. 2010;22(4):361–376.

[158] Li Y, Ma Z, Lu W, Li Y. Automatic removal of the eye blink artifact from EEG using an ICA-based template matching approach. Physiological measurement. 2006;27(4):425.

[159] Romero S, Mañanas MA, Barbanoj MJ. A comparative study of automatic techniques for ocular artifact reduction in spontaneous EEG signals based on clinical target variables: a simulation case. Computers in biology and medicine. 2008;38(3):348–360.

[160] Ghandeharion H, Erfanian A. A fully automatic ocular artifact suppression from EEG data using higher order statistics: Improved performance by wavelet analysis. Medical engineering & physics. 2010;32(7):720–729.

[161] Yang B, He L. Removal of ocular artifacts from EEG signals using ICA-RLS in BCI. In: Electronics, Computer and Applications, 2014 IEEE Workshop on. IEEE; 2014. p. 544–547.

[162] Joyce CA, Gorodnitsky IF, Kutas M. Automatic removal of eye movement and blink artifacts from EEG data using blind component separation. Psychophysiology. 2004;41(2):313–325.

[163] Klados MA, Papadelis C, Lithari C, Bamidis P. The removal of ocular artifacts from EEG signals: a comparison of performances for different methods. In: 4th European Conference of the International Federation for Medical and Biological Engineering. Springer; 2009. p. 1259–1263.

[164] Gao J, Yang Y, Sun J, Yu G. Automatic removal of various artifacts from EEG signals using combined methods. Journal of Clinical Neurophysiology. 2010;27(5):312–320.

[165] Leistritz L, Pester B, Doering A, Schiecke K, Babiloni F, Astolfi L, et al. Time-variant partial directed coherence for analysing connectivity: a methodological study. Philosophical Transactions of the Royal Society A: Mathematical, Physical and Engineering Sciences. 2013;371(1997):20110616.

[166] Piper D, Ungureanu M, Strungaru R, Schiecke K, Pester B, Leistritz L, et al. Time-variant connectivity analysis between epileptic EEG signals and between EEG-envelopes and HRV. In: E-Health and Bioengineering Conference (EHB), 2013. IEEE; 2013. p. 1–4.

[167] Gohel B, Jeong Y. Sensory modality-specific spatio-temporal dynamics in response to counting tasks. Neuroscience letters. 2014;581:20–25.

[168] Marek T, Tichavsky P, Dohnal G, et al. On the estimation of mutual information. In: Proceedings of ROBUST; 2008. .

[169] Sabeti M, Katebi S, Rastgar K. Source localization algorithms to find attention and memory circuits in the brain. Journal of King Saud University-Computer and Information Sciences. 2015;27(3):334–343.

[170] Yao J, Dewald JP. Evaluation of different cortical source localization methods using simulated and experimental EEG data. Neuroimage. 2005;25(2):369–382.

[171] Chowdhury R, Merlet I, Birot G, Kobayashi E, Nica A, Biraben A, et al. Complex patterns of spatially extended generators of epileptic activity: Comparison of source localization methods cMEM and 4-ExSo-MUSIC on high resolution EEG and MEG data. NeuroImage. 2016;143:175–195.

[172] Delorme A, Makeig S. EEGLAB: an open source toolbox for analysis of single-trial EEG dynamics including independent component analysis. Journal of neuroscience methods. 2004;134(1):9–21.

[173] Scherg M. Fundamentals of dipole source potential analysis. Auditory evoked magnetic fields and electric potentials Advances in audiology. 1990;6:40–69.

[174] Kavanagk RN, Darcey TM, Lehmann D, Fender DH. Evaluation of methods for three-dimensional localization of electrical sources in the human brain. Biomedical Engineering, IEEE Transactions on. 1978;(5):421–429.

[175] Field A. Discovering statistics using IBM SPSS statistics. Sage; 2013.

[176] Holm S. A simple sequentially rejective multiple test procedure. Scandinavian journal of statistics. 1979;p. 65–70.

[177] IBM Corp. IBM SPSS Statistics for Windows, Version 24.0. Armonk, NY: IBM Corp; 2016.

[178] Müller KR, Tangermann M, Dornhege G, Krauledat M, Curio G, Blankertz B. Machine learning for real-time single-trial EEG-analysis: from brain–computer interfacing to mental state monitoring. Journal of neuroscience methods. 2008;167(1):82–90.

[179] Delorme A, Mullen T, Kothe C, Acar ZA, Bigdely-Shamlo N, Vankov A, et al. EEGLAB, SIFT, NFT, BCILAB, and ERICA: new tools for advanced EEG processing. Computational intelligence and neuroscience. 2011;2011:10.

[180] Stopczynski A, Stahlhut C, Larsen JE, Petersen MK, Hansen LK. The smartphone brain scanner: a mobile real-time neuroimaging system. arXiv preprint arXiv:13040357. 2013;.

[181] Bigdely-Shamlo N, Mullen T, Kreutz-Delgado K, Makeig S. Measure projection analysis: a probabilistic approach to EEG source comparison and multi-subject inference. Neuroimage. 2013;72:287–303.

[182] Kong W, Zhou Z, Hu S, Zhang J, Babiloni F, Dai G. Automatic and Direct Identification of Blink Components from Scalp EEG. Sensors. 2013;13(8):10783–10801.

[183] Barbati G, Porcaro C, Zappasodi F, Rossini PM, Tecchio F. Optimization of an independent component analysis approach for artifact identification and removal in magnetoencephalographic signals. Clinical Neurophysiology. 2004;115(5):1220–1232.

[184] Romero S, Mananas M, Barbanoj MJ. Ocular reduction in EEG signals based on adaptive filtering, regression and blind source separation. Annals of biomedical engineering. 2009;37(1):176–191.

[185] Wallstrom GL, Kass RE, Miller A, Cohn JF, Fox NA. Automatic correction of ocular artifacts in the EEG: a comparison of regression-based and component-based methods. International journal of psychophysiology. 2004;53(2):105–119.

[186] Mantini D, Perrucci MG, Cugini S, Ferretti A, Romani GL, Del Gratta C. Complete artifact removal for EEG recorded during continuous fMRI using independent component analysis. Neuroimage. 2007;34(2):598–607.

[187] Cassani R, Falk TH, Fraga FJ, Kanda PA, Anghinah R. The effects of automated artifact removal algorithms on electroencephalography-based Alzheimer's disease diagnosis. Frontiers in aging neuroscience. 2014;6.

[188] Winkler I, Brandl S, Horn F, Waldburger E, Allefeld C, Tangermann M. Robust artifactual independent component classification for BCI practitioners. Journal of neural engineering. 2014;11(3):035013.

[189] Frølich L, Andersen TS, Mørup M. Classification of independent components of EEG into multiple artifact classes. Psychophysiology. 2015;52(1):32–45.

[190] Fernandez HZ. Evaluation and Comparsion of the Independent Components of Simultaneously Measured MEG and EEG Data. Univerlagtuberlin; 2009.

[191] Anderer P, Roberts S, Schlögl A, Gruber G, Klösch G, Herrmann W, et al. Artifact processing in computerized analysis of sleep EEG–a review. Neuropsychobiology. 1999;40(3):150–157.

[192] Welch PD. The use of fast Fourier transform for the estimation of power spectra: a method based on time averaging over short, modified periodograms. IEEE Transactions on audio and electroacoustics. 1967;15(2):70–73.

[193] Djemili R, Bourouba H, Korba MCA. Comparative Analysis of Spectral Estimation Methods for Brain-Computer Interfaces. 2nd Intl' Conference on Advances in Engineering Sciences and Applied Mathematics (ICAESAM'2014). 2014;p. 1–5.

[194] Goncharova I, McFarland DJ, Vaughan TM, Wolpaw JR. EMG contamination of EEG: spectral and topographical characteristics. Clinical Neurophysiology. 2003;114(9):1580–1593.

[195] Theodoridis S, Koutroumbas K. Pattern recognition and neural networks. In: Machine Learning and Its Applications. Springer; 2001. p. 169–195.

[196] Schneider KM. Techniques for improving the performance of naive bayes for text classification. In: Computational Linguistics and Intelligent Text Processing. Springer; 2005. p. 682–693.

[197] White DM, Van Cott CA. EEG artifacts in the intensive care unit setting. American journal of electroneurodiagnostic technology. 2010;50(1):8–25.

[198] Yeh YC, Wang WJ. QRS complexes detection for ECG signal: The Difference Operation Method. Computer methods and programs in biomedicine. 2008;91(3):245–254.

[199] Abbaspour S, Fallah A. Removing ECG Artifact from the Surface EMG Signal Using Adaptive Subtraction Technique. Journal of Biomedical Physics & Engineering. 2014;4(1):33.

[200] Billauer E. peakdet: Peak detection using MATLAB; 2012. Accessed: 2013-09-30. `http://www.billauer.co.il/peakdet.html`.

[201] Roach BJ, Mathalon DH. Event-related EEG time-frequency analysis: an overview of measures and an analysis of early gamma band phase locking in schizophrenia. Schizophrenia bulletin. 2008;34(5):907–926.

[202] Barbato G, Ficca G, Beatrice M, Casiello M, Muscettola G, Rinaldi F. Effects of sleep deprivation on spontaneous eye blink rate and alpha EEG power. Biological psychiatry. 1995;38(5):340–341.

[203] Carney LG, Hill RM. The nature of normal blinking patterns. Acta ophthalmologica. 1982;60(3):427–433.

[204] Friedman N, Geiger D, Goldszmidt M. Bayesian network classifiers. Machine learning. 1997;29(2-3):131–163.

[205] Langley P, Sage S. Induction of selective Bayesian classifiers. In: Proceedings of the Tenth international conference on Uncertainty in artificial intelligence. Morgan Kaufmann Publishers Inc.; 1994. p. 399–406.

[206] Rennie JD, Shih L, Teevan J, Karger DR, et al. Tackling the poor assumptions of naive bayes text classifiers. In: ICML. vol. 3. Washington DC); 2003. p. 616–623.

[207] Soundararajan KP, Schultz T. Learning Probabilistic Transfer Functions: A Comparative Study of Classifiers. In: Computer Graphics Forum. vol. 34. Wiley Online Library; 2015. p. 111–120.

[208] Sáez-Atienzar S, Martínez-Gómez J, Alonso-Barba JI, Puerta JM, Galindo MF, Jordán J, et al. Automatic quantification of the subcellular localization of chimeric GFP protein supported by a two-level Naive Bayes classifier. Expert Systems with Applications. 2015;42(3):1531–1537.

[209] Townsend J. Theoretical analysis of an alphabetic confusion matrix. Perception & Psychophysics. 1971;9(1):40–50.

[210] Ghaderi F, Kim SK, Kirchner EA. Effects of eye artifact removal methods on single trial P300 detection, a comparative study. Journal of neuroscience methods. 2014;221:41–47.

[211] Fielding AH, Bell JF. A review of methods for the assessment of prediction errors in conservation presence/absence models. Environmental conservation. 1997;24(01):38–49.

[212] Gorji HT, Koohpayezadeh A, Haddadnia J. Ocular Artifact Detection and Removing from EEG by wavelet families: A Comparative Study. Journal of Information Engineering and Applications. 2013;3(13):39–47.

[213] Croft R, Barry R. Removal of ocular artifact from the EEG: a review. Neurophysiologie Clinique/Clinical Neurophysiology. 2000;30(1):5–19.

[214] Gratton G. Dealing with artifacts: The EOG contamination of the event-related brain potential. Behavior Research Methods, Instruments, & Computers. 1998;30(1):44–53.

[215] Szibbo D, Luo A, Sullivan TJ. Removal of blink artifacts in single channel EEG. In: Engineering in Medicine and Biology Society (EMBC), 2012 Annual International Conference of the IEEE. IEEE; 2012. p. 3511–3514.

[216] Koles ZJ. The quantitative extraction and topographic mapping of the abnormal components in the clinical EEG. Electroencephalography and clinical Neurophysiology. 1991;79(6):440–447.

[217] Gasser T, Ziegler P, Gattaz WF. The deleterious effect of ocular artefacts on the quantitative EEG, and a remedy. European archives of psychiatry and clinical neuroscience. 1992;241(6):352–356.

[218] Croft RJ, Chandler JS, Barry RJ, Cooper NR, Clarke AR. EOG correction: a comparison of four methods. Psychophysiology. 2005;42(1):16–24.

[219] Zhou W, Gotman J. Automatic removal of eye movement artifacts from the EEG using ICA and the dipole model. Progress in Natural Science. 2009;19(9):1165–1170.

[220] Matiko JW, Beeby S, Tudor J. Real time eye blink noise removal from EEG signals using morphological component analysis. In: Engineering in Medicine and Biology Society (EMBC), 2013 35th Annual International Conference of the IEEE. IEEE; 2013. p. 13–16.

[221] Mateo J, Torres A, Sanchez-Morla E, Santos J. Eye Movement Artefact Suppression Using Volterra Filter for Electroencephalography Signals. Journal of Medical and Biological Engineering. 2015;35(3):395–405.

[222] Chang WD, Cha HS, Kim K, Im CH. Detection of eye blink artifacts from single prefrontal channel electroencephalogram. Computer Methods and Programs in Biomedicine. 2015;.

[223] Binias B, Palus H, Jaskot K. Real-time detection and filtering of eye movement and blink related artifacts in EEG. In: Methods and Models in Automation and Robotics (MMAR), 2015 20th International Conference on. IEEE; 2015. p. 903–908.

[224] Klein A, Skrandies W. A reliable statistical method to detect eyeblink-artefacts from electroencephalogram data only. Brain topography. 2013;26(4):558–568.

[225] Lange VM, Perret C, Laganaro M. Comparison of single-word and adjective-noun phrase production using event-related brain potentials. Cortex. 2015;67:15–29.

[226] Gonzalez-Moreno A, Aurtenetxe S, Lopez-Garcia ME, del Pozo F, Maestu F, Nevado A. Signal-to-noise ratio of the MEG signal after preprocessing. Journal of neuroscience methods. 2014;222:56–61.

[227] Chicherov V, Plomp G, Herzog MH. Neural correlates of visual crowding. Neuroimage. 2014;93:23–31.

[228] Liu Y, Bengson J, Huang H, Mangun GR, Ding M. Top-down modulation of neural activity in anticipatory visual attention: control mechanisms revealed by simultaneous EEG-fMRI. Cerebral Cortex. 2014;p. bhu204.

[229] Bekhtereva V, Sander C, Forschack N, Olbrich S, Hegerl U, Müller MM. Effects of EEG-vigilance regulation patterns on early perceptual processes in human visual cortex. Clinical Neurophysiology. 2014;125(1):98–107.

[230] Devuyst S, Dutoit T, Ravet T, Stenuit P, Kerkhofs M, Stanus E. Automatic processing of EEG-EOG-EMG artifacts in sleep stage classification. In: 13th International Conference on Biomedical Engineering. Springer; 2009. p. 146–150.

[231] Greco A, Mammone N, Morabito FC, Versaci M. Semi-Automatic Artifact Rejection Procedure based on Kurtosis, Renyi's Entropy and Independent Component Scalp Maps. In: IEC (Prague); 2005. p. 22–26.

[232] Durka PJ, Klekowicz H, Blinowska KJ, Szelenberger W, Niemcewicz S. A simple system for detection of EEG artifacts in polysomnographic recordings. Biomedical Engineering, IEEE Transactions on. 2003;50(4):526–528.

[233] Moretti D, Babiloni F, Carducci F, Cincotti F, Remondini E, Rossini P, et al. Computerized processing of EEG–EOG–EMG artifacts for multi-centric studies in EEG oscillations and event-related potentials. International Journal of Psychophysiology. 2003;47(3):199–216.

[234] Nazarpour K, Wongsawat Y, Sanei S, Chambers J, Oraintara S, et al. Removal of the eye-blink artifacts from EEGs via STF-TS modeling and robust minimum variance beamforming. Biomedical Engineering, IEEE Transactions on. 2008;55(9):2221–2231.

[235] Bhattacharyya S, Biswas A, Mukherjee J, Majumdar AK, Majumdar B, Mukherjee S, et al. Detection of artifacts from high energy bursts in neonatal EEG. Computers in biology and medicine. 2013;43(11):1804–1814.

[236] Wang Y, Toor SS, Gautam R, Henson DB. Blink frequency and duration during perimetry and their relationship to test-retest threshold variability. Investigative ophthalmology & visual science. 2011;52(7):4546–4550.

[237] Sovierzoski M, Argoud FI, De Azevedo FM, et al. Identifying eye blinks in EEG signal analysis. In: Information Technology and Applications in Biomedicine, 2008. ITAB 2008. International Conference on. IEEE; 2008. p. 406–409.

[238] Kandaswamy A, Krishnaveni V, Jayaraman S, Malmurugan N, Ramadoss K. Removal of ocular artifacts from EEG-A Survey. IETE journal of research. 2005;51(2):121–130.

[239] Krishnaveni V, Jayaraman S, Aravind S, Hariharasudhan V, Ramadoss K. Automatic identification and Removal of ocular artifacts from EEG using Wavelet transform. Measurement science review. 2006;6(4):45–57.

[240] Popescu TD. Blind separation of vibration signals and source change detection–Application to machine monitoring. Applied Mathematical Modelling. 2010;34(11):3408–3421.

[241] Kachenoura A, Albera L, Senhadji L. Blind source separation methods applied to synthesized polysomnographic recordings: a comparative study. In: Engineering in Medicine and Biology Society, 2007. EMBS 2007. 29th Annual International Conference of the IEEE. IEEE; 2007. p. 3868–3871.

[242] Zibulevsky M, Pearlmutter B, et al. Blind source separation by sparse decomposition in a signal dictionary. Neural computation. 2001;13(4):863–882.

[243] Gribonval R, Lesage S. A survey of sparse component analysis for blind source separation: principles, perspectives, and new challenges. In: ESANN'06 proceedings-14th European Symposium on Artificial Neural Networks. d-side publi.; 2006. p. 323–330.

[244] Donoho DL, Elad M. Optimally sparse representation in general (nonorthogonal) dictionaries via l1 minimization. Proceedings of the National Academy of Sciences. 2003;100(5):2197–2202.

[245] Li Y, Cichocki A, Amari SI. Sparse component analysis for blind source separation with less sensors than sources. Citeseer;. .

[246] Bofill P, Zibulevsky M. Underdetermined blind source separation using sparse representations. Signal processing. 2001;81(11):2353–2362.

[247] Marvasti F, Amini A, Haddadi F, Soltanolkotabi M, Khalaj BH, Aldroubi A, et al. A unified approach to sparse signal processing. EURASIP Journal on Advances in Signal Processing. 2012;2012(1):44. Available from: http://asp.eurasipjournals.com/content/2012/1/44.

[248] Mallat S. A wavelet tour of signal processing. Academic press; 1999.

[249] Rubinstein R, Zibulevsky M, Elad M. Double sparsity: Learning sparse dictionaries for sparse signal approximation. Signal Processing, IEEE Transactions on. 2010;58(3):1553–1564.

[250] Chen SS, Donoho DL, Saunders MA. Atomic decomposition by basis pursuit. SIAM journal on scientific computing. 1998;20(1):33–61.

[251] Yu X, Hu D, Xu J. Blind Source Separation: Theory and Applications. Wiley; 2014. Available from: https://books.google.co.uk/books?id=anBRAgAAQBAJ.

[252] Itano MS, Steinhauer C, Schmied JJ, Forthmann C, Liu P, Neumann AK, et al. Super-resolution imaging of C-type lectin and influenza hemagglutinin nanodomains on plasma membranes using blink microscopy. Biophysical journal. 2012;102(7):1534–1542.

[253] BAKHSHI AD, AHMED A, GULFAM SM, KHAQAN A, YASIN A, IQBAL S, et al. Estimation of Baseline Wander Characteristics in ECG Signals Using Adaptive Transversal Filter and Lomb's Periodogram Analysis. Przegląd Elektrotechniczny. 2013;89(5):107–110.

[254] Anderson CW, Stolz E, Shamsunder S, et al. Multivariate autoregressive models for classification of spontaneous electroencephalographic signals during mental tasks. Biomedical Engineering, IEEE Transactions on. 1998;45(3):277–286.

[255] Gouy-Pailler C, Sameni R, Congedo M, Jutten C. Iterative Subspace Decomposition for Ocular Artifact Removal from EEG Recordings. In: Adali T, Jutten C, Romano JMT, Barros AK, editors. Independent Component Analysis and Signal Separation. Springer Berlin Heidelberg; 2009. p. 419–426. Available from: http://link.springer.com/chapter/10.1007/978-3-642-00599-2_53.

[256] Gouy-Pailler C, Sameni R, Congedo M, Jutten C. Iterative subspace decomposition for ocular artifact removal from EEG recordings. In: Independent Component Analysis and Signal Separation. Springer; 2009. p. 419–426.

[257] Blackwood D, Muir W. Cognitive brain potentials and their application. The British Journal of Psychiatry. 1990;.

[258] Ansari Asl K, Chanel G, Pun T. A channel selection method for EEG classification in emotion assessment based on synchronization likelihood. 2007;.

[259] Lotte F. A Tutorial on EEG Signal-processing Techniques for Mental-state Recognition in Brain–Computer Interfaces. In: Guide to Brain-Computer Music Interfacing. Springer; 2014. p. 133–161.

[260] Cecotti H, Rivet B, Congedo M, Jutten C, Bertrand O, Maby E, et al. A robust sensor-selection method for P300 brain–computer interfaces. Journal of neural engineering. 2011;8(1):016001.

[261] Krusienski DJ, Sellers EW, McFarland DJ, Vaughan TM, Wolpaw JR. Toward enhanced P300 speller performance. Journal of neuroscience methods. 2008;167(1):15–21.

[262] Rakotomamonjy A, Guigue V. BCI competition III: dataset II-ensemble of SVMs for BCI P300 speller. Biomedical Engineering, IEEE Transactions on. 2008;55(3):1147–1154.

[263] Schröder M, Lal TN, Hinterberger T, Bogdan M, Hill NJ, Birbaumer N, et al. Robust EEG channel selection across subjects for brain-computer interfaces. EURASIP Journal on Applied Signal Processing. 2005;2005:3103–3112.

[264] Colwell K, Ryan D, Throckmorton C, Sellers E, Collins L. Channel selection methods for the P300 speller. Journal of neuroscience methods. 2014;232:6–15.

[265] Hoffmann U, Vesin JM, Ebrahimi T, Diserens K. An efficient P300-based brain–computer interface for disabled subjects. Journal of Neuroscience methods. 2008;167(1):115–125.

[266] Blankertz B, Losch F, Krauledat M, Dornhege G, Curio G, Muller KR. The Berlin Brain–Computer Interface: accurate performance from first-session in BCI-naive subjects. Biomedical Engineering, IEEE Transactions on. 2008;55(10):2452–2462.

[267] Guyon I, Weston J, Barnhill S, Vapnik V. Gene selection for cancer classification using support vector machines. Machine learning. 2002;46(1-3):389–422.

[268] Xu N, Gao X, Hong B, Miao X, Gao S, Yang F. BCI competition 2003-data set IIb: enhancing P 300 wave detection using ICA-based subspace projections for BCI applications. IEEE transactions on biomedical engineering. 2004;51(6):1067–1072.

[269] Serby H, Yom-Tov E, Inbar GF. An improved P300-based brain-computer interface. Neural Systems and Rehabilitation Engineering, IEEE Transactions on. 2005;13(1):89–98.

[270] Rivet B, Souloumiac A, Attina V, Gibert G. xDAWN algorithm to enhance evoked potentials: application to brain–computer interface. Biomedical Engineering, IEEE Transactions on. 2009;56(8):2035–2043.

[271] Rivet B, Cecotti H, Maby E, Mattout J. Impact of spatial filters during sensor selection in a visual P300 brain-computer interface. Brain topography. 2012;25(1):55–63.

[272] Zakeri Z, Samadi MRH, Cooke N, Jancovic P. Automatic ERP classification in EEG recordings from task-related independent components. In: Biomedical and Health Informatics (BHI), 2016 IEEE-EMBS International Conference on. IEEE; 2016. p. 288–291.

[273] Renard Y, Lotte F, Gibert G, Congedo M, Maby E, Delannoy V, et al. OpenViBE: an open-source software platform to design, test, and use brain-computer interfaces in real and virtual environments. Presence: teleoperators and virtual environments. 2010;19(1):35–53.